40183

National Library of Canada | Bibliothèque nationale du Canada

CANADIAN THESES ON MICROFICHE | THÈSES CANADIENNES SUR MICROFICHE

NAME OF AUTHOR/*NOM DE L'AUTEUR* Harold Richard Hooper

TITLE OF THESIS/*TITRE DE LA THÈSE* Energy Levels Below 2 MeV in ^{121}Sb and ^{123}Sb

UNIVERSITY/*UNIVERSITÉ* University of Alberta

DEGREE FOR WHICH THESIS WAS PRESENTED/*GRADE POUR LEQUEL CETTE THÈSE FUT PRÉSENTÉE* Doctor of Philosophy

YEAR THIS DEGREE CONFERRED/*ANNÉE D'OBTENTION DE CE GRADE* 1978

NAME OF SUPERVISOR/*NOM DU DIRECTEUR DE THÈSE* W. J. McDonald and D. M. Sheppard

Permission is hereby granted to the NATIONAL LIBRARY OF CANADA to microfilm this thesis and to lend or sell copies of the film.

The author reserves other publication rights, and neither the thesis nor extensive extracts from it may be printed or otherwise reproduced without the author's written permission.

L'autorisation est, par la présente, accordée à la BIBLIOTHÈQUE NATIONALE DU CANADA de microfilmer cette thèse et de prêter ou de vendre des exemplaires du film.

L'auteur se réserve les autres droits de publication; ni la thèse ni de longs extraits de celle-ci ne doivent être imprimés ou autrement reproduits sans l'autorisation écrite de l'auteur.

DATED/*DATÉ* June 9, 1978 SIGNED/*SIGNÉ* H. Richard Hooper

PERMANENT ADDRESS/*RÉSIDENCE FIXÉ* 2171 Bel-Air Drive,
Ottawa, Ontario,
K2C 0X2

NL-91 (3-74)

National Library of Canada

Cataloguing Branch
Canadian Theses Division

Ottawa, Canada
K1A 0N4

Bibliothèque nationale du Canada

Direction du catalogage
Division des thèses canadiennes

NOTICE

The quality of this microfiche is heavily dependent upon the quality of the original thesis submitted for microfilming. Every effort has been made to ensure the highest quality of reproduction possible.

If pages are missing, contact the university which granted the degree.

Some pages may have indistinct print especially if the original pages were typed with a poor typewriter ribbon or if the university sent us a poor photocopy.

Previously copyrighted materials (journal articles, published tests, etc.) are not filmed.

Reproduction in full or in part of this film is governed by the Canadian Copyright Act, R.S.C. 1970, c. C-30. Please read the authorization forms which accompany this thesis.

THIS DISSERTATION
HAS BEEN MICROFILMED
EXACTLY AS RECEIVED

AVIS

La qualité de cette microfiche dépend grandement de la qualité de la thèse soumise au microfilmage. Nous avons tout fait pour assurer une qualité supérieure de reproduction.

S'il manque des pages, veuillez communiquer avec l'université qui a conféré le grade.

La qualité d'impression de certaines pages peut laisser à désirer, surtout si les pages originales ont été dactylographiées à l'aide d'un ruban usé ou si l'université nous a fait parvenir une photocopie de mauvaise qualité.

Les documents qui font déjà l'objet d'un droit d'auteur (articles de revue, examens publiés, etc.) ne sont pas microfilmés.

La reproduction, même partielle, de ce microfilm est soumise à la Loi canadienne sur le droit d'auteur, SRC 1970, c. C-30. Veuillez prendre connaissance des formules d'autorisation qui accompagnent cette thèse.

LA THÈSE A ÉTÉ
MICROFILMÉE TELLE QUE
NOUS L'AVONS REÇUE

THE UNIVERSITY OF ALBERTA

ENERGY LEVELS BELOW 2 MeV IN ^{121}Sb AND ^{123}Sb

by

© HAROLD RICHARD HOOPER

A THESIS

SUBMITTED TO THE FACULTY OF GRADUATE STUDIES AND RESEARCH

IN PARTIAL FULFILMENT OF THE REQUIREMENTS FOR THE DEGREE

OF DOCTOR OF PHILOSOPHY

DEPARTMENT OF PHYSICS

EDMONTON, ALBERTA

FALL, 1978

THE UNIVERSITY OF ALBERTA

FACULTY OF GRADUATE STUDIES AND RESEARCH

The undersigned certify that they have read, and recommend to the Faculty of Graduate Studies and Research, for acceptance, a thesis entitled Energy Levels Below 2 MeV in ^{121}Sb and ^{123}Sb

submitted by Harold Richard Hooper

in partial fulfilment of the requirements for the degree of Doctor of Philosophy.

J. M. McDonald
Co-supervisor

Douglas M. Sheppard
Co-supervisor

G. B. Hudson

A. McNamara

G. C. Neilson

J. C. Waddington
External Examiner

DATE June 1, 1978

ABSTRACT

Energy levels below 2 MeV in ^{121}Sb and ^{123}Sb have been studied using the ^{121,123}Sb(n,n'γ) reactions. Excited states and the γ-ray decay of these isotopes were investigated and compared with previous results. γ-ray angular distributions have also been measured, and spins and γ-ray multipole mixing ratios deduced. Definite spin assignments have been made for the 947 (9/2), 1025 (7/2), 1036 (9/2) and 1145 (9/2) keV levels in ^{121}Sb, and for the 1030 (9/2) keV level in ^{123}Sb.

A complementary study of energy levels in ^{121}Sb has also been made using the ^{120}Sn(p,γ) reaction. The results of this experiment are compared with those of the (n,n'γ) experiment.

Model calculations have been carried out using the intermediate coupling model. General calculations were undertaken for the odd mass Sb isotopes with $115 \leqslant A \leqslant 125$ and for the odd mass In isotopes with $113 \leqslant A \leqslant 123$, while detailed model calculations of electromagnetic observables were done for the ^{121}Sb and ^{123}Sb nuclei. The model predictions are compared with the present and past experimental results, and are found to be in reasonable agreement with them.

ACKNOWLEDGEMENTS

I would like to express my thanks to my supervisors, Dr. D.M. Sheppard and Dr. W.J. McDonald, and to our lab director Dr. G.C. Neilson, for their guidance, criticism and support of my work.

I also wish to thank my co-workers in the various $(n,n'\gamma)$ studies, Dr. Hugh Siefken, Dr. Peter Green and Dr. John Davidson, for many helpful discussions and, more important, for being there at three in the morning when I needed them. A special thanks to John for fathering EVA, and also for always being so enthusiastic.

I am indebted to Jim Easton for answering my many questions about the computers, and also for being a great skip in curling. Thanks also to "Uncle" Jock Elliott, who was always willing, at any hour of the day or night, to explain why the machine wasn't working.

I wish to thank all the technical staff for keeping things running when I needed them. Thanks also to the secretarial staff for their friendliness, and particular to Greta who was such an avid curler, and never complained about having to throw lead rock all the time.

My most sincere thanks to all my fellow graduate students, both past and present, for their encouragement and humour. I really appreciated being dragged off either running or for a beer on various occasions.

Finally I thank my wife Ione for all her love, support

and patience over these past four years. I promise that I'll never mention antimony again.

The financial support of the National Research Council of Canada is gratefully acknowledged.

To Ione

June, 1978.

TABLE OF CONTENTS

CHAPTER		PAGE
I	INTRODUCTION	1
II	EXPERIMENTAL DETAILS	4
	2.1 The Small-Sample Method for Studying γ-Ray Angular Distributions from the (n,n'γ) Reaction	4
	2.2 The ^{121,123}Sb(n,n'γ)^{121,123}Sb Experiment	8
	2.3 The ^{120}Sn(p,γ)^{121}Sb Experiment	14
III	EXPERIMENTAL RESULTS	15
	3.1 General Results and Analysis	15
	3.2 The Excited States of ^{121}Sb	25
	a) Levels at 0, 37, 507 and 573 keV	25
	b) Levels at 947 and 1322 keV	26
	c) Level at 1025 keV	28
	d) Level at 1036 keV	30
	e) Level at 1140 keV	30
	f) Level at 1145 keV	33
	g) Level at 1386 keV	36
	h) Levels above 1400 keV	36
	3.3 The Excited States of ^{123}Sb	41
	a) Levels at 0, 160, 542 and 712 keV	41
	b) Level at 1030 keV	43
	c) Level at 1089 keV	43
	d) Level at 1182 keV	43
	e) Level at 1260 keV	46
	f) Level at 1337 keV	46
	g) Levels above 1400 keV	46
IV	BACKGROUND TO THE MODEL CALCULATIONS	50
	4.1 Introduction	50
	4.2 The Intermediate Coupling Model	52
	a) General Comments	52
	b) The Formalism	54

CHAPTER PAGE

4.3 Electromagnetic Properties 62

V DISCUSSION OF MODEL CALCULATIONS AND EXPERIMENTAL RESULTS 69

5.1 Input Parameters for Model Calculations 69

a) The CUPPLE3 Calculations 69
b) The MOMENT Calculations 85

5.2 Energy Levels of ^{121}Sb and ^{123}Sb Below 2 MeV 87

VI CONCLUSIONS 111

REFERENCES 115

APPENDIX A PHASE CONSISTENT ELECTROMAGNETIC MULTIPOLE OPERATORS 118

APPENDIX B COMPUTING DETAILS OF THE PROGRAMS CUPPLE3 AND MOMENT 125

B.1 The Program CUPPLE3 125

B.2 The Program MOMENT 130

LIST OF TABLES

Table	Description	Page
1.	γ-rays from ^{121}Sb and ^{123}Sb observed in the $(n,n'\gamma)$ and (p,γ) experiments.	16
2.	A comparison of γ-ray energies measured in this study with some previous measurements.	17
3.	Energy levels in ^{121}Sb and ^{123}Sb as deduced in this work.	18
4.	Experimental spin values and mixing ratios in ^{121}Sb.	23
5.	Experimental spin values and mixing ratios in ^{123}Sb.	24
6.	Reduced matrix elements for the boson creation operators.	61
7.	Coupling strenghth parameters ξ_λ deduced from experimental $B(E\lambda)\downarrow$ values compared with strength parameters used in the CUPPLE3 calculations.	71
8.	Input parameters for CUPPLE3.	74
9.	a) Experimentally measured and model calculated energies for the lowest single-hole levels in the odd mass In nuclei.	75
	b) Experimentally measured and model calculated spectroscopic factors for the lowest single-hole levels in the odd mass In nuclei.	76
10.	a) Experimentally measured and model calculated energies for the lowest single-particle and two-particle-one-hole levels in the odd mass Sb nuclei.	77
	b) Experimentally measured and model calculated spectroscopic factors for the lowest single-hole levels in the odd mass Sb nuclei.	79
11.	Model predicted energy eigenvectors for ^{123}Sb.	90
12.	Model predicted energy eigenvectors for ^{123}Sb.	92

Table	Description	Page
13.	Model predicted and experimentally observed electromagnetic properties of ^{121}Sb.	93
14.	Model predicted and experimentally observed electromagnetic properties of ^{123}Sb.	94
15.	Qualitative results for experiments exciting ^{121}Sb.	96
16.	Qualitative results for experiments exciting ^{123}Sb.	97
17.	Input cards for CUPPLE3.	126
18.	Input cards for MOMENT.	131

LIST OF FIGURES

Figure		Page
1.	Comparison between a normal γ-ray angular distribution experiment and one using the $(n,n'\gamma)$ reaction.	6
2.	Part of a typical γ-ray spectrum, both with and without time-of-flight (TOF) gating.	11
3.	Electronics used in the $^{121,123}Sb(n,n'\gamma)$ Experiment.	12
4.	Energy level and decay scheme for ^{121}Sb as deduced in this work.	19
5.	Energy level and decay scheme for ^{123}Sb as deduced in this work.	20
6.	Energy level and decay scheme for ^{121}Sb as deduced by Barnard et al. (Ba71).	21
7.	Energy level and decay scheme for ^{123}Sb as deduced by Barnard et al. (Ba71).	22
8.	Level at 573 keV; angular distribution of 573 keV γ-ray.	27
9.	Level at 947 keV a) angular distribution of 910 keV γ-ray. b) χ^2/df	29
10.	Level at 1025 keV a) angular distribution of 1025 keV γ-ray. b) χ^2/df	31
11.	Level at 1036 keV a) angular distribution of 989 keV γ-ray. b) χ^2/df	32
12.	Level at 1145 keV a) χ^2/df curve for 1108 keV γ-ray. b) χ^2/df curve for 1145 keV γ-ray.	34
	c) angular distribution of 1108 keV γ-ray. d) angular distribution of 1145 keV γ-ray.	35
13.	Level at 1386 keV a) angular distribution of 1386 keV γ-ray. b) χ^2/df	37
14.	Level at 542 keV; angular distribution of 542 keV γ-ray.	42

Figure		Page
15.	Level at 1030 keV a) angular distribution of 1030 keV γ-ray. b) χ^2/df	44
16.	Level at 1089 keV a) angular distribution of 1089 keV γ-ray. b) χ^2/df	45
17.	Level at 1182 keV a) angular distribution of 1021 keV γ-ray. b) χ^2/df	47
18.	Level at 1337 keV a) angular distribution of 1337 keV γ-ray. b) χ^2/df	48
19.	A comparison of the model generated eigenvalues and the experimentally measured level energies for the lowest single-hole states in the odd mass In isotopes.	81
20.	A comparison of the model generated eigenvalues and the experimentally measured level energies for the lowest single-partile and two-particle-one-hole states in the odd mass Sb isotopes.	82
21.	Model calculated energies as a function of the quadrupole coupling strength parameter ξ_2 for the four lowest levels in ^{121}Sb.	86
22.	A comparison of model predicted and experimental energy levels in ^{121}Sb	88
23.	A comparison of model predicted and experimental energy levels in ^{123}Sb	89

Chapter I

Introduction

A number of experimental studies (Ho71, Ba71, Au72, Bo73, Co73, An75, Ka77, St77) have previously been carried out on the two naturally occuring antimony (Sb) isotopes, ^{121}Sb and ^{123}Sb. These experiments have made use of such reactions as the (^{3}He,d) stripping reaction, the (t,α) pickup reaction, (d,d') inelastic scattering, various coulomb excitation reactions, and (γ,γ') resonance-scattering. Despite the many experimental measurements made in these studies, the information available for energy levels above 1 MeV in these nuclei is still quite incomplete. Many of the studies noted above were selective in the levels they populated, and furthermore many of the charged particle studies exhibited poor energy resolution. These two factors make the correlation of results from different experiments difficult. As well, few measurements have been made of the spins of these levels.

The (n,n'γ) reaction does not suffer from the difficulties mentioned above. For incident neutron energies of less than 10 MeV, this reaction is not overly selective in the levels it populates. In addition, excellent energy resolution can be obtained provided the emitted γ-ray is detected. An earlier study of the Sb nuclei (Ba71) made use of this reaction to study level energies and γ-ray branching ratios. The recent

development, however, of a new experimental technique at the University of Alberta Nuclear Research Centre (Da76) makes it practical to determine level spins using this reaction. A study was therefore undertaken of energy levels below 2 MeV in ^{121}Sb and ^{123}Sb using the $(n,n'\gamma)$ reaction. As well, a study of ^{121}Sb using the ^{120}Sn(p,γ) reaction was carried out in order to complement the $(n,n'\gamma)$ work.

One of the fundamental goals of nuclear physics has been to understand and explain the structure of nuclei. While it is obvious that the properties of a nucleus must in some way be determined by the characteristics of the individual nucleons which make up the nucleus, most nuclei contain too many nucleons to permit simple calculations based on the individual nucleon parameters. The problem of understanding nuclear structure is greatly simplified if it is possible to correlate the properties of many nucleons, and express these correlations in terms of collective parameters. There is, of course, considerable experimental evidence for the correlation of nucleon parameters in nuclei, and many nuclei exhibit various forms of collective motion.

A basic model of nuclear structure which couples the collective motions of many nucleons to the independent parameters of a few nucleons is the intermediate coupling model. The odd-mass Sb nuclei, with one proton outside the

Z = 50 closed shell, are examples of nuclei for which simple intermediate coupling model calculations can be attempted. In these nuclei the single-particle parameters of the extra-core proton are coupled to the vibrational structure of the doubly even tin (Sn) core. Model calculations of this type have been carried out in the present study, and a comparison made between experimental measurements and model predictions. This comparison is useful for two reasons. It indicates to what extent the various assumptions implicit in the model calculations are valid. It also provides a convenient framework with which to discuss and interpret both the present and previous experimental results.

Chapter II

Experimental Details

2.1 The Small-Sample Method for Studying γ-Ray Angular Distributions from the (n,n'γ) Reaction

A useful tool in nuclear structure studies is a measurement of the angular distribution of γ-rays emitted following a nuclear reaction (Ro67). γ-ray angular distributions provide information about the spins of the nuclear levels involved in a γ-ray decay, and can also be used to measure the multipole mixing ratio of emitted γ-radiation. This mixing ratio information can be useful when studying other properties of the nuclear levels, such as their parities. Of course the amount of information obtained from an angular distribution experiment depends to a large extent on the nature of the nuclear reaction used to excite a nucleus. The (n,n'γ) reaction is particularly advantageous in this sort of a study because there is no coulomb barrier. Hence this reaction can be used on heavier (A>100) nuclei where charged particle studies are difficult. Furthermore, since for low incident neutron energies (<10 MeV) this reaction is a compound one, the strength with which it populates a particular nuclear level is dependent only on the energy and spin of the excited level relative to the ground state, and not on subtler properties of the nuclear structure. Hence this reaction is not overly selective in the nuclear levels it populates, as are many other reactions.

From an experimental point of view, however, the difficulties in working with neutrons are considerable. Nevertheless, a technique has been developed at this lab for measuring γ-ray angular distributions using the $(n,n'\gamma)$ reaction (Da76). For completeness, the details of this technique are given below.

Fig. 1 shows schematically the difference between a normal γ-ray angular distribution experiment and one using a neutron production source. In the normal experiment the incident charged particle beam is collimated, monoenergetic and of reasonably high flux. The angular distribution is obtained by measuring the relative number of γ-rays emitted as a function of the angle of emission Θ, where Θ is measured with respect to the incident beam. In an inelastic neutron scattering experiment, however, the necessity of good counting statistics requires that the scatterer be fairly large, and that it be placed close to the neutron production target. In this arrangement the flux of neutrons through the scatterer is produced by a nuclear reaction such as $^3H(p,n)^3He$ and is neither monoenergetic nor collimated. If the γ-ray yield is measured as a function of the angle Θ, where Θ is measured relative to the incident charged particle beam, then a distorted γ-ray angular distribution is obtained; a distribution which averages over the incident neutron direction, energy and flux. As well, the distribution is

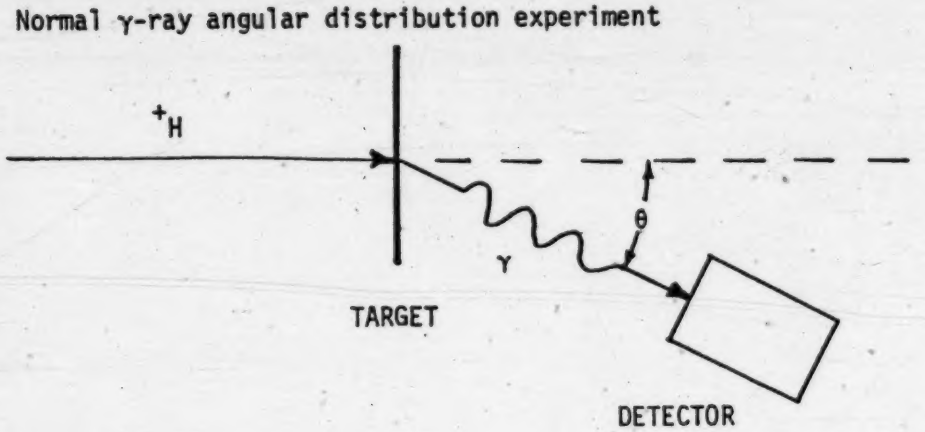

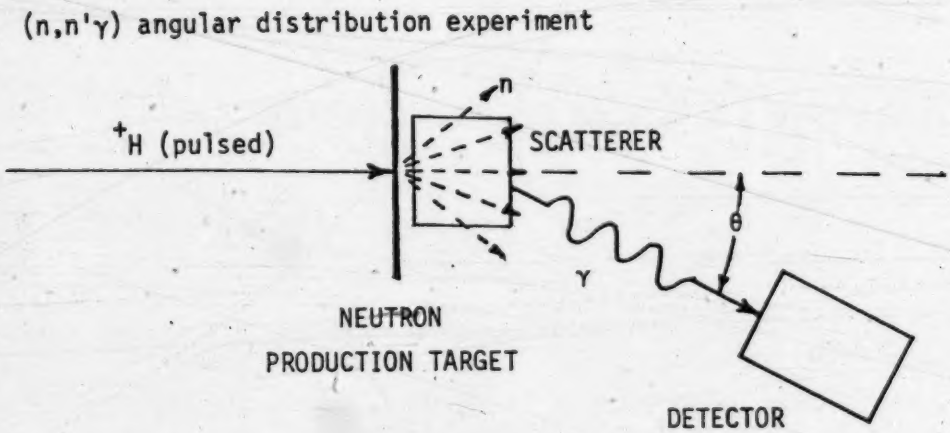

Fig. 1 Comparison between a normal γ-ray angular distribution experiment and one using the (n,n'γ) reaction.

further distorted by such factors as the finite thickness of the neutron production target, and γ-ray absorption within the scatterer itself.

In a single step γ-ray transition, a nucleus in an initial excited state of spin J_i and parity π_i decays by the emission of a γ-ray with multipole mixing ratio δ to a final state of spin J_f and parity π_f. If the nucleus has been initially excited by the (n,n') reaction, and if J_i, π_i, J_f, π_f and δ are known, then it is possible to calculate, using the Compound Nuclear Statistical Model (Sh66), the relative γ-ray yield at any angle Θ provided the incident neutron direction, energy and flux are given. For most nuclear decays of interest, J_f and π_f are known. Therefore a computer program was written which, for particular values of J_i, π_i and δ, integrates over all possible neutron directions and energies and produces a distorted theoretical angular distribution. This program, called EVA (Da76a), also takes into account such effects as neutron and γ-ray absorption within the scatterer, the thickness of the neutron production target, and the finite area of the charged particle beam spot on the neutron production target.

EVA compares the distorted angular distributions it generates to the experimental angular distributions using a standard χ^2 test for goodness of fit. In this way definite values of J_i and δ can often be deduced. The initial state

parity π_i cannot normally be determined since angular distribution measurements are insensitive to it.

2.2 The $^{121,123}Sb(n,n'\gamma)^{121,123}Sb$ Experiment

The neutron scatterer consisted of a cylinder of natural Sb powder (57.2% ^{121}Sb, 42.8% ^{123}Sb) of length 1.59 cm and radius 0.87 cm. The Sb powder had a mass of 13.5 g and was contained in a thin-walled nylon tube. The cylindrical scatterer was aligned axially with the beam at a separation distance of 0.8 cm from the neutron production target.

Neutrons with maximum energies ranging from 1.5 to 2.7 MeV were produced using the $^{3}H(p,n)^{3}He$ reaction. Excitation curves were measured for γ-rays produced in the $^{121,123}Sb(n,n'\gamma)$ reaction, and maximum neutron energies were chosen for each angular distribution run so that there was no appreciable feeding of the levels of interest from higher excited states. The tritium target consisted of a 3.27 mg/cm^2 layer of metallic erbium deposited on a tantalum backing with tritium absorbed in the erbium layer at a 1:1 atomic ratio. The energy spread in the neutron beam due to the target thickness was typically 150 keV.

A 10 ns pulsed proton beam with a 2 MHz repetition rate and average current of about 0.7 μA was provided by the University of Alberta Van de Graaff accelerator. Typical runs required an accumulated charge of 10 mC per

angle. γ-rays were detected in two Ge(Li) detectors placed about 50 cm from the scatterer, and a stationary NE213 liquid scintillator neutron detector was used to monitor total neutron flux. Signals from the detectors were analysed and stored in an on-line computer, with signals from the Ge(Li) detectors being sorted both as a function of energy and as a function of time, measured relative to a signal from a pulsed proton beam pickoff. A ^{137}Cs source was placed close to the Ge(Li) detectors in order to monitor dead time and gain stability within the system. The γ-ray energy spectra were calibrated using the 573.16 ± 0.13 keV and 1385.5 ± 0.4 keV γ-rays from ^{121}Sb. The energies of these two γ-rays were measured in the (p,γ) experiment.

The Ge(Li) timing spectra proved to be quite useful in reducing neutron-induced background in the γ-ray energy spectra. Because the protons were pulsed, so too were the neutrons produced in the neutron production target and the γ-rays created in the scatterer. After any one pulse of protons, the γ-rays would arrive at the Ge(Li) detectors ahead of the neutrons because of their higher velocity. Two distinct peaks could therefore be distinguished in the timing spectra; one due to the pulse of γ-rays and the other due to the pulse of neutrons. By sorting to the energy spectra only those signals which fell in the γ-ray time peak, background from neutron induced reactions within the Ge(Li) detectors could be significantly reduced. This

time-of-flight gating is illustrated in fig. 2, which shows a typical γ-ray spectrum both with and without time-of-flight gating. Fig. 3 outlines the electronics used during the experiment.

One limit on the amount of information which could be obtained from these γ-ray angular distribution measurements was predetermined by a basic feature of angular distribution theory. It is well known that the anisotropy in a particular γ-ray angular distribution is dependent on the alignment of the nuclear level emitting the γ-radiation. An excited nuclear state will only be appreciably aligned by any nuclear reaction if the spin of the excited state is higher than the ground state spin. Hence, since the ground state spins of ^{121}Sb and ^{123}Sb are 5/2 and 7/2 respectively, little information will be forthcoming from γ-ray angular distribution measurements for levels with spins less than 7/2 in ^{121}Sb, and less than 9/2 in ^{123}Sb.

The advantage in using a natural Sb scatterer was that the natural Sb was readily available and inexpensive. The cost of separated Sb isotopes was found to be prohibitively high, considering that this type of experiment requires a sample with a mass of at least a few grams. However, using a natural Sb scatterer introduced the problem that a γ-ray observed in the ^{121,123}Sb(n,n'γ) reaction cannot definitely be assigned to either one of the two Sb isotopes unless

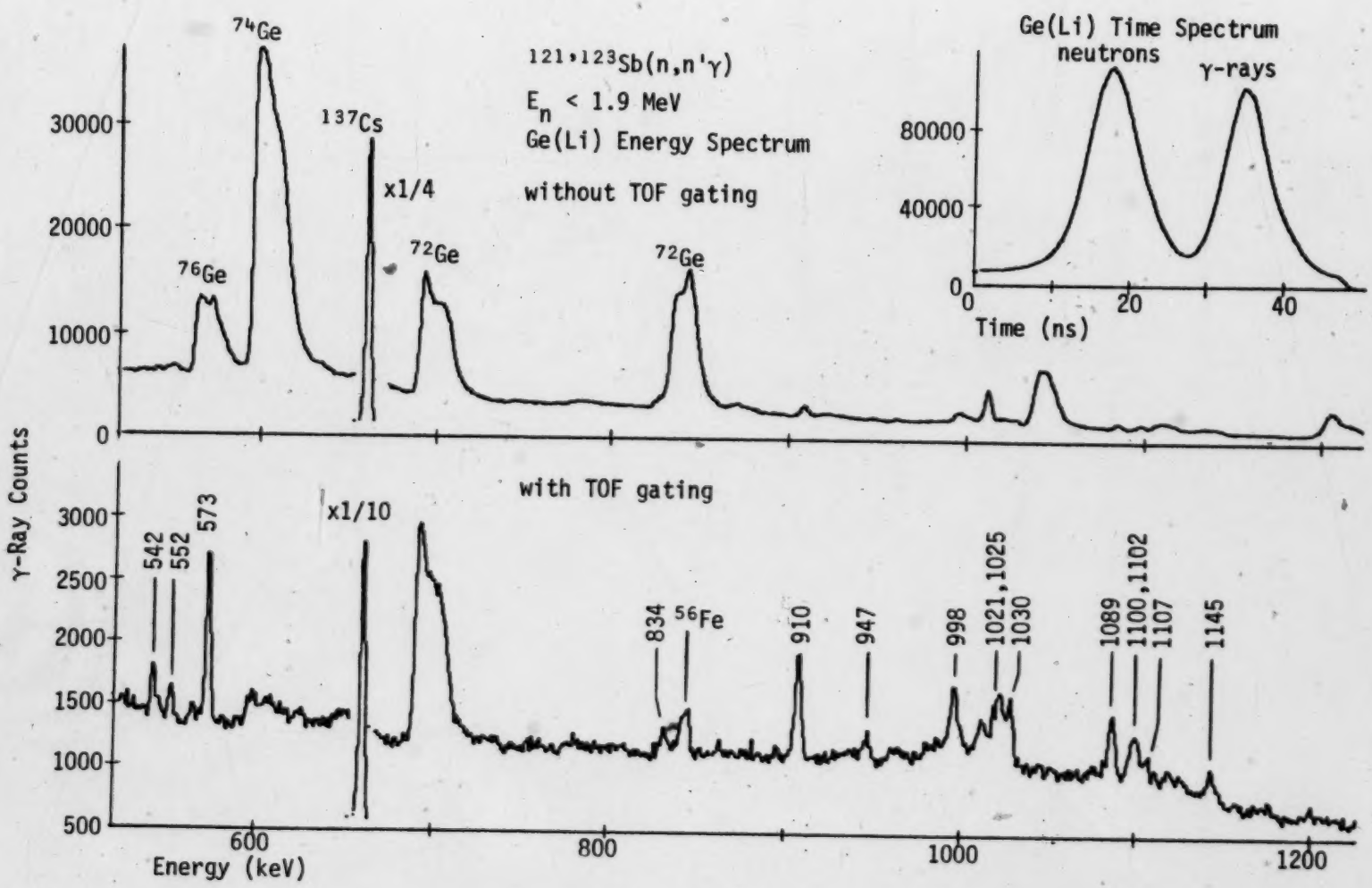

Fig. 2 Part of a typical γ-ray spectrum, both with and without time-of-flight (TOF) gating. The Ge(Li) detector was at an angle $\theta = 50^{o}$. The energies in keV for γ-rays from Sb are indicated, and large background peaks are noted.

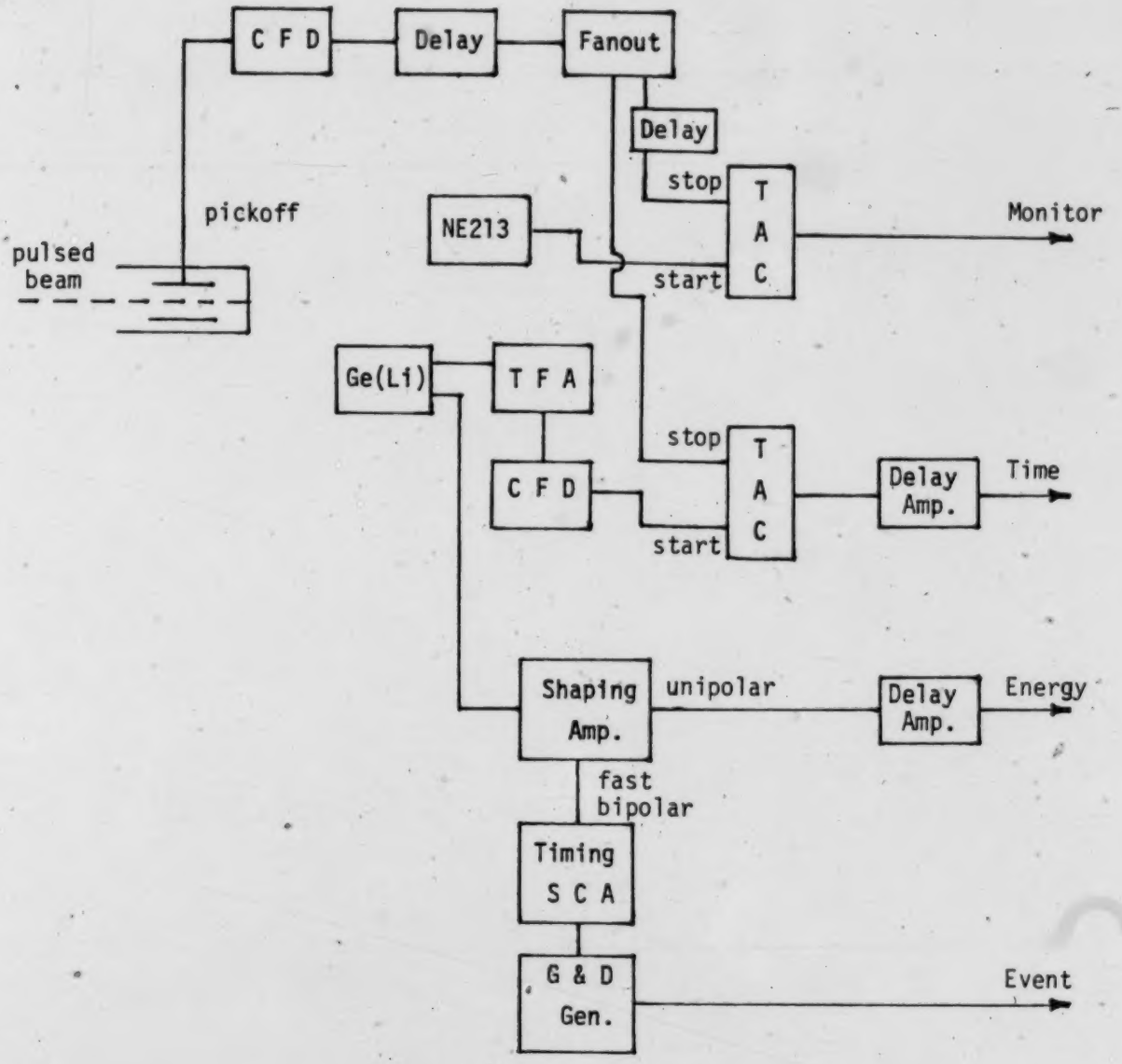

Fig. 3a Electronics used in the $^{121,123}Sb(n,n'\gamma)$ experiment.

Abbreviations used in this figure are explained in fig. 3b.

During the experiment two Ge(Li) detectors were used, each with its own set of electronics.

CFD--constant fraction discriminator

Ge(Li)--lithium drifted germanium γ-ray detector

G & D--gate and delay generator
Gen.

NE213--liquid scintillator neutron detector

TAC--time to amplitude converter

TFA--timing filter amplifier

Timing--timing single channel analyser
SCA

Fig. 3b) Abbreviations used in fig. 3a).

that γ-ray has already been observed in a previous work. Therefore, a short experiment using a thin ^{120}Sn target and the $^{120}Sn(p,\gamma)^{121}Sb$ reaction was carried out to aid in the assignment of γ-rays.

2.3 The $^{120}Sn(p,\gamma)^{121}Sb$ Experiment

The target used in this experiment consisted of a separated Sn isotope (>98% ^{120}Sn) in the form of SnO_2 evaporated to a thickness of about 3.5 mg/cm^2 onto a Ta backing. A blank Ta backing was also employed in order to observe the background spectrum.

A d.c. proton beam with an energy of 3.4 MeV and an average current of 3 μA was used to bombard the target. This beam energy was chosen because it was the highest energy which could be used without crossing the threshold for the $^{120}Sn(p,n)^{120}Sb$ reaction. γ-rays were detected in a Ge(Li) detector placed about 1 cm from the target at an angle of approximately 50° to the proton beam direction. A γ-ray energy spectrum was accumulated in an on-line computer. The energy spectrum was calibrated using ^{133}Ba, ^{137}Cs and ^{60}Co γ-ray sources. Spectra were typically accumulated for about 240 minutes.

Chapter III

Experimental Results

3.1 General Results and Analysis

Table 1 lists the γ-rays observed in the $(n,n'\gamma)$ and/or the (p,γ) experiments which have been assigned to either ^{121}Sb or ^{123}Sb. Errors listed in table 1 are purely statistical in nature. Table 2 compares some of the present γ-ray measurements with the results of two previous experiments.

Energy level and decay schemes could be constructed using the γ-ray energies listed in table 1, and with the help of previously published level schemes, and γ-ray threshold information obtained from the $(n,n'\gamma)$ experiment. Table 3 lists the excited states of ^{121}Sb and ^{123}Sb as deduced in this work, and figs. 4 and 5 illustrate the decay schemes. A detailed discussion of the levels and their assignment is given later in the chapter. For comparison, figs. 6 and 7 show decay schemes for ^{121}Sb and ^{123}Sb deduced in an earlier $(n,n'\gamma)$ experiment (Ba71).

Tables 4 and 5 list the results of the γ-ray angular distribution measurements. In order to evaluate the angular distribution data, the alignment of the initial state in a particular γ-decay was calculated using the Compound Nuclear Statistical Model (Sh66) and the optical model parameters of Wilmore and Hodgson (Wi64). The computer code EVA was used to calculate distorted

Gamma Ray Energy in keV		
$(n,n'\gamma)$[a]	(p,γ)[b]	Combined
282.5 ±0.3		282.5 ±0.3
374.9 ±0.2	374.9 ±0.2	374.9 ±0.2
381.8 ±0.2		381.8 ±0.2
391.3 ±0.2		391.3 ±0.2
470.2 ±0.2	470.40±0.13	470.34±0.13
542.1 ±0.2		542.1 ±0.2
552.2 ±0.2		552.2 ±0.2
(573.16±0.13)	573.16±0.13	573.16±0.13
834.2 ±0.2	834.1 ±0.3	834.2 ±0.2
898.1 ±0.3	898.2 ±0.3	898.1 ±0.3
910.0 ±0.2	(^{67}Ga)	910.0 ±0.2
940.1 ±0.4	939.9 ±0.3	940.0 ±0.3
947.6 ±0.3	(??)[c]	947.6 ±0.3
998.7 ±0.3	(^{64}Zn)	998.7 ±0.3
1021.3 ±0.3		1021.3 ±0.3
1025.1 ±0.3	1024.8 ±0.2	1024.9 ±0.2
1030.5 ±0.3		1030.5 ±0.3
1088.8 ±0.4		1088.8 ±0.4
1100.2 ±0.6		1100.2 ±0.6
1102.4 ±0.5	1102.4 ±0.4	1102.4 ±0.4
1107.7 ±0.4	(^{69}Ga)	1107.7 ±0.4
1144.9 ±0.4	1145.0 ±0.4	1145.0 ±0.4
1176.5 ±0.5		1176.5 ±0.5
1337.8 ±0.5	(^{69}Ga)	1337.8 ±0.5
(1385.5 ±0.4)	1385.5 ±0.4	1385.5 ±0.4
1406.8 ±0.7	1407.0 ±0.5	1406.9 ±0.5
1410.2 ±0.6	1410.2 ±0.4	1410.2 ±0.4
1425.5 ±0.6		1425.5 ±0.6
	1437.3 ±0.6	1437.3 ±0.6
	1470.8 ±0.6	1470.8 ±0.6
	1473.3 ±1.6	1473.3 ±1.6
	1481.8 ±0.6	1481.8 ±0.6
1509.2 ±0.7	1508.7 ±0.8	1509.0 ±0.7
1514.6 ±1.2		1514.6 ±1.2
1519.0 ±0.8	1519.4 ±0.4	1519.3 ±0.4
1575.5 ±0.7	1575.4 ±0.7	1575.4 ±0.7
1590.3 ±1.2	1590.5 ±0.6	1590.5 ±0.6
1735.9 ±0.7	1736.5 ±0.5	1736.3 ±0.5
1810.8 ±0.7	1811.0 ±0.6	1810.9 ±0.6

[a] Energies in brackets were used to calibrate the $(n,n'\gamma)$ spectra. See text for details of energy calibration.

[b] In cases where a background contaminant peak may have obscured an Sb peak, the contaminant is listed in brackets.

[c] See comment in chapter III concerning this background γ-ray.

Table 1 γ-rays from ^{121}Sb and ^{123}Sb observed in the $(n,n'\gamma)$ and (p,γ) experiments.

Gamma Ray Energy in keV					
This Study	Previous Studies				
	Ref. An75		Ref. Ra74	Ref. Bo73	
282.5±0.2	281.7±0.1				
381.8±0.2	381.6±0.1		381.7±0.4		
391.3±0.2	391.3±0.1				
470.34±0.13	470.6±0.1				
542.1±0.2	541.9±0.1		542.2±0.4		
552.2±0.2			552.2±0.4		
573.16±0.13	573.0±0.1				
910.0±0.2	909.8±0.5				
998.7±0.3	998.4±0.1				
1021.3±0.3	1021.8±0.3		1021.0±0.2		
1024.9±0.2	1024.9±0.1			1025.±1.	
1030.5±0.3	1030.4±0.2		1030.23±0.10	1030.±1.	
1088.8±0.4	1088.6±0.2		1088.64±0.10	1089.±1.	
1100.2±0.6			1100.5±0.4		
1107.7±0.4	1107.6±0.1				
1145.0±0.4	1144.8±0.1			1144.±1.	
1176.5±0.5			1177.06±0.20		
1337.8±0.5			1337.44±0.20		
1385.5±0.4	1386.2±0.1			1385.±1.	
1425.5±0.6				1423.±3.	
1514.6±1.2				1512.±2.	
1736.3±0.5				1736.±1.	
1810.9±0.6				1810.±1.	

Table 2 A comparison of γ-ray energies measured in this study with some previous measurements.

Nucleus	Level Energy (keV) This Study[a]	Other Works	Ref.[b]
^{121}Sb	(37.15±0.02)	37.15±0.02	1
	507.49±0.13	507.54±0.05	1
	573.16±0.13	573.08±0.05	1
	947.3 ±0.2	947.0 ±0.5	2
	1024.9 ±0.2	1024.9 ±0.1	2
	1035.9 ±0.3	1035.6 ±0.1	2
	1139.6 ±0.4	1139.3 ±1.0	1
	1145.0 ±0.3	1144.8 ±0.1	2
	1322.2 ±0.3	1325.	3
	1385.5 ±0.4	1386.2 ±0.1	2
	1407.3 ±0.2	1408. ±2.	4
	1427.4 ±0.3	1426.8 ±0.1	2
	1447.5 ±0.3	1446. ±5.	1
	1471.3 ±0.3	*1473. ±2.	4
	1474.5 ±0.6	*1476. ±2.	4
	1509.0 ±0.7		
	1519.2 ±0.3	1521. ±2.	4
	*1575.4 ±0.7		
	*1612.6 ±0.7		
	1627.7 ±0.6	1630. ±2.	4
	1736.3 ±0.5	1736. ±1.	5
	1810.9 ±0.6	1810. ±1.	5
^{123}Sb	(160.33±0.05)	160.33±0.05	6
	542.1 ±0.2	541.9 ±0.1	2
	712.5 ±0.2	712.5 ±0.4	6
	1030.5 ±0.3	1030.23±0.10	6
	1088.8 ±0.4	1088.64±0.10	6
	1181.6 ±0.3	1181.27±0.14	6
	1260.5 ±0.6	1260.9 ±0.4	6
	1337.3 ±0.5	1337.42±0.14	6
	1514.6 ±1.2	1512. ±2.	5
	*1585.8 ±0.6	1574. ±10.	7

[a] Levels shown in brackets were observed in the present study, but the energies quoted are from previous works. Levels preceded by an asterix are tentatative.

[b] References: 1-Ho71, 2-An75, 3-St77, 4-Ba71, 5-Bo73, 6-Ra74, 7-Ba66.

Table 3 Energy levels in ^{121}Sb and ^{123}Sb as deduced in this work. For comparison, levels from previous experiments which appear to correspond to ones seen in this study are also listed.

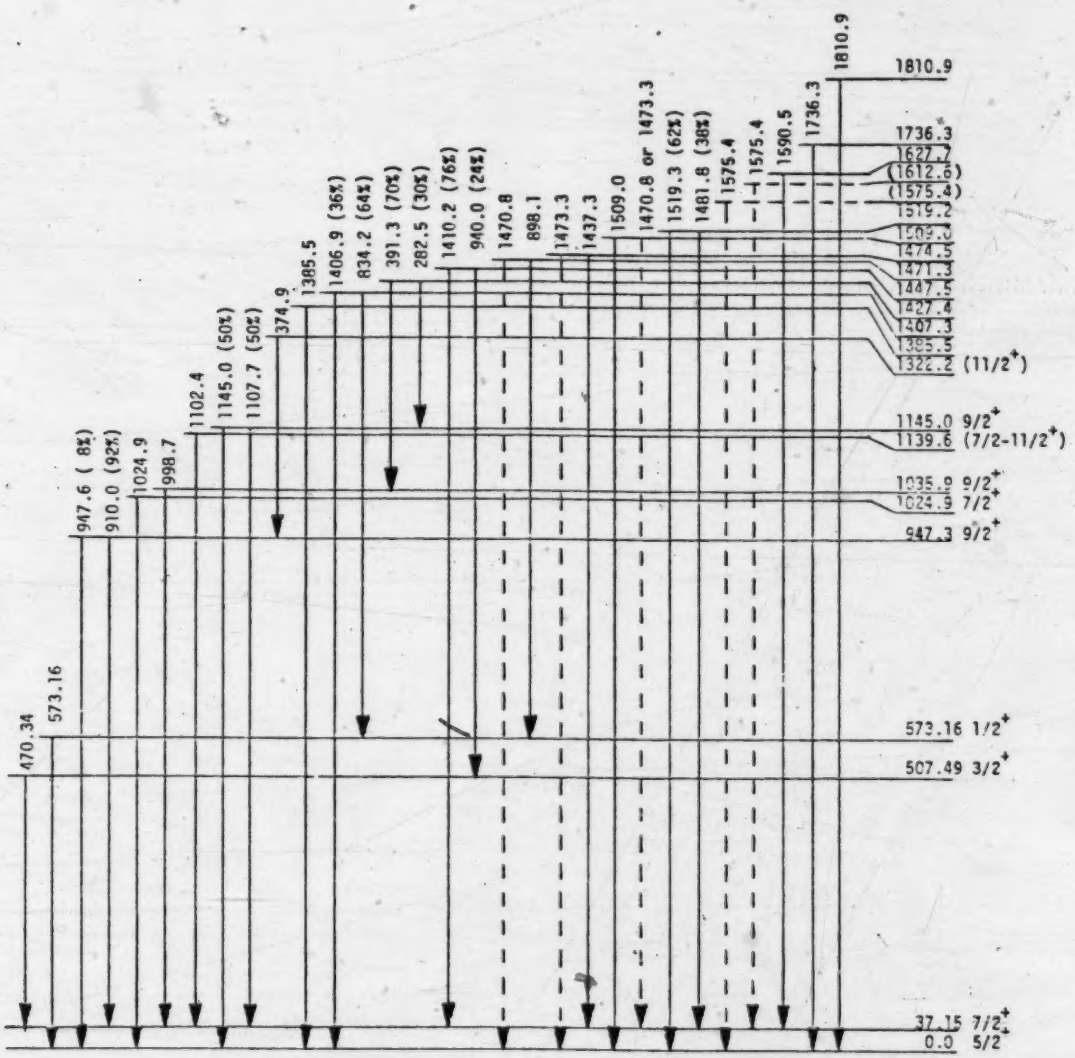

Fig. 4 Energy level and decay scheme for ^{121}Sb as deduced in this work. Only those γ-rays observed in the present study are shown. All energies are in keV.

γ-ray branching ratios are taken from Ba71, with the exception of the decay of the 1448 keV level for which the branching ratio was calculated from this work. Errors in these branching ratios may be as high as 20%.

Spin assignments for the four lowest levels are from Ho71, while definite assignments for higher levels are from the present study. Tentative assignments for the 1140 keV level are from Ba71, and the tentative assignment for the 1322 keV level is from St77.

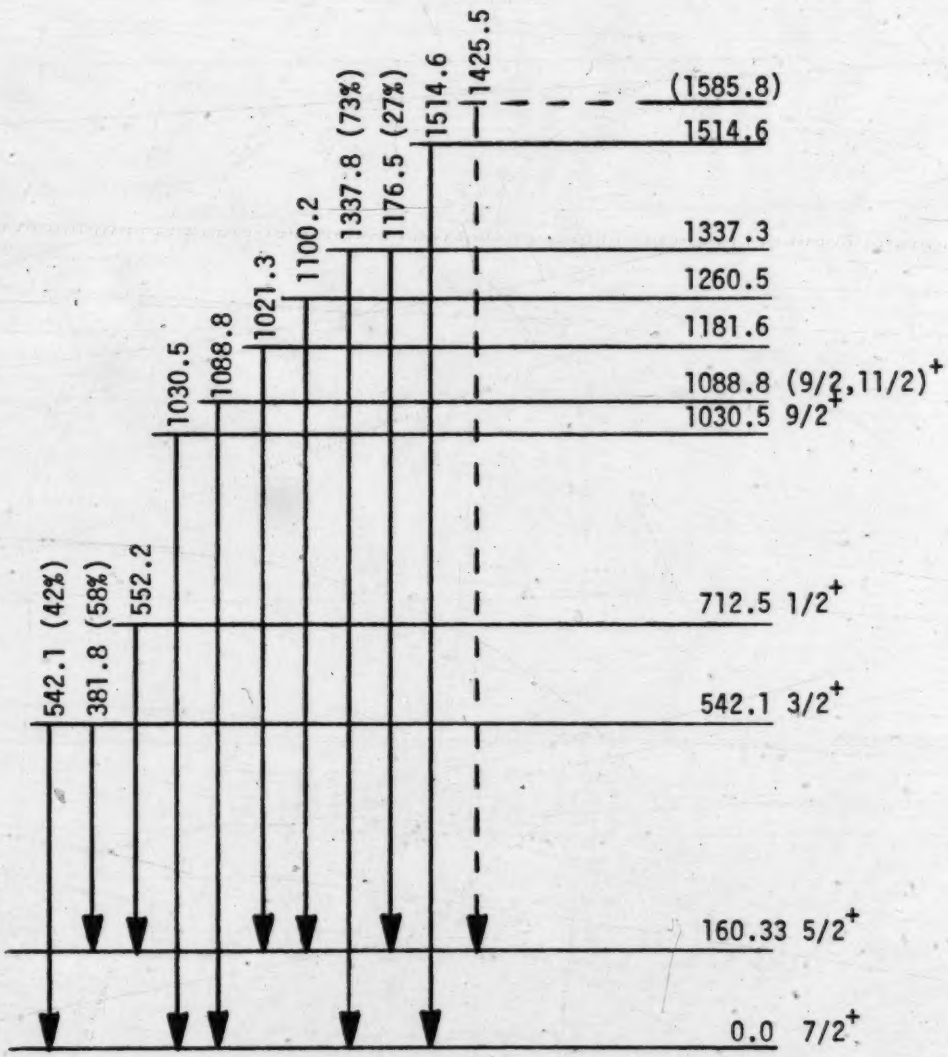

Fig. 5 Energy level and decay scheme for ^{123}Sb as deduced in this work.

Spin assignments for the four lowest levels are from Au72. The spin assignment for the 1030 keV level is from the present study, and the tentative assignment for the 1089 keV level is from Ba71 and the present study.

For further details see the caption of fig. 4.

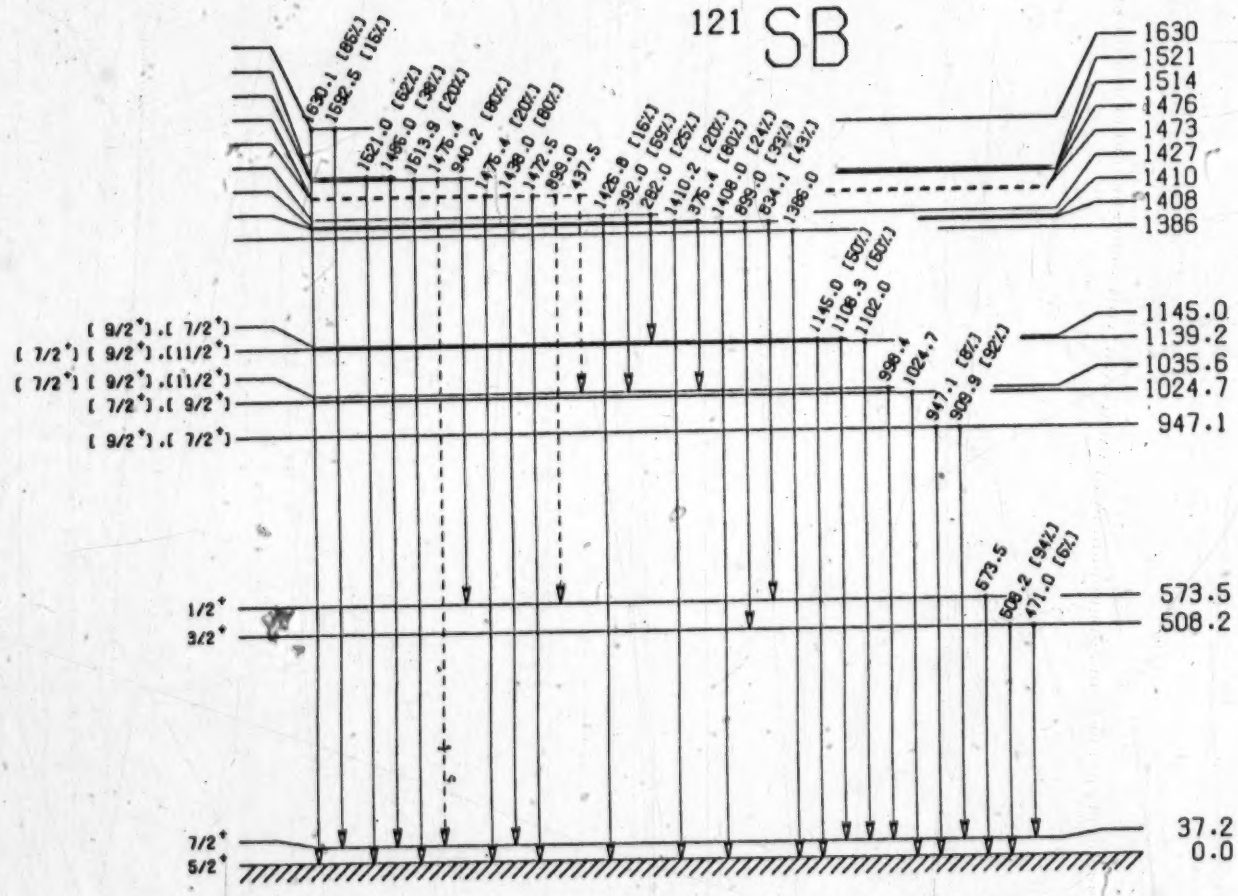

Fig. 6 Energy level and decay scheme for ^{121}Sb as deduced by Barnard et al. (Ba71). This experiment also made use of the (n,n'γ) reaction and natural Sb targets. Uncertainties in level energies are about 1 keV for levels below 1200 keV, and 2 keV for levels above 1200 keV. Errors in branching ratios may be as high as 20%.

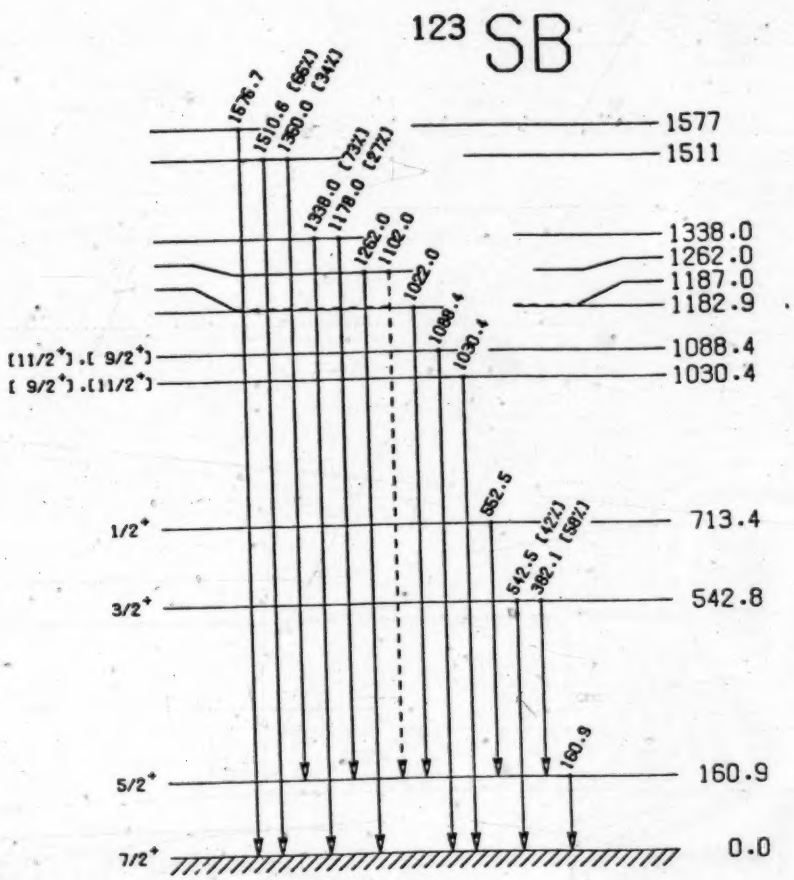

Fig. 7 Energy level and decay scheme for ^{123}Sb as deduced by Barnard et al. (Ba71). See the caption to fig. 6 for further details.

Level Energy (keV)	γ-Ray Energy (keV)	$J_i^{\pi_i} \rightarrow J_f^{\pi_f}$	arctanδ [a] (deg)
947	947	$9/2 \rightarrow 5/2^+$	All δ
	910	$9/2 \rightarrow 7/2^+$	13(6) 67(6)
1025	1025	$7/2 \rightarrow 5/2^+$	4→75
1036	999	$9/2 \rightarrow 7/2^+$	19(11) 61(11)
1145	1145	$9/2 \rightarrow 5/2^+$	-90→-56 -33→31 60→90
	1108	$9/2 \rightarrow 7/2^+$	6→74
1386	1386	$1/2 \rightarrow 5/2^+$	All δ
		$3/2 \rightarrow 5/2^+$	All δ
		$5/2 \rightarrow 5/2^+$	All δ
		$7/2 \rightarrow 5/2^+$	All δ
		$9/2 \rightarrow 5/2^+$	-90→-85 -4→90

[a] arctanδ is given in degrees. The numbers in parentheses give the uncertainties in degrees. The phase convention of Rose and Brink (Ro67) has been used.

Table 4 Experimental spin values and mixing ratios in ^{121}Sb

Level Energy (keV)	γ-Ray Energy (keV)	$J_i^\pi \rightarrow J_f^\pi$	arctan δ [a] (deg)
1030	1030	$9/2 \rightarrow 7/2^+$	9→72
1089	1089	$3/2 \rightarrow 7/2^+$	-90→-14 69→90
		$5/2 \rightarrow 7/2^+$	-89→-9
		$9/2 \rightarrow 7/2^+$	-81→-18
		$11/2 \rightarrow 7/2^+$	-89(12) 3(12)
1182	1021	$1/2 \rightarrow 5/2^+$	All δ
		$3/2 \rightarrow 5/2^+$	All δ
		$5/2 \rightarrow 5/2^+$	-90→-56 -2→90
		$7/2 \rightarrow 5/2^+$	All δ
		$9/2 \rightarrow 5/2^+$	All δ
1337	1337	$1/2 \rightarrow 7/2^+$	0 [b]
		$3/2 \rightarrow 7/2^+$	All δ
		$5/2 \rightarrow 7/2^+$	-7→89
		$7/2 \rightarrow 7/2^+$	All δ
		$9/2 \rightarrow 7/2^+$	-90→-88 -10→90
		$11/2 \rightarrow 7/2^+$	19→75

[a] Same as in table 4.

[b] The radiation was assumed to be pure octupole.

Table 5 Experimental spin values and mixing ratios in ^{123}Sb

theoretical angular distributions for comparison with the data. The uncertainties associated with the experimental points were purely statistical in nature. Plots of χ^2 per degree of freedom (χ^2/df) as a function of initial state spin J_i and γ-ray multipole mixing ratio δ were generated, with values of J_i ranging from $J_f - 3$ to $J_f + 3$. Combinations of J_i and δ for which the minima in $\chi^2(J_i, \delta)$ fell above the 0.1% confidence limit were rejected (En64). Values of J_i and δ which were not rejected, and which have not been ruled out as a result of previous work, are listed in tables 4 and 5. The errors reported in the mixing ratios are calculated according to the $\chi^2_{min}+1$ rule (Ro75). In cases where the mixing ratio error could not be calculated according to this rule, a range of values is listed corresponding to $\chi^2 \leqslant \chi^2_{min}+1$. The signs of the mixing ratios are in accordance with the phase convention of Rose and Brink (Ro67).

3.2 The Excited States of ^{121}Sb

(a) Levels at 0, 37, 507 and 573 keV

The first four states in ^{121}Sb have been studied extensively in previous works (Ho71). The energy of the 37.15 ± 0.02 keV level listed in table 3 is taken from Nuclear Data Sheets (Ho71). The energy of the second excited state, 507.49 ± 0.13 keV, has been deduced from the 470.34 keV transition to the first excited state, while the energy of the 573.16 ± 0.13 keV level is the same as that

for the 573.16 keV γ-ray. The 507-->0 keV transition observed in previous works (Ba71,An75) was hidden in this study by the background 511 keV γ-ray.

These four levels have known spin-parities of $5/2^+$, $7/2^+$, $3/2^+$ and $1/2^+$ respectively. A graph of angular distribution data for the 573-->0 keV, $1/2^+$-->$5/2^+$ transition is shown in fig. 8. For this case, of course, the angular distribution is expected to be isotropic apart from the distortions produced in the experiment.

(b) Levels at 947 and 1322 keV

An energy of 947.3 ± 0.2 keV was assigned to the fourth excited state in ^{121}Sb on the basis of the 947.6 and 910.0 keV γ-rays seen in the (n,n'γ) experiment. In the (p,γ) experiment, the 910 keV γ-ray was hidden by a background γ-ray from ^{67}Ga. The source of a 948.8 ± 0.3 keV γ-ray visible in the target-in spectrum, but not in the background spectrum of the (p,γ) experiment, has not been identified. However, it does not correspond in energy to the 947.6 ± 0.3 keV γ-ray observed in the (n,n'γ) experiment.

A spin assignment of 9/2 was made for the 947 keV level, with arctan for the 910 keV transition equal to either 13° ± 6° or 67° ± 6°. Previous suggestions that this state has positive parity (Ho71,Ba71) are further strengthened by the fact that arctanδ for the 910 keV γ-ray

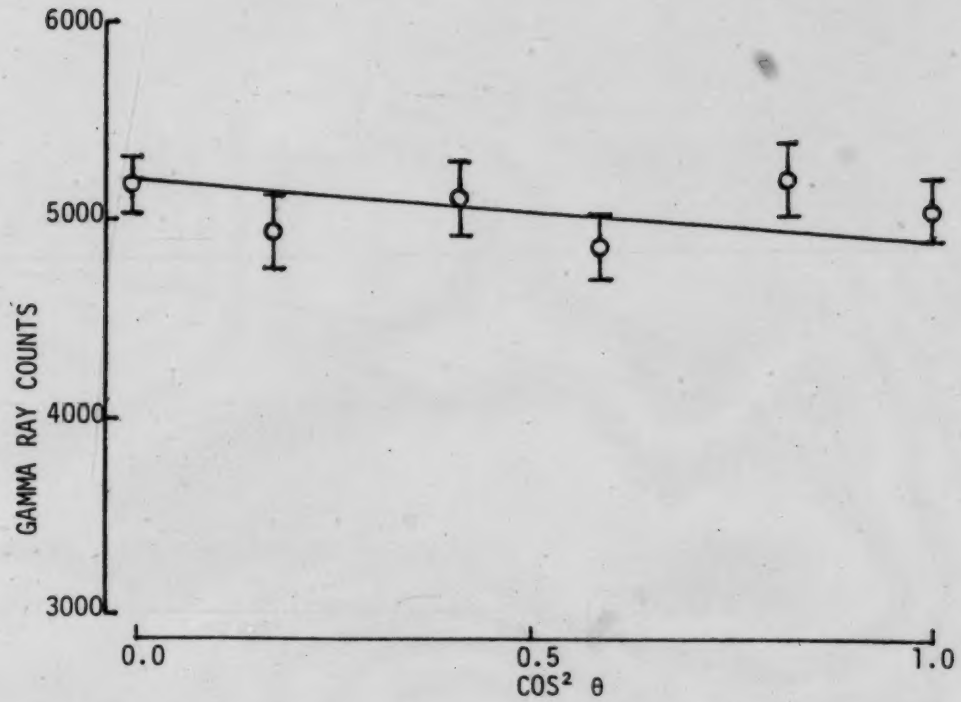

Fig. 8 For each γ-ray transition, the experimental angular distribution was measured a number of times. In this and following figures only one sample angular distribution is illustrated for each transition. The errors shown are purely statistical in nature. The smooth lines drawn through the data in this and following figures are theoretical angular distributions generated using the computer code EVA.

In this figure, data is shown for the 573 → 0 keV transition. The theoretical calculation is for a $1/2^+ \rightarrow 5/2^+$ transition with a mixing ratio $\delta = 0$.

is not consistent with zero. A $9/2^- \rightarrow 7/2^+$, M2/E1 transition would be expected to have a mixing ratio of zero. The value of arctanδ for the 947-->0 keV transition is consistent with zero, however, as would be expected for an M3/E2 transition. Fig. 9a) shows a graph of angular distribution data and fig. 9b) a plot of χ^2/df vs arctanδ for the 910 keV transition.

Stwertka et al. (St77) have recently proposed that the 947 keV level is the band head for a $\Delta J = 1$ rotational band. Similar bands have been seen in other Sb nuclei (Ga75). According to Stwertka, the first excited state in this band decays to the band head with the emission of a 375 keV γ-ray. A 374.9 ± 0.2 keV γ-ray observed during the present study in both the $(n,n'\gamma)$ and (p,γ) spectra appears to correspond to the above transition. Therefore, a level with an energy of 1322.2 ± 0.3 keV has been included in the present level scheme. The spin-parity of this level should be, according to Stwertka, $11/2^+$. Accurate angular distribution measurements to test this proposal could not be made in the present study, however, due to the overlap of the 375 keV γ-ray with a background 377.5 keV γ-ray.

(c) Level at 1025 keV

This level has a measured energy of 1024.9 ± 0.2 keV, based on its 1024.9 keV decay to the ground state. It has been assigned a spin of 7/2, with a value of arctanδ for

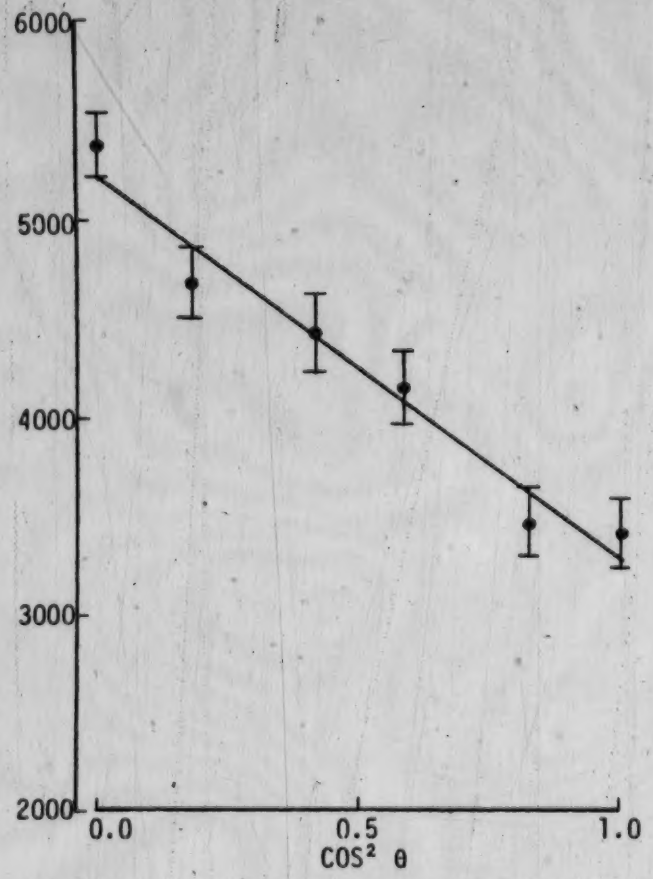

Fig. 9 a) A sample angular distribution for the 947 → 37 keV transition. The theoretical curve is for a $9/2^+ \rightarrow 7/2^+$ transition with arctanδ = 66°.

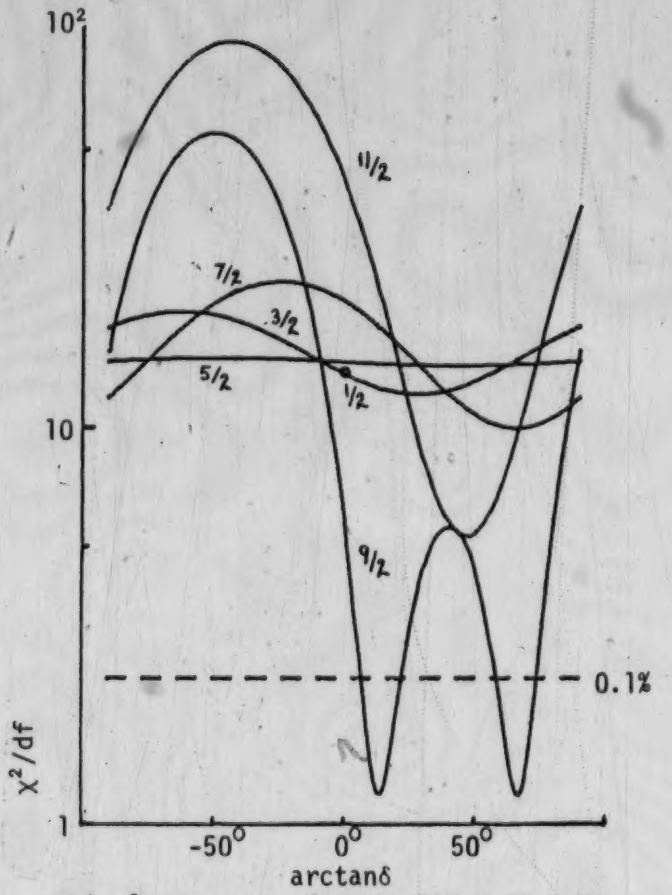

b) χ^2/df curves for the 947 → 37 keV transition. The χ^2/df curves in this and following figures represent all the experimental data for each transition.

the 1025 keV transition between 4° and 75°. Positive parity has previously been suggested for this level (Ba71). A graph of angular distribution data and a plot of χ^2/df vs arctanδ are shown in fig. 10.

(d) Level at 1036 keV

This level was found to decay to the first excited state via the 998.7 kev γ-ray, and therefore has a deduced energy of 1035.9 ± 0.3 keV. The 999 keV γ-ray was observed in the (n,n'γ) experiment, but could not be seen in the (p,γ) experiment due to large background peak from ^{64}Zn.

The 1036 keV level could be assigned a definite spin of 9/2 with possible values of arctanδ for the 999 keV transition of 19° ± 11° or 61° ± 11°. The fact that arctanδ was inconsistent with zero strengthens an earlier suggestion that this state has positive parity (Ho71,Ba71). A graph of an experimental angular distribution and a plot of χ^2/df vs arctan are shown in fig. 11.

(e) Level at 1140 keV

On the basis of the 1102.4 keV γ-ray observed in both the (n,n'γ) and (p,γ) experiments, the measured energy for this level is 1139.6 ± 0.4 keV. In the (n,n'γ) experiment the 1102 keV γ-ray was part of a doublet with the 1100 keV γ-ray from the 1260-->160 keV transition in ^{123}Sb. Because of the close proximity of these two γ-rays, it was

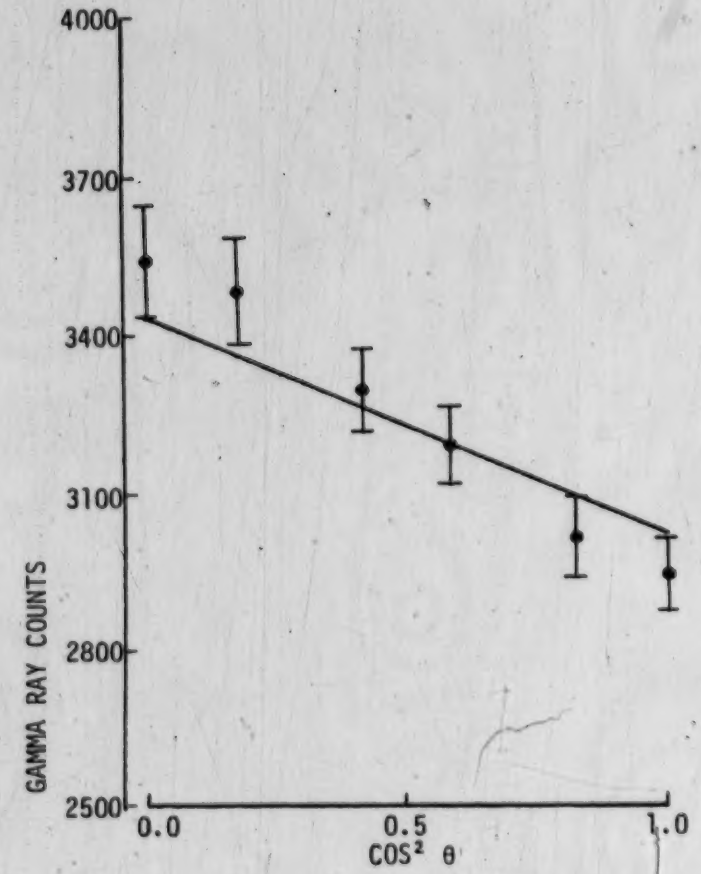

Fig. 10 a) A sample angular distribution for the 1025 → 0 keV transition. The theoretical curve is for a $7/2 \rightarrow 5/2^+$ transition with $\arctan\delta = 40^\circ$.

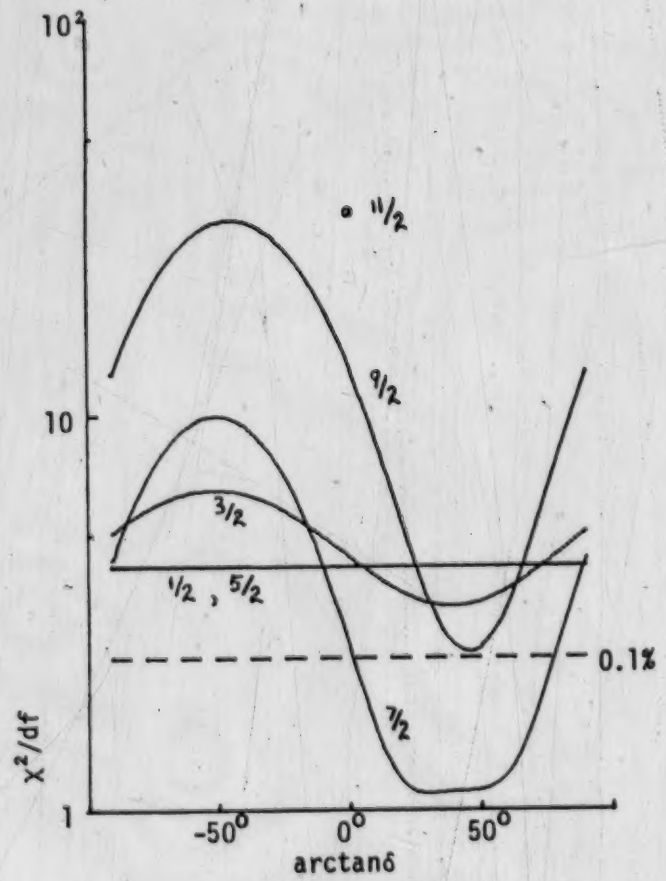

b) χ^2/df curves for the 1025 → 0 keV transition.

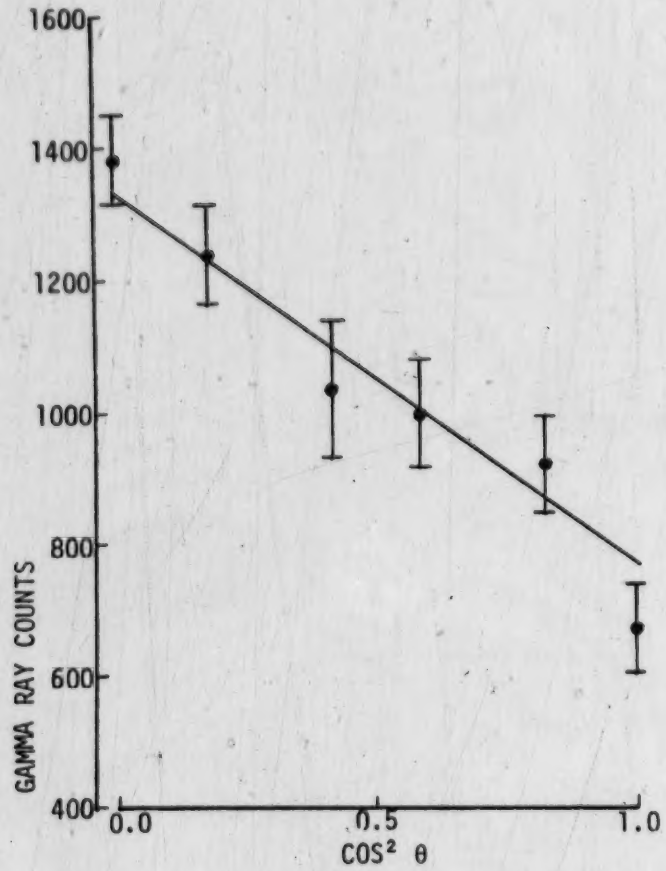

Fig. 11 b) A sample angular distribution for the 1036 → 37 keV transition. The theoretical curve is for a $9/2 \rightarrow 7/2^+$ transition with arctanδ = 19°.

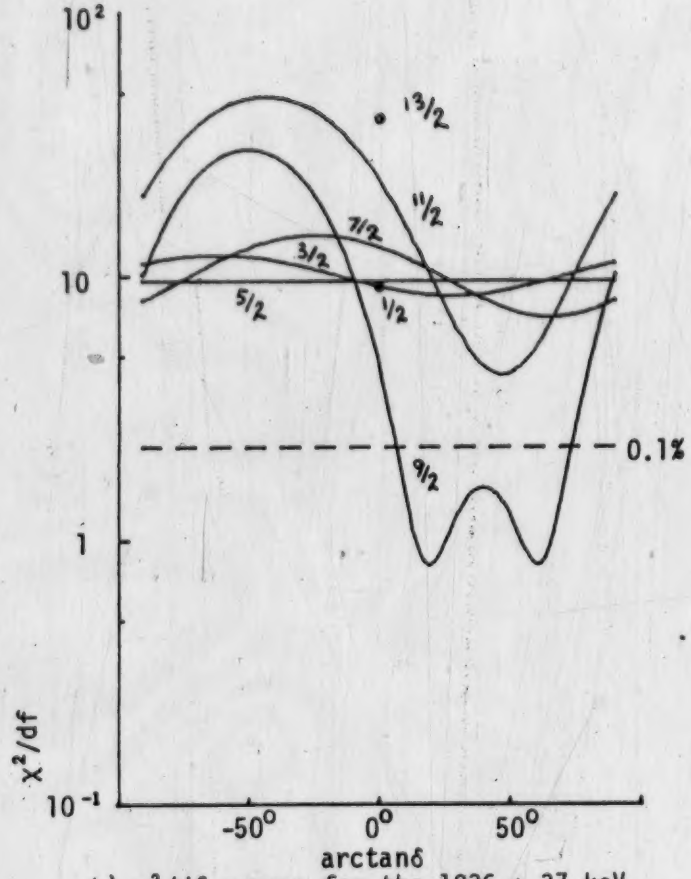

b) χ^2/df curves for the 1036 → 37 keV transition.

impossible to extract peak areas with sufficient accuracy to permit angular distribution measurements. Spin-parities of $9/2^+$ or $11/2^+$ have previously been suggested for this level (Bo73).

(f) Level at 1145 keV

Based on the energies of the 1145.0 and 1107.7 keV γ-rays, the energy of this level was calculated to be 1145.0 ± 0.3 keV. Although the 1145 keV γ-ray was observed in the (p,γ) experiment, the 1108 keV γ-ray could not be distinguished in this experiment due to a background peak from ^{69}Ga. As shown in figs. 12a) and 12b), a definite spin assignment of 9/2 was deduced from the 1108 keV transition for a value of arctan between 6° and 74°. A spin assignment of 11/2 was permitted at the 0.5% confidence level by the 1108 keV γ-ray angular distribution data, but could be rejected on the basis of the 1145 keV γ-ray data. Figs. 12c) and 12d) show graphs of angular distribution data for the 1108 keV and 1145 keV transitions.

Previous experiments have suggested positive parity for this state (Ba71,Bo73).

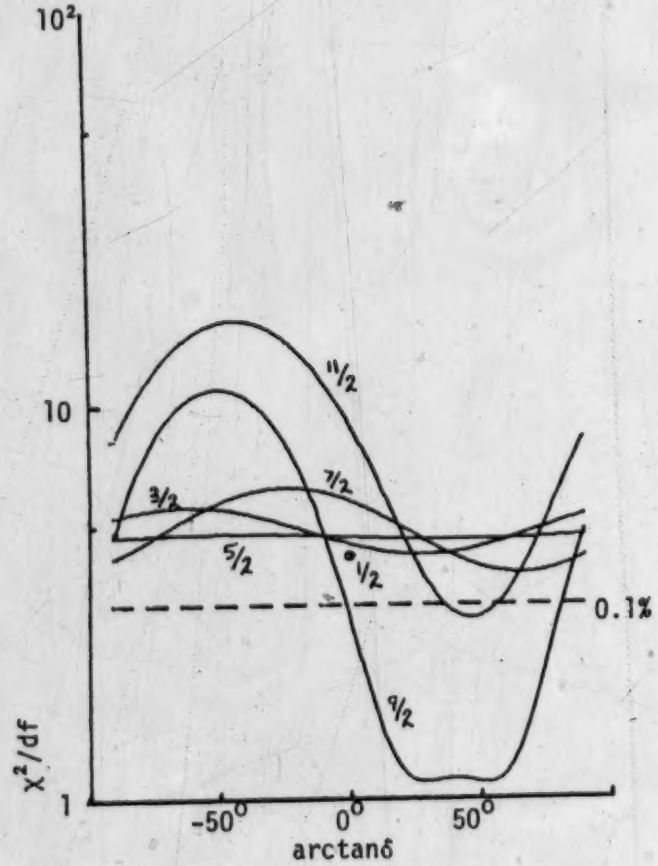

Fig. 12 a) χ^2/df curves for the 1145 → 37 keV transition.

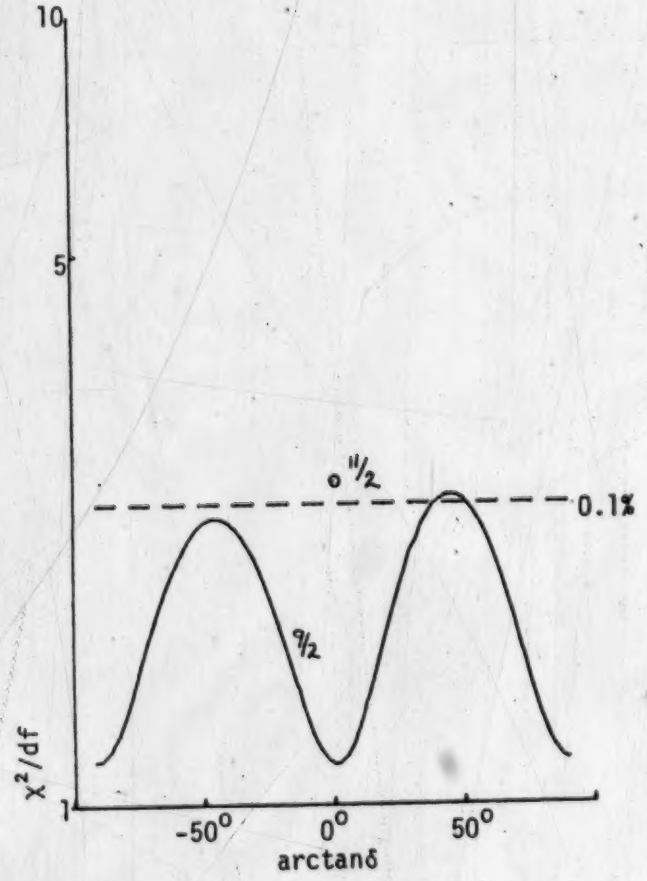

b) χ^2/df curves for the 1145 → 0 keV transition.

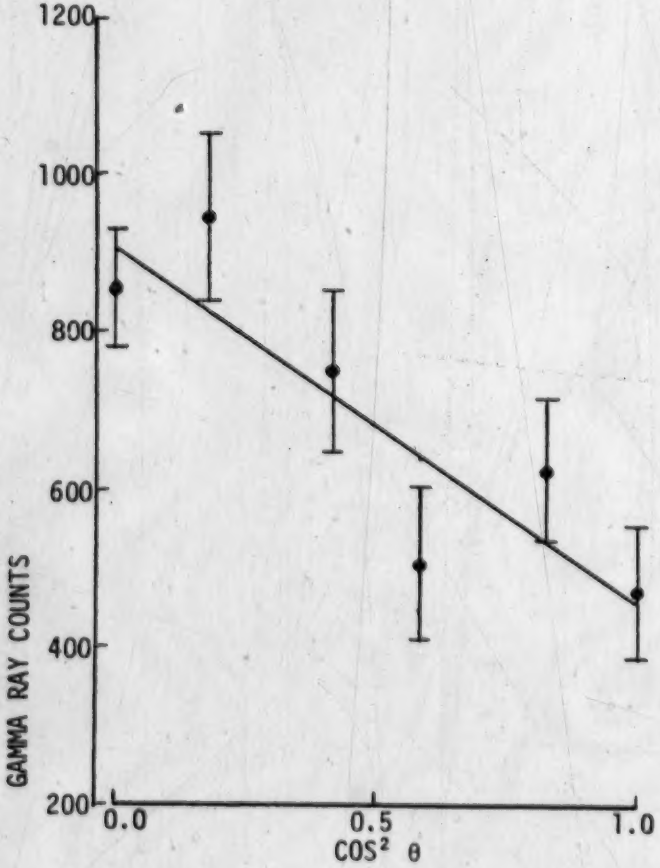

Fig. 12 c) A sample angular distribution for the 1145 → 37 keV transition. The theoretical curve is for a $9/2 \rightarrow 7/2^+$ transition with $\arctan\delta = 52^0$.

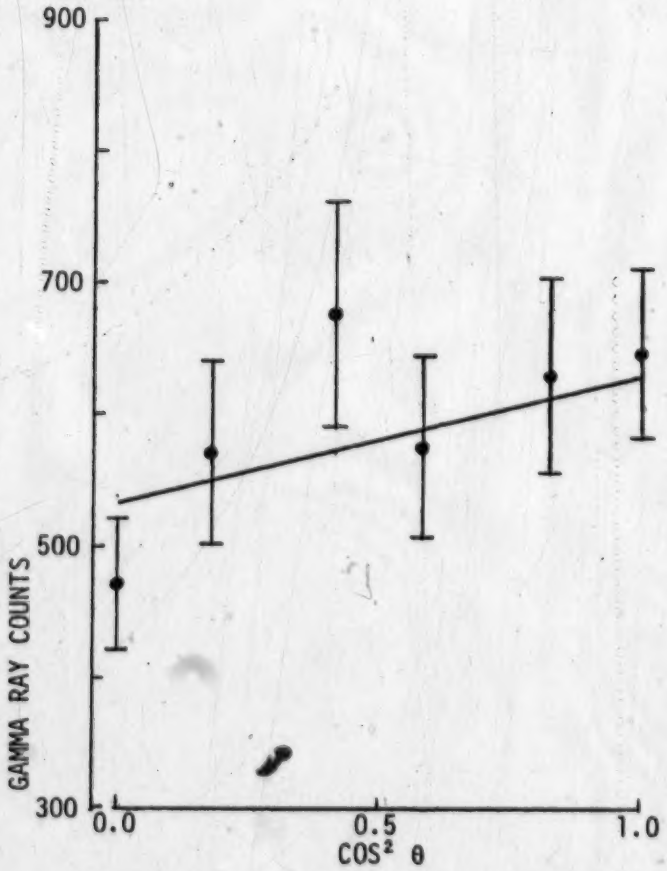

d) A sample angular distribution for the 1145 → 0 keV transition. The theoretical curve is for a $9/2 \rightarrow 5/2^+$ transition with $\arctan\delta = 1^0$.

(g) Level at 1386 keV

An energy of 1385.5 ± 0.4 keV was deduced for this level from the 1385.5 keV γ-ray seen in both the (n,n'γ) and (p,γ) experiments. A previous paper has proposed a spin-parity of $3/2^+$ for this level (Bo73). The results of the present study were consistent with this assignment, since the measured angular distribution for this transition was isotropic. Fig. 13a) shows a measured angular distribution fitted for a $3/2^+$ initial state, and fig. 13b) a plot of χ^2/df vs $\arctan\delta$.

(h) Levels Above 1400 keV

Many of the excited states above 1400 keV have only recently been proposed, and the energy level scheme in this region is still in some doubt. Barnard et al. (Ba71), in a study which also made use of the (n,n'γ) reaction and natural Sb targets, suggested the existence of a number of levels above 1400 keV which had not previously been reported. Most of these assignments were made on the basis of γ-ray energy sums, with the uncertainties for γ-ray energies being about 2 keV. Since the present work improved on these γ-ray uncertainties, the evidence for the existence of many of these levels could either be strengthened or challenged. Unfortunately, most of the transitions were rather weak, and therefore angular distribution measurements were not possible.

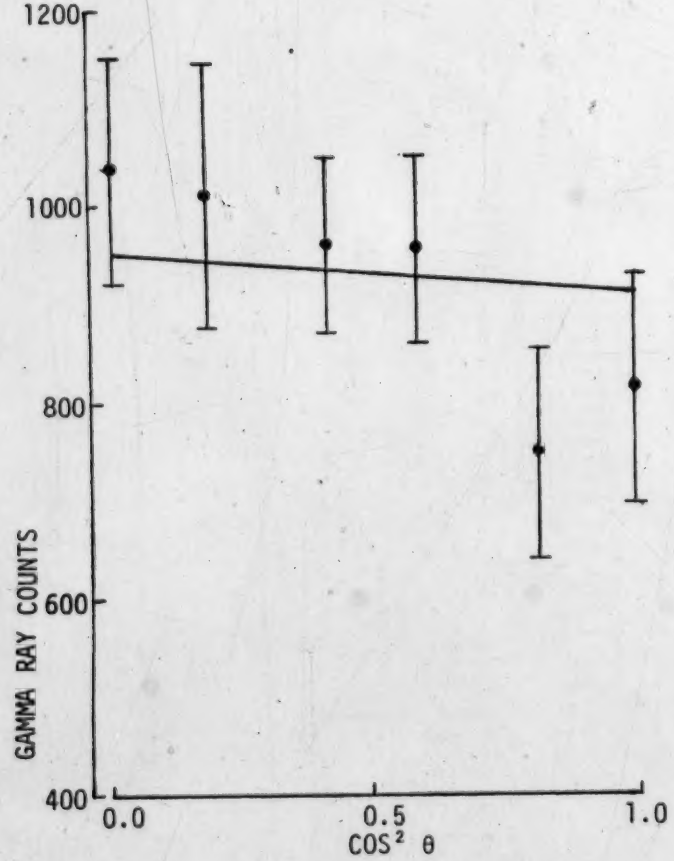

Fig. 13 a) A sample angular distribution for the 1386 → 0 keV transition. The theoretical curve is for a $3/2 \rightarrow 5/2^+$ transition with arctanδ = 68°.

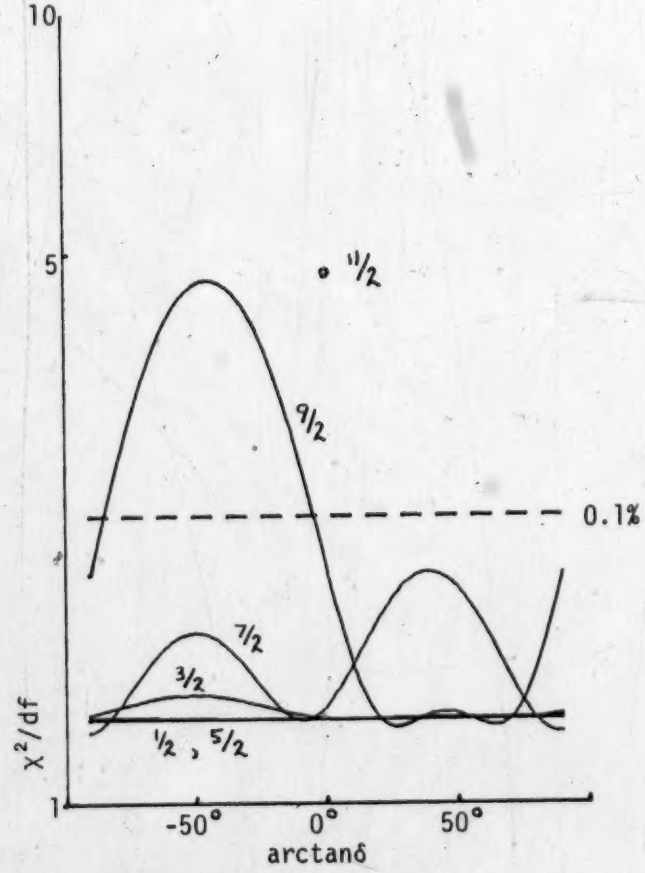

b) χ^2/df curves for the 1386 → 0 keV transition.

The existence of a level with an energy of 1407.3 ± 0.2 keV was confirmed on the basis of the 1406.9 keV γ-ray and the 834.2 keV γ-ray observed in both the (n,n'γ) and (p,γ) experiments.

A level with an energy of 1423 ± 5 keV has been reported in a number of previous experiments (Ho71). Barnard et al. reported a level at 1427 ± 2 kev which decayed via three γ-ray branches with energies of 1427, 392 and 282 keV. These three γ-rays were also observed in a recent coulomb excitation experiment, which made use of both natural Sb targets and isotopically enriched targets (An75). The authors of this study noted that the 1427 keV γ-ray was quite weak compared to the 392 and 282 keV γ-rays. In the present work, however, the energies of these three γ-rays were no longer consistent with their originating from a single level. As well, the threshold for the 1425 keV γ-ray seemed to indicate that this γ-ray originated from a level above 1500 keV. Therefore a level has been proposed with an energy of 1427.4 ± 0.3 keV which decays to the 1035.9 and 1145.0 keV levels via the 391.3 and 282.5 keV γ-rays respectively. The 1425 keV γ-ray will be considered later during the discussion of the levels in ^{123}Sb. It should be noted here that these three γ-rays were not observed in the (p,γ) experiment.

A level with an energy of 1446 ± 5 keV has been observed in previous works (Ho71), but was not specified in

the paper by Barnard et al. Barnard did propose a level at 1410 ± 2 keV which was assumed to decay to the ground state via a 1410 keV γ-ray, and to the excited state at 1036 keV via a 375 keV γ-ray. However, the 375 keV γ-ray appears to originate, as stated earlier, from the 1322 keV level. Therefore, on the basis of energy sums a level with an energy of 1447.5 ± 0.3 keV is proposed. This level is assumed to decay to the first excited state with the emission of a 1410.2 keV γ-ray, and to the second excited state with the emission of a 940.0 keV γ-ray. These two γ-rays were observed in both the $(n,n'\gamma)$ and (p,γ) experiments. It should be noted here that a possible spin-parity assignment of $11/2^-$ proposed for this level (Bo73) is not consistent with the decay of this level to the second excited state, which has a known spin-parity of $3/2^+$.

Levels at 1471.3 ± 0.3 and 1474.5 ± 0.6 keV were observed in accordance with the work of Barnard et al., although the 1474 keV level appeared to be quite weakly populated. These level energies were assigned on the basis of the 898.1 keV decay of the 1471 keV level to the 573 keV level, and the 1437.3 keV decay of the 1474 keV level to the 37 keV level. γ-rays with energies of 1470.8 ± 0.6 keV and 1473.3 ± 1.6 keV which could correspond to ground state decays of these levels were observed in the (p,γ) experiment. However, either one of these γ-rays may have originated from the 1509 keV level, which is discussed

below. These two γ-rays were not seen in the $(n,n'\gamma)$ experiment, while the 1471-->1036 keV transition observed by Barnard was hidden by a large background peak, possibly from ^{23}Na, in both the $(n,n'\gamma)$ and (p,γ) spectra.

In his work, Barnard assigned a level with an energy of 1514 ± 2 keV to ^{121}Sb and a level with an energy of 1511 ± 2 keV to ^{123}Sb. However, since the 1509.0 keV γ-ray was observed in this study in both the $(n,n'\gamma)$ and (p,γ) experiments, but the 1514.6 keV γ-ray was seen only in the $(n,n'\gamma)$ experiment, the 1515 keV level has been assigned to ^{123}Sb while a level with an energy of 1509.0 ± 0.7 keV is proposed for ^{121}Sb. The 1509 keV level may decay to the first excited state in ^{121}Sb through the emission of either the 1470.8 keV or 1473.3 keV γ-ray mentioned above.

Further excited states were observed at energies of 1519.2 ± 0.3 keV and 1627.7 ± 0.6 keV in accordance with the work of Barnard et al. The 1628 keV transition observed by Barnard was obscured by a background peak, possibly from ^{20}Ne, in both the $(n,n'\gamma)$ and (p,γ) spectra.

A γ-ray with an energy of 1575.4 ± 0.7 keV was observed in both the $(n,n'\gamma)$ and (p,γ) experiments. Based on the threshold energy for observing this γ-ray in the $(n,n'\gamma)$ experiment, this γ-ray may originate from either a level with an energy of 1575.4 keV decaying to the ground state, or a level of energy 1612.6 keV decaying to the first excited state. Levels at either of these energies

have not be observed in previous experiments.

Levels at energies of 1736.3 ± 0.5 keV and 1810.9 ± 0.6 keV were assigned on the basis of the 1736.3 and 1810.9 keV γ-rays present in both the $(n,n'\gamma)$ and (p,γ) spectra. Level energies of 1736 ± 1 keV and 1810 ± 1 keV have previously been reported for these levels (Bo73). The 1736 keV level was assigned a definite spin-parity of $1/2^+$ by Nuclear Data Sheets (Ho71), but this assignment has since been disputed (Bo73).

3.3 The Excited States of ^{123}Sb

(a) Levels at 0, 160, 542 and 712 keV

The first four states in ^{123}Sb have been studied extensively in the past (Au72), and have known spin-parities of $7/2^+$, $5/2^+$, $3/2^+$ and $1/2^+$ respectively. The energy of the first excited state, 160.33 ± 0.05 keV, was taken from a recent radioactive decay study (Ra74). The energy of the second excited state was deduced to be 542.1 ± 0.2 keV based on the 542.1 and 381.8 keV transitions, and the energy of the third excited state was determined to be 712.5 ± 0.2 keV based on the 552.2 keV transition.

An experimental angular distribution is shown in fig. 14 for the 542-->0 keV, $3/2^+$-->$7/2^+$ transition. For this transition arctanδ was set equal to zero, as would be expected for an M3/E2 transition.

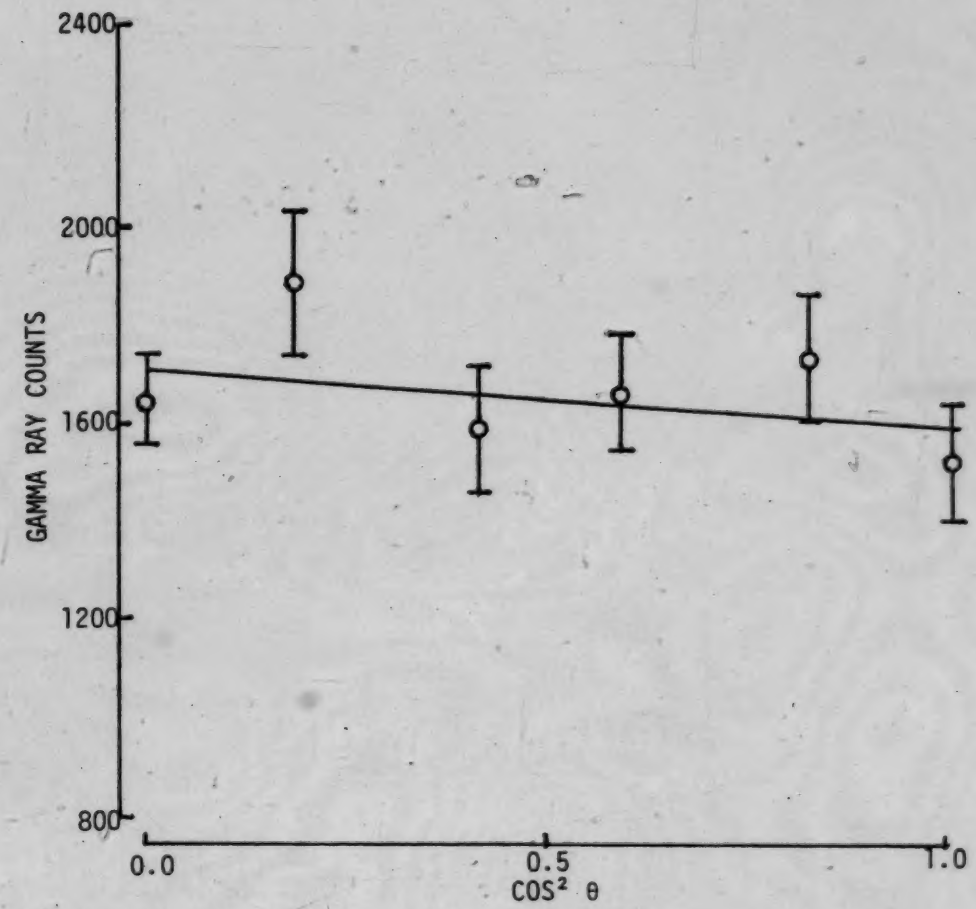

Fig. 14 A sample angular distribution for the 542 → 0 keV transition. The theoretical curve is for a $3/2^+ \rightarrow 7/2^+$ transition with $\arctan\delta = 0^\circ$.

(b) Level at 1030 keV

This level decays to the ground state with the emission of a γ-ray of energy 1030.5 ± 0.3 keV. A spin assignment of 9/2 has been made for this level, with arctanδ ranging from 9° to 72°. Positive parity has previously been assigned to this level (Au72). A graph of angular distribution data and a plot of χ^2/df vs arctanδ for the 1030-->0 keV transition are shown in fig. 15.

(c) Level at 1089 keV

This state decays to the ground state with the emission of a γ-ray of energy 1088.8 ± 0.4 keV. A spin-parity of $11/2^+$ has previously been proposed for this level (Bo73). As can be seen in the plot of χ^2/df vs arctanδ shown in fig. 16, the present work is consistent with this spin assignment, but also permits other spin choices. The value of arctanδ deduced assuming this level has a spin-parity of $11/2^+$ is consistent with zero degrees, which is what would be expected for an $11/2^+ \rightarrow 7/2^+$, M3/E2 transition.

(d) Level at 1182 keV

On the basis of the 1021.3 keV transition to the first excited state, this level was assigned an energy of 1181.6 ± 0.3 keV. Spin-parity assignments of $7/2^+$ or $9/2^+$ have previously been suggested for this level (Bo73). The

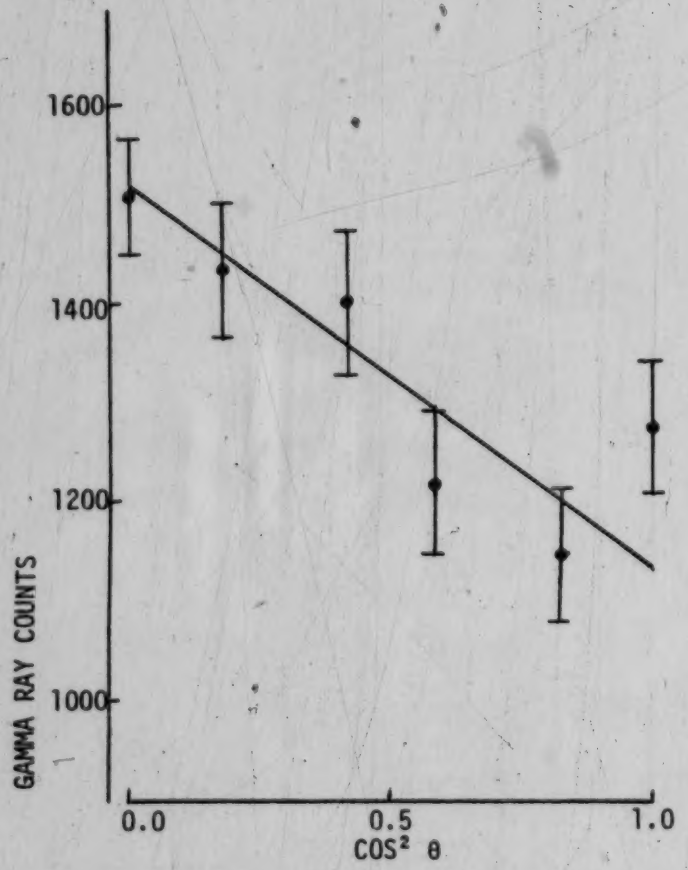

Fig. 15 a) A sample angular distribution for the 1030 → 0 keV transition. The theoretical curve is for a $9/2 \rightarrow 7/2^+$ transition with arctanδ = 33°.

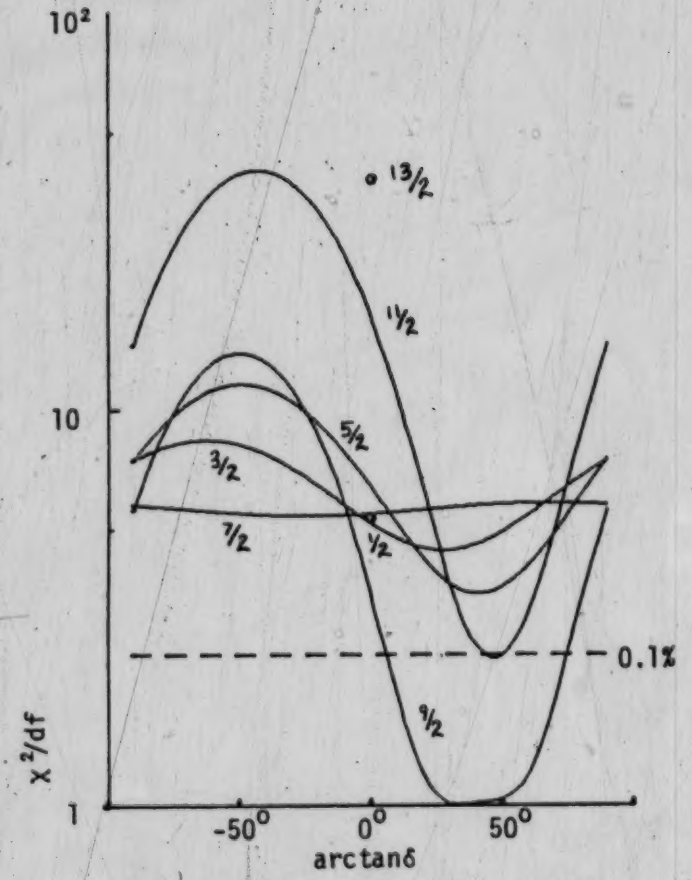

b) χ^2/df curves for the 1030 → 0 keV transition.

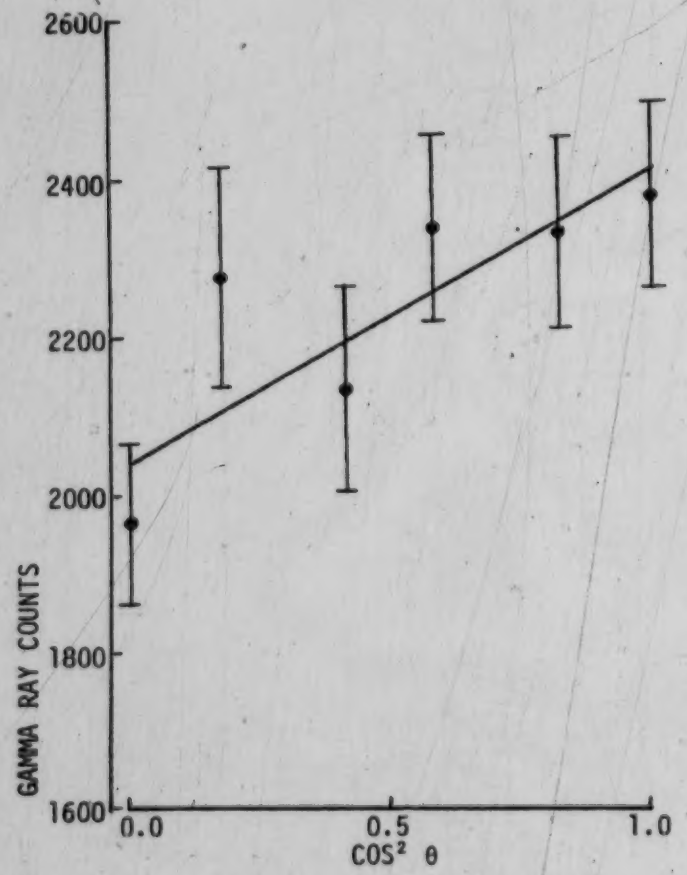

Fig. 16 a) A sample angular distribution for the 1089 → 0 keV transition. The theoretical curve is for a $11/2 \rightarrow 7/2^+$ transition with arctanδ = 3°.

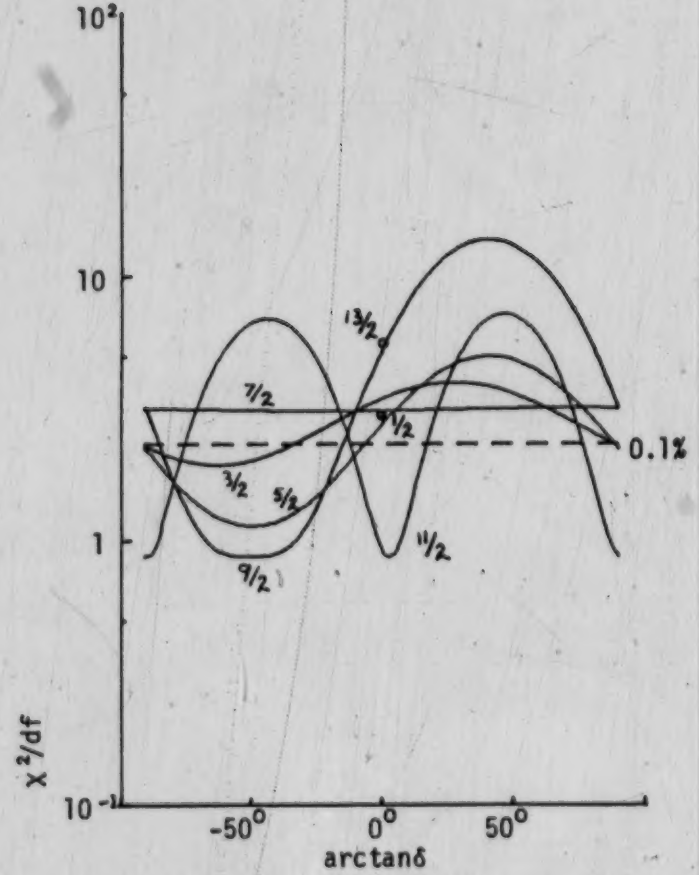

b) χ^2/df curves for the 1089 → 0 keV transition.

plot of χ^2/df vs arctanδ shown in fig. 17 is clearly consistent with these and many other spin assignments.

(e) Level at 1260 keV

This level has been assigned an energy of 1260.5 ± 0.6 keV on the basis of the 1100.2 keV transition to the first excited state. A transition to the ground state reported by Barnard et al. was obscured in this work by a background peak.

Because of the close proximity of the 1100 keV γ-ray to the 1102 keV γ-ray, accurate angular distribution measurements could not be made.

(f) Level at 1337 keV

Based on the 1337.8 keV transition to the ground state and the 1176.5 keV transition to the first excited state, an energy of 1337.3 ± 0.5 keV was deduced for this level. As can be seen from the plot of χ^2/df vs arctanδ for the 1337 keV transition shown in fig. 18, no spin assignment could be made for this level.

(g) Levels Above 1400 keV

A 1514.6 keV γ-ray was observed in the (n,n'γ) experiment but not in the (p,γ) experiment, and hence a level with energy 1514.6 ± 1.2 keV has been proposed for

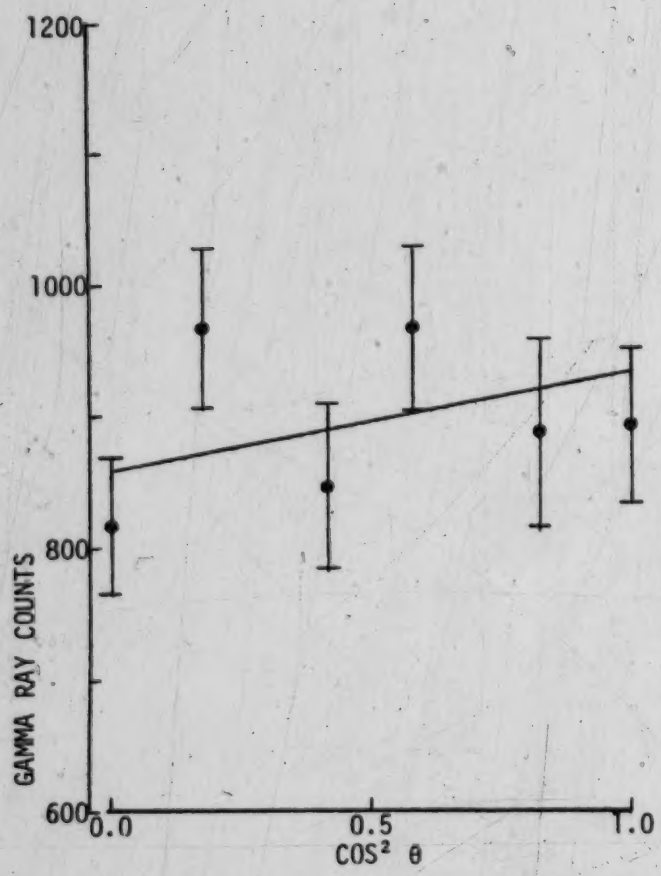

Fig. 17 a) A sample angular distribution for the 1182 → 160 keV transition.

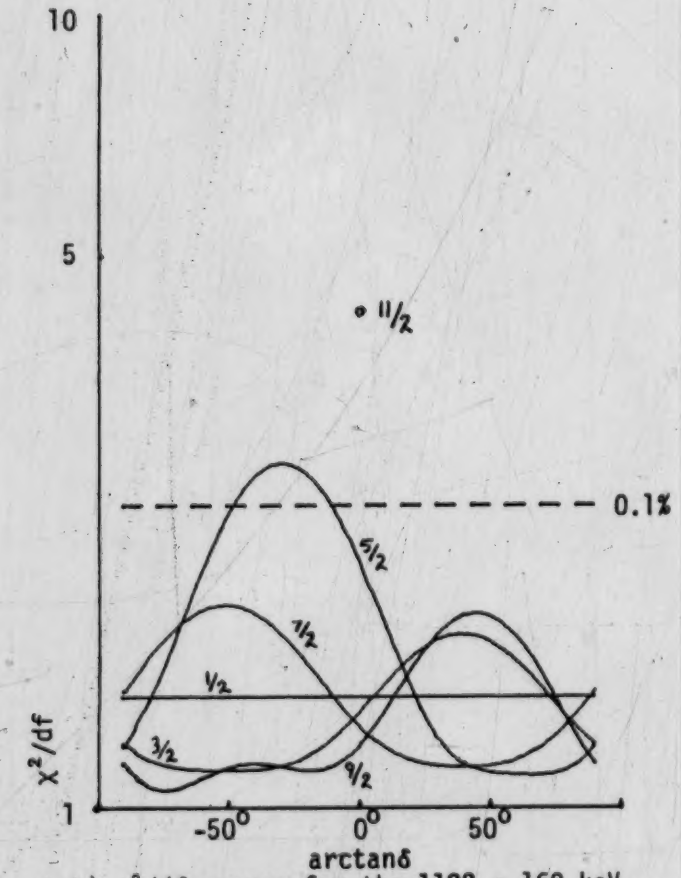

b) χ^2/df curves for the 1182 → 160 keV transition.

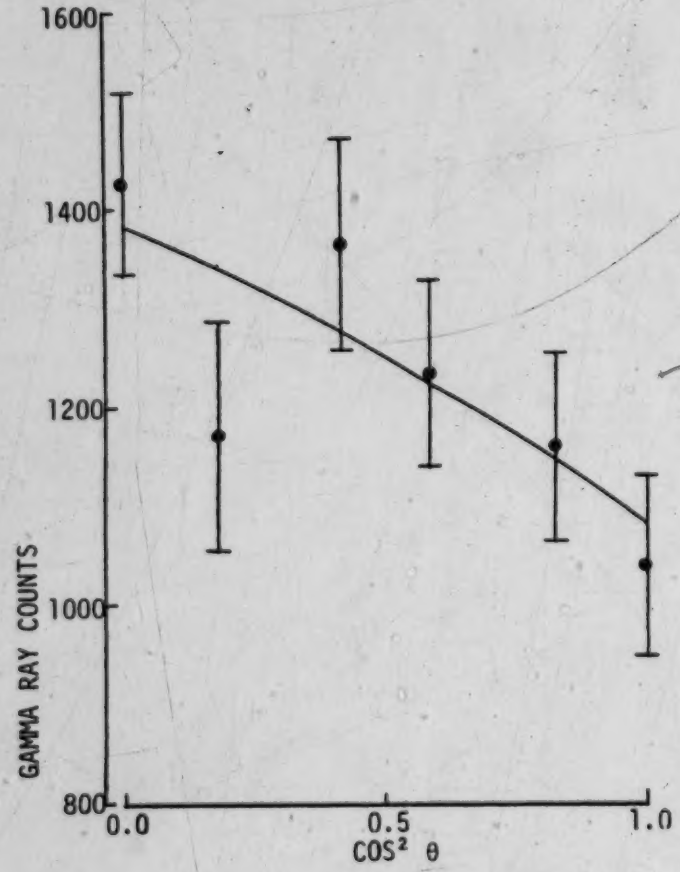

Fig. 18 a) A sample angular distribution for the 1337 → 0 keV transition. The theoretical curve is for a $9/2 \rightarrow 7/2^+$ transition with arctanδ = 57°.

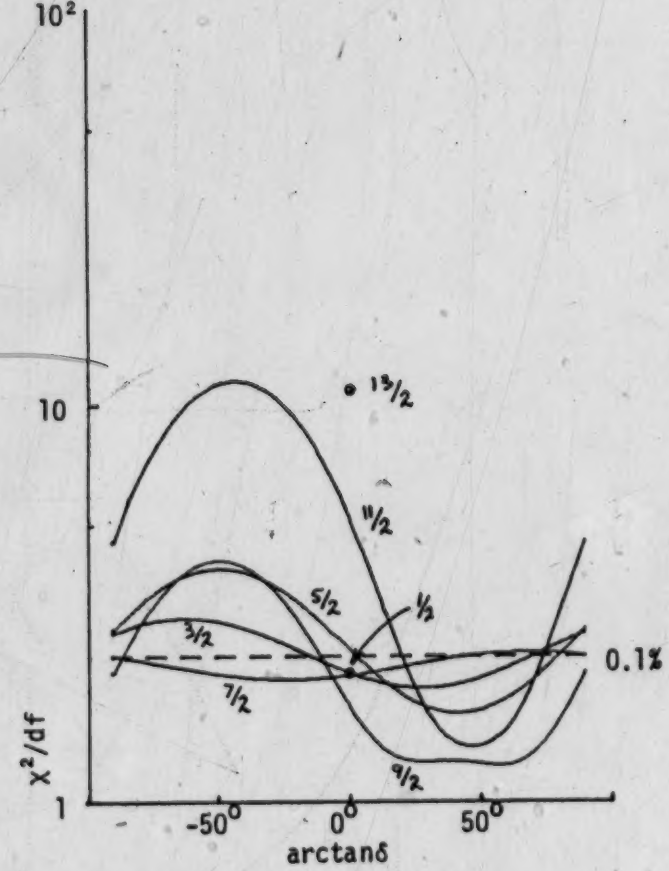

b) χ^2/df curves for the 1337 → 0 keV transition.

^{123}Sb. This level is probably the level observed by Barnes et al. (Ba66) in a (^{3}He,d) experiment with an energy of 1502 ± 10 keV, and in a (d,d') experiment with an energy of 1510 ± 5 keV. A 1350 keV γ-ray observed by Barnard (Ba71), corresponding to a transition from this level to the first excited state, was not observed in the present study due to the presence of a background peak.

A 1577 ± 2 keV level assigned to ^{123}Sb by Barnard was assigned to ^{121}Sb in the present work because the 1575 keV γ-ray through which the level decays was observed in both the (p,γ) and (n,n'γ) experiments. Barnard's assignment of this level to ^{123}Sb was based on an earlier observation of a level at 1574 ± 10 keV in a (^{3}He,d) experiment (Ba66). However, a level at energy 1585.8 ± 0.6 keV has been tentatively proposed in the present work on the basis of a 1425.5 keV γ-ray. This γ-ray has already been mentioned in a discussion of the ^{121}Sb results. From threshold information, the 1425 keV γ-ray appeared to be coming from a level with an energy between 1500 and about 1700 keV. Only a level at energy 1586 keV decaying to the first excited state of ^{123}Sb would be consistent with this threshold requirement, and hence this level has been proposed.

Chapter IV

Background to the Model Calculations

4.1 Introduction

Since the even mass Sn isotopes, with Z = 50, are semi-closed-shell nuclei, the odd mass Sb isotopes, with Z = 51, should be particularly suited to interpretation using nuclear shell theory. There are several models available for carrying out this type of a calculation, but in general these models can be categorized as either microscopic or macroscopic models. The kind of model used in a particular problem will depend on the purpose of the calculation.

Microscopic models attempt to derive the structure of a nucleus in terms of the nucleon-nucleon forces acting between the nucleons within the nucleus. Both the collective, coherent motion for all the nucleons, and the independent particle motions of individual nucleons are determined using a free nucleon-nucleon interaction Hamiltonian. A modified BCS (Bardeen, Cooper, Schrieffer) theory of superconductivity is often used in this type of a calculation (see for example Ba60, Ki63), and calculations of this sort have been carried out for nuclei in the Sn region (Ba71a).

Macroscopic models differ from microscopic models in that they treat the collective and single-particle motions of the nucleons separately. No attempt is made to

understand the collective motion in terms of a fundamental nucleon-nucleon potential, but instead the coherent rotations or vibrations of all the nucleons are described phenomenologically. A popular model of this type, the unified model, couples the independent motion of nucleons in some common potential to the motion of the potential itself. Since the potential is generated by the nucleons themselves, its motion represents the collective, coherent motion of all the nucleons.

From a theoretical point of view, microscopic models are most appealing since "it has always been the aspiration of nuclear theorists to derive the properties of finite nuclei starting for the free nucleon-nucleon interaction" (Ba71a). However, calculations of this sort can become very complicated if realistic interactions are used for the nucleon-nucleon potential. Furthermore, whereas these techniques can be quite useful in predicting qualitatively how nuclear structure will vary as a function of atomic weight over a range of isotopes, they are often not nearly as successful in describing the detailed quantitative structure of a single nucleus. Macroscopic models, on the other hand, are usually more successful in predicting the quantitative structure of individual nuclei, primarily because these models are to a certain extent empirical in form.

In the present study the model calculations were

intended to illuminate the experimental results obtained in this and earlier works. Hence, a unified model approach using the intermediate coupling model was employed, since this model could provide good quantitative results for levels in the nuclei of interest. The calculations were reasonably straightforward, and could readily be compared with such experimental observables as level energies and spectroscopic factors, and γ-ray transition rates. Details of these model calculations are given below, while the results of the calculations are compared with experimental observations in the next chapter.

4.2 The Intermediate Coupling Model

a) General Comments

The intermediate coupling model is a theoretical model used to describe the nuclear structure of nuclei close to closed shells. In its simplest form, this model couples a single nucleon in various single-particle states outside a closed shell to the collective states of the "magic", or closed core. For the Sb isotopes, the 51st proton in a single-particle state outside the Z = 50 closed shell is coupled to the vibrational states of the doubly even Sn core. In this way, the energy, spin, parity and electromagnetic properties of nuclear states can be calculated, and the electromagnetic transition rates for transitions between various states predicted.

A number of papers have been published discussing the odd mass Sb isotopes in terms of the intermediate coupling model (Se70,Va70,Va71,Va73). The present study follows closely the work of Vanden Berghe and Degriech (Va73), but makes use of the notation of Green (Gr73). The details of these calculations are as follows.

1. The vibrational core states are composed of up to three quadrupole phonons, up to two octupole phonons, or up to two quadrupole phonons coupled to one octupole phonon.

2. Both single-particle states, and two-particle-one-hole (2p1h) states can be coupled to the core states. For simplicity it is assumed that, for 2p1h states, the two particles lie in the same orbital and are coupled to spin zero. This assumption will be justified later. The permitted single-particle orbitals for Sb are the 1g7/2, 2d5/2, 2d3/2, 3s1/2 and 1h11/2 states, while the permitted hole orbitals are the 1g9/2, 2p1/2 and 2p3/2 states.

Detailed calculations were made for only the ^{121}Sb and ^{123}Sb nuclei, although some limited calculations were also carried out for all the odd mass Sb isotopes with $115 \leqslant A \leqslant 125$ and all the odd mass In isotopes with $113 \leqslant A \leqslant 123$. These calculations aided in the choice of input parameters for the ^{121}Sb and ^{123}Sb calculations. For the In isotope calculations, the model made use of single-hole and two-hole-one-particle states rather than single-particle and two-particle-one-hole states.

A concise outline of the model formalism is given below.

b) The Formalism

It is useful to begin by introducing a convenient wave function notation. Following the notation of Vanden Berghe and Degriech (Va73), wave functions for single-particle states are written as

$$|j\,(N_1R_1N_2R_2)R\,;I\;M\rangle$$

where N_1 quadrupole phonons couple to spin R_1, N_2 octupole phonons couple to spin R_2, R_1 and R_2 couple to core spin R, and the core spin R couples with the single-particle spin j to total spin I and spin projection M. The single-particle state $|jm\rangle$ is formed by coupling the particle spin 1/2 and orbital spin l to total particle spin j.

Wavefunctions for the 2p1h terms are written as

$$|(j_1)^2 0 j_3(N_1R_1N_2R_2)R\,;I\;M\rangle$$

where the core part is the same as above, but now the two particles in orbital j_1 couple to spin zero, while the core spin R couples with the hole spin j_3 to total spin I and spin projection M. The two particle state is coupled to spin zero because this state is by far the lowest in energy. For two protons in the 2d5/2 or 1g7/2 orbitals coupled via a two-body force, the next two particle state, with a spin-parity of 2^+, would be expected to be at least

one MeV higher in energy than the 0^+ state[1].

These basis wavefunctions can be decomposed into their single-particle or 2p1h terms and core terms as follows:

$$|J\ (N_1R_1N_2R_2)R\ ;I\ M\ > = \sum_{mM_R} (jR;mM_R|IM) \times |jm\rangle\ |(N_1R_1N_2R_2)RM_R\rangle$$

$$|(j_1)^2 0j_3(N_1R_1N_2R_2)R\ ;I\ M\ > = \sum_{m_3M_R} (j_3R;m_3M_R|IM) \times |j_3m_3\rangle\ |(N_1R_1N_2R_2)RM\ > \qquad (4\text{-}1)$$

Eigenstates with an energy $E^{(\alpha)}$ can be expanded in terms of these basis states;

$$|E^{(\alpha)};I\ M\ > = \sum_{\substack{jN_1N_2\\R_1R_2R}} A_\alpha(J\ (N_1R_1N_2R_2)R\ ;I\ M\ ) \times |J\ (N_1R_1N_2R_2)R\ ;I\ M\ > + \sum_{\substack{j_1j_3N_1N_2\\R_1R_2R}} A_\alpha((j_1)^2 0j_3(N_1R_1N_2R_2)R\ ;I\ M\ ) \times |(j_1)^2 0j_3(N_1R_1N_2R_2)R\ ;I\ M\ > \qquad (4\text{-}2)$$

where the A_α are expansion coefficients. The problem at hand is to solve the Schrodinger equation

$$H|E^{(\alpha)};I\ M\ > = E^{(\alpha)}|E^{(\alpha)};I\ M\ >$$

$$\text{or} \quad < E^{(\alpha)};I\ M|H|E^{(\alpha)};I\ M\ > = E^{(\alpha)} \qquad (4\text{-}3)$$

where H is the total Hamiltonian. This is accomplished by calculating the matrix elements in the matrix $\langle IM|H|IM\rangle$ where

$$|IM\rangle = \sum_{\substack{jN_1N_2\\R_1R_2R}} |J\ (N_1R_1N_2R_2)R\ ;I\ M\ > + \sum_{\substack{j_1j_3N_1N_2\\R_1R_2R}} |(j_1)^2 0j_3(N_1R_1N_2R_2)R\ ;I\ M\ > \qquad (4\text{-}4)$$

and then diagonalizing this matrix.

[1]See forinstance deS74, pages 279-290, 369

In the intermediate coupling model, the total Hamiltonian for a nucleus can be expanded as

$$H = H_c + H_{sp} + H_{int} \qquad (4\text{-}5)$$

where H_c is the core Hamiltonian, H_{sp} is the single-particle or 2p1h Hamiltonian, and H_{int} represents the interaction between the single-particle or 2p1h state and the core. The Hamiltonian is designed so that H_c only operates on the core part of the basis wavefunctions, while H_{sp} operates only on the single-particle or 2p1h portions of these states.

Following the notation of Green, if the nuclear surface vibrations are expanded as

$$R(\theta,\phi) = R_0\left[1 + \sum_{\lambda=2}^{3}\sum_{\mu=-\lambda}^{\lambda} \alpha^*_{\lambda\mu} Y_{\lambda\mu}(\theta,\phi)\right] \qquad (4\text{-}6)$$

then

$$H_c = \tfrac{1}{2}\sum_{\lambda\mu}\left(B_\lambda|\dot{\alpha}_{\lambda\mu}|^2 + C_\lambda|\alpha_{\lambda\mu}|^2\right) \qquad (4\text{-}7)$$

where B_λ is the inertial parameter and C_λ the surface stiffness. The frequency of the vibrations is

$$\omega_\lambda = \left(\frac{C_\lambda}{B_\lambda}\right)^{1/2} . \qquad (4\text{-}8)$$

It is convenient to introduce the vibrator creation and annihilation operators $b^+_{\lambda\mu}$ and $b_{\lambda\mu}$, defined by the equations

$$b_{\lambda\mu} = \frac{B_\lambda}{(2B_\lambda\hbar\omega_\lambda)^{1/2}}\left[\omega_\lambda \alpha^+_{\lambda\mu} + i\dot{\alpha}^+_{\lambda\mu}\right]$$

$$b^{+}_{\lambda\mu} = \frac{B_\lambda}{(2B_\lambda\hbar\omega_\lambda)^{1/2}} \left[\omega_\lambda \alpha_{\lambda\mu} - i\dot{\alpha}_{\lambda\mu}\right] \qquad (4\text{-}9)$$

The collective Hamiltonian can then be rewritten as

$$H_c = \sum_{\lambda\mu} (b^{+}_{\lambda\mu} b_{\lambda\mu} + 1/2). \qquad (4\text{-}10)$$

Thus

$$H_c |(N_1 R_1 N_2 R_2) R M_R\rangle$$
$$= [\hbar\omega_2(N_1+5/2) + \hbar\omega_3(N_2+7/2)] |(N_1 R_1 N_2 R_2) R M\rangle \qquad (4\text{-}11)$$

The single-particle Hamiltonian H_{sp} is defined so that

$$H_{sp}|jm\rangle = \epsilon_j |jm\rangle \qquad (4\text{-}12)$$

where ϵ_j is the single-particle energy corresponding to particle orbit j. For 2p1h states,

$$H_{sp}|(j_1)^2 0 j_3 m_3\rangle = (\epsilon_{j_3} + 2\epsilon_{j_1} - E_{res})|(j_1)^2 0 j_3 m_3\rangle \qquad (4\text{-}13)$$

where ϵ_{j_3} is the hole orbit energy, ϵ_{j_1} is the particle orbit energy, and E_{res} is the residual interaction energy. E_{res} is the energy gained when the two protons in orbital j_1 couple to spin zero. E_{res} is often taken to have the form

$$E_{res} = (2j_1+1)G_{pair} \qquad (4\text{-}14)$$

where $G_{pair} = 27/A$ MeV for protons[1].

The matrix elements containing H_c and H_{sp} are therefore:

[1]See deS74, page 643

$$\langle J'(N_1'R_1'N_2'R_2')R';IM|H_c+H_{sp}|J(N_1R_1N_2R_2)R;IM\rangle$$
$$= [\hbar\omega_2(N_1+5/2) + \hbar\omega_3(N_2+7/2) + \epsilon_j]\ \delta_{N_1N_1'}\delta_{N_2N_2'}\delta_{R_1R_1'} \quad (4\text{-}15)$$
$$\times \delta_{R_2R_2'}\delta_{RR'}\delta_{jj'}$$

$$\langle (J_1')^2 0 J_3'(N_1'R_1'N_2'R_2')R';IM|H_c+H_{sp}|(J_1)^2 0 J_3(N_1R_1N_2R_2)R;IM\rangle$$
$$= [\hbar\omega_2(N_1+5/2) + \hbar\omega_3(N_2+7/2) + \epsilon_{j_3} + 2\epsilon_{j_1} - E_{res}]$$
$$\times \delta_{N_1N_1'}\delta_{N_2N_2'}\delta_{R_1R_1'}\delta_{R_2R_2'}\delta_{RR'}\delta_{j_1j_1'}\delta_{j_3j_3'} \quad (4\text{-}16)$$

and

$$\langle J'(N_1'R_1'N_2'R_2')R';IM|H_c+H_{sp}|(J_1)^2 0 J_3(N_1R_1N_2R_2)R;IM\rangle = 0 . \quad (4\text{-}17)$$

The interaction Hamiltonian, H_{int}, can be deduced by performing a Taylor expansion of a single-particle potential $V(r,R)$, where R has been defined in equation 4-6, about a spherical potential $V(r,R_0)$:

$$V(r,R) = V(r,R_0) + (R-R_0)\left.\frac{\partial V}{\partial R}\right|_{R_0} + \cdots \quad (4\text{-}18)$$

The second and higher order terms in this equation represent H_{int}. H_{int} can thus be expressed to first order in $\alpha_{\lambda\mu}$ as

$$H_{int} = -k(r)\sum_{\lambda\mu}\alpha^*_{\lambda\mu}Y_{\lambda\mu}(\theta,\phi) \quad (4\text{-}19)$$

where r, θ and ϕ are the particle coordinates, and

$$k(r) \equiv -R_0\left.\frac{\partial V}{\partial R}\right|_{R_0} . \quad (4\text{-}20)$$

A first order expansion should be sufficient since the amplitudes of the vibrations are expected to be small compared to the radius of the nucleus, and hence $\alpha_{\lambda\mu} \ll 1$. The radial dependence, k(r), will depend both on the shape of the potential $V(r,R)$ and on the quantum numbers of the

single-particle states. It has been shown, however, that $k \equiv \langle n'\ell' | k(r) | n\ell \rangle$ is reasonably insensitive to the values of n, ℓ, n' and ℓ', and can be considered to be a constant (Br60).

H_{int} can be rewritten in terms of the phonon creation and annihilation operators (equation 9) as

$$H_{int} = -\sum_{\lambda} \frac{\pi}{\hat{\lambda}}^{1/2} \hbar\omega_\lambda \xi_\lambda \times \sum_{\mu} (-)^{\mu} \left[b^{+}_{\lambda,-\mu} + (-)^{\mu} b_{\lambda\mu} \right] Y_{\lambda\mu}(\theta,\phi) \qquad (4\text{-}21)$$

where $\hat{\lambda} \equiv (2\lambda+1)^{1/2}$, and the dimensionless coupling parameter ξ_λ has been introduced. ξ_λ is defined as

$$\xi_\lambda \equiv \left(\frac{2\lambda+1}{2\pi\hbar\omega_\lambda C_\lambda} \right)^{1/2} K \qquad (4\text{-}22)$$

Using this expression the matrix elements of H_{int} can be calculated. After a considerable amount of Racah algebra, it can be shown that

$$\langle J'(N_1'R_1'N_2'R_2')R'; IM | H_{int} | J(N_1R_1N_2R_2)R; IM \rangle = -\sum_{\lambda} \frac{\pi}{\hat{\lambda}}^{1/2} \hbar\omega_\lambda \xi_\lambda (-)^{R'+j-I} \langle J' \| Y_\lambda \| J \rangle \times Q_\lambda(N_1'R_1'N_2'R_2'R'N_1R_1N_2R_2R)\, W(R'J'RJ;I\lambda), \qquad (4\text{-}23)$$

$$\langle (J_1')^2 0 J_3'(N_1'R_1'N_2'R_2')R'; IM | H_{int} | (J_1)^2 0 J_3(N_1R_1N_2R_2)R; IM \rangle = -\sum_{\lambda} (-)^{\lambda+1} \frac{\pi}{\hat{\lambda}}^{1/2} \hbar\omega_\lambda \xi_\lambda (-)^{R'+j_3-I} \langle J_3' \| Y_\lambda \| J_3 \rangle \times Q_\lambda(N_1'R_1'N_2'R_2'R'N_1R_1N_2R_2R)\, W(R'J_3'RJ_3;I\lambda), \qquad (4\text{-}24)$$

and

$$\langle J'(N_1'R_1'N_2'R_2')R';IM|H_{int}|(J_1)^2OJ_3(N_1R_1N_2R_2)R;IM\rangle$$
$$= \frac{(2)^{1/2}}{\hat{J}'}\sum_\lambda(-)^\lambda\prod^{1/2}\hbar\omega_\lambda\,\xi_\lambda\,(-)^{R'+j_1-I}\quad\langle J'\|Y_\lambda\|J_3\rangle$$
$$\times Q_\lambda(N_1'R_1'N_2'R_2'R'N_1R_1N_2R_2R)\;W(R'J'RJ_3;I\lambda)$$

(4-25)

or

$$\langle(J_1')^2OJ_3'(N_1'R_1'N_2'R_2')R';IM|H_{int}|J\,(N_1R_1N_2R_2)R;IM\rangle$$
$$= \frac{(2)^{1/2}}{\hat{J}}\sum_\lambda(-)^\lambda\prod^{1/2}\hbar\omega_\lambda\,\xi_\lambda\,(-)^{R'+j-I}\quad\langle J_3'\|Y_\lambda\|J\rangle$$
$$\times Q_\lambda(N_1'R_1'N_2'R_2'R'N_1R_1N_2R_2R)\;W(R'J_3'RJ;I\lambda),$$

(4-26)

where W(abcd;ef) is a Racah coefficient, and

$$Q_2(N_1'R_1'N_2'R_2'R'N_1R_1N_2R_2R)$$
$$= \hat{R}\hat{R}'\,\delta_{N_1N_1'}\,\delta_{R_1R_1'}\;W(R2R_2R_1';R'R_1)$$
$$[\langle N_1'R_1'\|b_2^+\|N_1R_1\rangle + (-)^{R_1-R_1'}\langle N_1R_1\|b_2^+\|N_1'R_1'\rangle]$$

(4-27)

$$Q_3(N_1R_1N_2R_2R\;N_1R_1N_2R_2R)$$
$$= \hat{R}\hat{R}'\,\delta_{N_1N_1'}\,\delta_{R_1R_1'}\;(-)^{R-R'}\;W(R3R_1R_2';R'R_2)$$
$$[(-)^{R_2-R_2'}\langle N_2'R_2'\|b_3^+\|N_2R_2\rangle + \langle N_2R_2\|b_3^+\|N_2'R_2'\rangle].$$

(4-28)

A detailed derivation of the reduced matrix elements $\langle N'R'\|b_\lambda^+\|NR\rangle$ for the phonon creation operators is given by Green (Gr73). A list of values of $\langle N'R'\|b_\lambda^+\|NR\rangle$ for all cases of interest in this study is given in table 6.

Equations 4-23 through 4-26 above deal with the case of single-particle or two-particle-one-hole terms coupled to a vibrating core, as is the case for the odd mass Sb isotopes. In order to deal with single-hole or two-hole-

λ	N'	R'	N	R	$(\langle N'R' \| b^{\dagger}_{\lambda} \| NR \rangle)^2$ [a]
2	1	2	0	0	5
	2	0	1	2	2
	2	2	1	2	10
	2	4	1	2	18
	3	2	2	0	7
	3	0	2	2	3
	3	2	2	2	20/7
	3	3	2	2	15
	3	4	2	2	99/7
	3	2	2	4	36/7
	3	3	2	4	*6 [b]
	3	4	2	4	90/7
	3	6	2	4	39
3	1	3	0	0	7
	2	0	1	3	2
	2	2	1	3	10
	2	4	1	3	18
	2	6	1	3	26

[a] $(\langle N'R' \| b^{\dagger}_{\lambda} \| NR \rangle)^2$ is non-zero only if $N'=N+1$.

[b] The presence of an asterisk preceding a number indicates that the reduced matrix element is given by the negative square root of that number.

Table 6 Reduced matrix elements for the boson creation operators.

one-particle terms which would be encountered in such nuclei as the odd mass In isotopes, these equations must be modified slightly. Equations 4-23 and 4-24 must in these cases be multiplied by a further phase factor of $(-)^{\lambda+1}$, while equations 4-25 and 4-26 would be multiplied by a further phase of $(-)^{\lambda}$.

The reduced matrix element for the spherical harmonics can be shown to be[1]

$$\langle J' \| Y_\lambda \| J \rangle = \tfrac{1}{2}[1+(-)^{\ell+\ell'+\lambda}] \frac{\hat{J}\hat{\lambda}}{(4\pi)^{1/2}} (-)^{J-J'+\lambda} (J\lambda;-\tfrac{1}{2}0|J'-\tfrac{1}{2}) \quad (4\text{-}29)$$

Using these equations, therfore, it is possible to calculate all the matrix elements in the matrix $\langle IM|H|IM\rangle$, where $|IM\rangle$ is defined in equation 4-4 above. By diagonalizing this matrix, the energy eigenvalues $E^{(\alpha)}$ and eigenstates $|E^{(\alpha)};I\ M\rangle$ can be calculated.

4.3 Electromagnetic Properties

Once the energy eigenstates $|E^{(\alpha)};IM\rangle$ are known, it becomes possible to calculate certain electromagnetic properties of the nucleus being studied. In particular, magnetic dipole and electric quadrupole moments, γ-ray branching ratios, and multipole mixing ratios can be calculated.

In order to deduce these quantities it is necessary to

[1]See for example the appendix of deS63

solve matrix elements of the form

$$\langle E^{(\beta)};I'M' \mid \mathcal{H}(M1,\mu) \mid E^{(\alpha)};I\ M\rangle$$

and $\langle E^{(\beta)};I'M' \mid \mathcal{H}(E2,\mu) \mid E^{(\alpha)};I\ M\rangle$

where $\mathcal{H}(M1,\mu)$ is the magnetic dipole operator, and $\mathcal{H}(E2,\mu)$ is the electric quadrupole operator. These matrix elements will have solutions of the form

$$\begin{aligned}
&\langle E^{(\beta)};I'M' \mid \mathcal{H}(A) \mid E^{(\alpha)};I\ M\rangle \\
&= \sum A_\beta(J'(N_1'R_1'N_2'R_2')R';I'M')A_\alpha(J\,(N_1R_1N_2R_2)R;I\ M) \\
&\quad \langle J'(N_1'R_1'N_2'R_2')R';I'M' \mid \mathcal{H}(A) \mid J\,(N_1R_1N_2R_2)R;I\ M\rangle \\
&+ \sum A_\beta(J'(N_1'R_1'N_2'R_2')R';I'M')A_\alpha((J_1)^20J_3(N_1R_1N_2R_2)R;I\ M) \\
&\quad \langle J'(N_1'R_1'N_2'R_2')R';I'M' \mid \mathcal{H}(A) \mid (J_1)^20J_3(N_1R_1N_2R_2)R;I\ M\rangle \\
&+ \sum A_\beta((J_1')^20J_3'(N_1'R_1'N_2'R_2')R';I'M')A_\alpha(J\,(N_1R_1N_2R_2)R;I\ M) \\
&\quad \langle (J_1')^20J_3'(N_1'R_1'N_2'R_2')R';I'M' \mid \mathcal{H}(A) \mid J\,(N_1R_1N_2R_2)R;I\ M\rangle \\
&+ \sum A_\beta((J_1')^20J_3'(N_1'R_1'N_2'R_2')R';I'M') \\
&\qquad \times A_\alpha((J_1)^20J_3(N_1R_1N_2R_2)R;I\ M) \qquad (4\text{-}30) \\
&\quad \langle (J_1')^20J_3'(N_1'R_1'N_2'R_2')R';I'M' \mid \mathcal{H}(A) \mid (J_1)^20J_3(N_1R_1N_2R_2)R;I\ M\rangle
\end{aligned}$$

where the summations are over all primed and unprimed variables except I, I', M and M', and $\mathcal{H}(A)$ represents either $\mathcal{H}(M1,\mu)$ or $\mathcal{H}(E2,\mu)$.

Expressions for the magnetic dipole and electric quadrupole operators are deduced in appendix A. The magnetic dipole operator is defined as

$$\mathcal{H}(M1,\mu) = \left(\frac{3}{4\pi}\right)^{1/2}(g_L l_\mu + g_S S_\mu + g_R R_\mu)\beta \qquad (4\text{-}31)$$

where β denotes the nuclear magneton

$$\beta \equiv \frac{ek}{2m_q c} \qquad (4\text{-}32)$$

and g_l, g_s and g_R are the g factors for the orbital, spin and core angular momenta respectively.

Since $\mathcal{H}(M1,\mu)$ is a component of an irreducible tensor operator, the reduced matrix elements $\langle I'\|\mathcal{H}(M1)\|I\rangle$ can be deduced rather than the matrix elements $\langle I'M'|\mathcal{H}(M1,\mu)|I\ M\rangle$. These reduced matrix elements are defined by the equation

$$\langle I'M'|\mathcal{H}(M1,\mu)|I\ M\rangle = (\hat{I}')^{-1}\,(I1;M\mu|I'M')\,\langle I'\|\mathcal{H}(M1)\|I\rangle. \qquad (4\text{-}33)$$

Using Racah algebra and the single-particle and 2p1h wavefunctions defined earlier, it can be shown that

$$\begin{aligned}
&\langle J'(N_1'R_1'N_2'R_2')R';I'\|\mathcal{H}(M1)\|J\,(N_1R_1N_2R_2)R\;;I\rangle \\
&= (3/4\pi)^{1/2}\hat{I}\hat{I}'\,\delta_{N_1N_1'}\delta_{R_1R_1'}\delta_{N_2N_2'}\delta_{R_2R_2'}\delta_{ll'} \\
&\times\Big\{\delta_{jj'}\,g_R\hat{R}\hat{R}'\,(-)^{I-I'+R-R'}W(1RI'J;R'I) \\
&\times[\hat{R}_1[R_1(R_1+1)]^{1/2}W(1RR_1R_2;R'R_1) \\
&\quad +\hat{R}_2[R_2(R_2+1)]^{1/2}W(1RR_2R_1;R'R_2)] \\
&+\delta_{ll'}\hat{J}\hat{J}'\,W(1JI'R;J'I) \\
&\times[g_l\hat{l}[l(l+1)]^{1/2}W(1lJ'1/2;lJ) \\
&\quad +(-)^{j-j'}\,g_s\sqrt{3/2}\,W(1\,1/2\,J'l;1/2\,J)]\Big\}, \qquad (4\text{-}34)
\end{aligned}$$

$$\begin{aligned}
&\langle(J_1')^2OJ_3'(N_1'R_1'N_2'R_2')R';I'\|\mathcal{H}(M1)\|(J_1)^2OJ_3(N_1R_1N_2R_2)R\;;I\rangle \\
&= (3/4\pi)^{1/2}\hat{I}\hat{I}'\,\delta_{N_1N_1'}\delta_{R_1R_1'}\delta_{N_2N_2'}\delta_{R_2R_2'}\delta_{l_1l_1'}\delta_{j_1j_1'} \\
&\times\Big\{\delta_{j_2j_2'}\,g_R\hat{R}\hat{R}'\,(-)^{I-I'+R-R'}W(1RI'J_3;R'I) \\
&\times[\hat{R}_1[R_1(R_1+1)]^{1/2}W(1RR_1R_2;R'R_1)
\end{aligned}$$

$$+\hat{R}_2[R_2(R_2+1)]^{1/2}\,W(1RR_2R_1;R'R_2)]$$

$$+\delta_{RR'}\,\mathfrak{J}_3\mathfrak{J}_3'\,W(1J_3I'R;J_3'I)$$

$$\times\left[g_L\hat{\ell}_3[\ell_3(\ell_3+1)]^{1/2}W(1\ell_3J'1/2;\ell_3J_3)\right.$$

$$\left.+(-)^{J_3-J_3'}\,g_S\sqrt{3/2}\;\;W(1\,1/2\;J_3'\ell_3;1/2\,J_3)\right]\Big\}, \qquad (4\text{-}35)$$

and

$$\langle J'(N_1'R_1'N_2'R_2')R';I'\|\mathfrak{M}(M1)\|(J_1)^2OJ_3(N_1R_1N_2R_2)R;I\rangle$$

$$=\frac{(2)^{1/2}}{\hat{J}'}\delta_{J_1J_1'}(3/4\pi)^{1/2}\hat{T}\hat{T}'\,\delta_{N_1N_1'}\delta_{R_1R_1'}\delta_{N_2N_2'}\delta_{R_2R_2'}\delta_{RR'}\delta_{\ell_3\ell'}$$

$$\times\mathfrak{J}_3\mathfrak{J}'\,W(1J_3I'R;J'I)$$

$$\times\left[g_L\hat{\ell}_3[\ell_3(\ell_3+1)]^{1/2}W(1\ell_3J'1/2;\ell_3J_3)\right.$$

$$\left.+g_S(-)^{J_3-J'}\sqrt{3/2}\;\;W(1\,1/2\;J'\ell_3;1/2\,J_3)\right] \qquad (4\text{-}36)$$

or

$$\langle(J_1')^2OJ_3'(N_1'R_1'N_2'R_2')R';I'\|\mathfrak{M}(M1)\|J(N_1R_1N_2R_2)R;I\rangle$$

$$=\frac{(2)^{1/2}}{\hat{J}'}\delta_{JJ'}(3/4\pi)^{1/2}\hat{T}\hat{T}'\,\delta_{N_1N_1'}\delta_{R_1R_1'}\delta_{N_2N_2'}\delta_{R_2R_2'}\delta_{RR'}\delta_{\ell\ell'}$$

$$\times\mathfrak{J}\mathfrak{J}_3'\,W(1JI'R;J_3'I)$$

$$\left[g_L\hat{\ell}[\ell(\ell+1)]^{1/2}W(1\ell J_3'1/2;\ell J)\right.$$

$$\left.+g_S(-)^{J-J_3'}\sqrt{3/2}\;\;W(1\,1/2\;J_3'\ell;1/2\,J)\right] \qquad (4\text{-}37)$$

The electric quadrupole operator for a nucleus with one extra-core proton is given in appendix A as

$$\mathfrak{M}(E2,\mu)=\frac{3}{4\pi}e(Z-1)R_o^2\sqrt{\frac{\hbar\omega_2}{2C_2}}\;(b_{2\mu}^{+}+(-)^{\mu}b_{2-\mu})$$

$$+er^2Y_{2\mu} \qquad (4\text{-}38)$$

where R_o is the mean radius of the nucleus and C_2 is the surface stiffness for quadrupole vibrations. Since the vibrations are assumed to be small, and the equilibrium shape of the nucleus is spherical, the expectation value of r^2 can be approximated as $3/5R_o^2$.

Since the $\mathfrak{M}(E2)$ operator is obviously an irreducible

tensor operator, the reduced matrix elements $\langle I' \| \mathfrak{M}(E2) \| I \rangle$ defined by

$$\langle I' M' | \mathfrak{M}(E2,\mu) | I\ M \rangle = (\hat{I}')^{-1}\ (I2; M\mu | I' M')\ \langle I' \| \mathfrak{M}(E2) \| I \rangle \tag{4-39}$$

can again be used.

Defining two constants $\mathfrak{M}_1$ and $\mathfrak{M}_2$ as

$$\mathfrak{M}_1 \equiv \frac{3}{5}\, e\, R_0^2 \tag{4-40}$$

and

$$\mathfrak{M}_2 \equiv \frac{3}{4\pi}\ (Z-1)\, e\, R_0^2 \sqrt{\frac{\kappa \omega_2}{2C_2}} \tag{4-41}$$

it can be shown that

$$\begin{aligned}
&\langle J'(N_1' R_1' N_2' R_2') R' ; I' \| \mathfrak{M}(E2) \| J\ (N_1 R_1 N_2 R_2) R\ ; I \rangle \\
&\quad = \hat{I}\hat{I}' \Big\{ [\mathfrak{M}_2\ \delta_{JJ'} (-)^{I-I'+R-R'} \\
&\qquad \times W(2RI'J; R'I)\ Q_2(N_1' R_1' N_2' R_2' R' N_1 R_1 N_2 R_2 R)] \\
&\qquad + [\mathfrak{M}_1\ \delta_{N,N_1'}\ \delta_{R,R_1'}\ \delta_{N_2 N_2'}\ \delta_{R_2 R_2'}\ \delta_{RR'} \\
&\qquad \times W(2JI'R; J'I)\ \langle J' \| Y_2 \| J \rangle] \Big\} \ , \qquad (4-42)
\end{aligned}$$

$$\begin{aligned}
&\langle (J_1')^2 0 J_3' (N_1' R_1' N_2' R_2') R' ; I' \| \mathfrak{M}(E2) \| (J_1)^2 0 J_3 (N_1 R_1 N_2 R_2) R\ ; I \rangle \\
&\quad = \hat{I}\hat{I}' \Big\{ [\mathfrak{M}_2\ \delta_{J_3,J_3'} (-)^{I-I'+R-R'} \\
&\qquad \times W(2RI'J_3; R'I)\ Q_2(N_1' R_1' N_2' R_2' R' N_1 R_1 N_2 R_2 R)] \\
&\qquad - [\mathfrak{M}_1\ \delta_{N,N_1'}\ \delta_{R,R_1'}\ \delta_{N_2 N_2'}\ \delta_{R_2 R_2'}\ \delta_{RR'} \\
&\qquad \times W(2J_3 I'R; J_3 I)\ \langle J_3' \| Y_2 \| J_3 \rangle] \Big\}\ \delta_{J_1,J_1'}, \qquad (4-43)
\end{aligned}$$

and

$$\langle J'(N_1'R_1'N_2'R_2')R';I'\|\mathcal{M}(E2)\|(J_1)^2 0 J_3(N_1R_1N_2R_2)R;I\rangle$$
$$= -\frac{(2)^{1/2}}{J}\,\eta_1\,\Pi\Pi'\,\delta_{N_1N_1'}\delta_{R_1R_1'}\delta_{N_2N_2'}\delta_{R_2R_2'}\delta_{RR'}\delta_{JJ'}\delta_{J_1J_1'}$$
$$\times W(2J_3I'R;J'I)\,\langle J'\|Y_2\|J_3\rangle \qquad (4\text{-}44)$$

or

$$\langle (J_1')^2 0 J_3'(N_1'R_1'N_2'R_2')R';I'\|\mathcal{M}(E2)\|J(N_1R_1N_2R_2)R;I\rangle$$
$$= -\frac{(2)^{1/2}}{J}\,\eta_1\,\Pi\Pi'\,\delta_{N_1N_1'}\delta_{R_1R_1'}\delta_{N_2N_2'}\delta_{R_2R_2'}\delta_{RR'}\delta_{JJ_1'}$$
$$\times W(2JI'R;J_3'I)\,\langle J_3'\|Y_2\|J\rangle. \qquad (4\text{-}45)$$

As shown in appendix A, the magnetic dipole moment $\mu^{(\alpha)}$ and electric quadrupole moment $Q^{(\alpha)}$ for an eigenstate $|E^{(\alpha)};I\rangle$ can be expressed as follows:

$$\mu^{(\alpha)} = \sqrt{\frac{I}{(I+1)(2I+1)}}\,\sqrt{\frac{4\pi}{3}}\,\langle E^{(\alpha)};I\|\mathcal{M}(M1)\|E^{(\alpha)};I\rangle. \qquad (4\text{-}46)$$

and

$$Q^{(\alpha)} = \sqrt{\frac{I(2I-1)}{(2I+3)(2I+1)(I+1)}}\,\sqrt{\frac{16\pi}{5}}\,\langle E^{(\alpha)};I\|\mathcal{M}(E2)\|E^{(\alpha)};I\rangle \qquad (4\text{-}47)$$

In order to calculate the branching ratio for a particular γ-ray decay, it is necessary to calculate the transition probability for that transition and all competing transitions. The transition probability for a decay from level $|E^{(\alpha)};I\ M\rangle$ to level $|E^{(\beta)};I'M'\rangle$ via M1 and/or E2 radiation is given as (see appendix A)

$$W(E^{(\alpha)}\rightarrow E^{(\beta)}) = \frac{16\pi c}{9}\frac{e^2}{(\hbar c)^4}\,E_\gamma^{\,3}$$
$$\times\left[B(M1) + \frac{3}{100}\left(\frac{E_\gamma}{\hbar c}\right)^2 B(E2)\right] \qquad (4\text{-}48)$$

where

$$B(M1) = \frac{1}{(2I+1)e^2} |\langle E^{(\beta)}; I' \| \mathfrak{M}(M1) \| E^{(\alpha)}; I \rangle|^2 \quad (4\text{-}49)$$

and

$$B(E2) = \frac{1}{(2I+1)e^2} |\langle E^{(\beta)}; I' \| \mathfrak{M}(E2) \| E^{(\alpha)}; I \rangle|^2 \quad (4\text{-}50)$$

The mixing ratio for an E2/M1 transition between these two levels is deduced in appendix A to be

$$\delta = -\sqrt{\frac{3}{100}} \frac{E_\gamma}{\hbar c} \frac{\langle E^{(\beta)}; I' \| \mathfrak{M}(E2) \| E^{(\alpha)}; I \rangle}{\langle E^{(\beta)}; I' \| \mathfrak{M}(M1) \| E^{(\alpha)}; I \rangle} \quad (4\text{-}51)$$

where the sign of δ is consistent with the phase convention of Rose and Brink (Ro67).

Chapter V

Discussion of Model Calculations and Experimental Results

5.1 Input Parameters for Model Calculations

In order to carry out the model calculations described in the previous chapter, two computer programs have been written. CUPPLE3 is a program designed to carry out intermediate coupling model calculations and hence to generate energy eigenvectors and eigenvalues. MOMENT is a program designed to calculate the electromagnetic observables described in chapter IV using as input the energy eigenvectors generated by CUPPLE3. The computing details of these two programs are given in appendix B.

a) The CUPPLE3 Calculations

Input parameters to CUPPLE3 include the quadrupole and octupole phonon energies ($\hbar\omega_2$ and $\hbar\omega_3$), the coupling strength parameters (ξ_2 and ξ_3), the particle and hole orbital energies (ϵ_j and $\epsilon_{j'}$), the pairing energy (G_{pair}), and a maximum energy cutoff which excludes from the calculations any basis states whose unperterbed energies are above the cutoff. Certain of these parameters were fixed throughout the calculations. An upper energy cutoff of 5 MeV was used for most of the calculations, since only states below 2 MeV were being considered. In a few instances, for reasons which will be explained later, a higher cutoff was used. G_{pair} was set equal to 27/A MeV,

as explained in chapter IV, and $\hbar\omega_2$ and $\hbar\omega_3$ were assumed to be equal to the energies of the lowest 2^+ and 3^- states respectively in the appropriate even mass Sn nucleus.

ξ_2 and ξ_3 were also predetermined by considering experimental data taken from the even mass Sn nuclei. The reduced matrix element $B(E\lambda)\uparrow$ for exciting a one phonon state in an even mass Sn nucleus can be expressed as[1]

$$B(E\lambda)\uparrow = (2\lambda+1)\frac{\hbar\omega_\lambda}{2C_\lambda}\left(\frac{3}{4\pi}ZeR_o^\lambda\right)^2$$

$$= \pi\left(\frac{\hbar\omega_\lambda\xi_\lambda}{K}\frac{3}{4\pi}ZeR_o^\lambda\right)^2 \qquad (5\text{-}1)$$

where the definition of ξ_λ given in chapter IV, equation 4-22, has been used. Thus

$$\xi_\lambda = \sqrt{\frac{B(E\lambda)\uparrow}{\pi}}\frac{K}{\hbar\omega_\lambda}\left(\frac{3}{4\pi}ZeR_o^\lambda\right)^{-1} \qquad (5\text{-}2)$$

Using a value of k = 40 MeV (Br60) and experimentally measured $B(E\lambda)$ values, it was possible to calculate the ξ_λ values. Values of $\hbar\omega_\lambda$ and ξ_λ determined from the Sn nuclei are listed in table 7. For reasons which will be discussed shortly, the calculated ξ_λ values were in fact varied to a certain extent during the CUPPLE3 calculations.

The particle and hole orbital energies, ϵ_j and $\epsilon_{j'}$, were variable during the CUPPLE3 calculations, and were adjusted to obtain a "best" fit between the model calculations and experimental results. For this comparison, two types of experimental observables were

[1] see for example deS74, page 476

Sn Isotope	Exp. Ref.[a]	λ	$\hbar\omega_\lambda$ (MeV)	$B(E\lambda)\uparrow$ (e^2b^λ)[b]	ξ_λ Calculated from $B(E\lambda)\uparrow$[c]	ξ_λ Used in CUPPLE3 calculations
114	1,3	2	1.300	0.25(5)	2.1	1.5
		3	2.275	0.16(6)	1.3→2.0	1.7
116	1,2,	2	1.294	0.216(5)	2.0	1.6
	4	3	2.266	0.22(9)	1.5→2.3	1.7
118	1,2,	2	1.230	0.216(5)	2.1	1.7
	5	3	2.310	0.17(7)	1.3→2.0	1.5
120	2,6	2	1.171	0.203(4)	2.1	1.8
		3	2.400	0.11(1)	1.2→1.3	1.3
122	1,2,	2	1.140	0.196(4)	2.1	1.8
	7	3	2.492	0.13(2)	1.2→1.4	1.3
124	1,2,	2	1.131	0.161(4)	1.9	1.8
	8	3	2.612	0.20(8)	1.2→1.8	1.5

[a]References: 1-Al64, 2-St70, 3-Ki75, 4-Ca75, 5-Ca76, 6-Ko76, 7-Be72, 8-Be73.

[b]The uncertainties in the $B(E\lambda)\uparrow$ values are given in parentheses.

[c]Due to the large relative errors in the $B(E3)\uparrow$ values, a range of ξ_3 values is given for each isotope.

Table 7 Coupling strength parameters ξ_λ deduced from experimental $B(E\lambda)\uparrow$ values compared with strength parameters used in the CUPPLE3 calculations.

used. Experimental level energies for the lowest states of each spin were compared with the energy eigenvalues generated during the model calculations. As well, experimentally measured spectroscopic factors could be compared with spectroscopic factors calculated using the model deduced eigenvectors.

Spectroscopic factors for a proton stripping reaction, such as the (^{3}He,d) reaction, on an even mass Sn target are given by (Va73)

$$S_{lj}^{(\alpha)} = |A_\alpha(j(0000)0;J)|^2 \qquad (5\text{-}3)$$

where the A_α coefficients are as defined in equation 4-2 of chapter IV. These spectroscopic factors are normalized so that

$$\sum_\alpha S_{lj}^{(\alpha)} = 1. \qquad (5\text{-}4)$$

Spectroscopic factors for a proton pickup reaction, such as the (t,α) reaction, on the even mass Te nuclei are calculated in one of two ways depending on whether a proton is picked up from above or below the Z = 50 closed shell. The ground state of an even mass Te nucleus is assumed to have a zero phonon core coupled to two protons resting in any one of the single-particle states above the Z = 50 closed shell. The two protons are assumed to be coupled to spin zero. The Te ground state wavefunction can therefore be written as (Co73)

$$|g^{(5.5)};0^+\rangle = \sum_j B((j)^2 0(0000)0;0)|(j)^2 0(0000)0;0\rangle \qquad (5\text{-}5)$$

where the B coefficients are similar to the A_α coefficients

mentioned above. The sum over j is over all the single-proton levels above the Z = 50 closed shell. In a pickup reaction, if the proton is picked up from a level above the closed shell, then (Va73)

$$S_{lj}^{(\alpha)} = 2|B((j)^2 0(0000)0;0)\ A_{\alpha}(j(0000)0;j)|^2. \qquad (5\text{-}6)$$

This spectroscopic factor is normalized so that

$$\sum_{\alpha(l_j)} S_{l_j}^{(\alpha)} = 2. \qquad (5\text{-}7)$$

If the proton is picked up from below the closed shell, then (Va73)

$$S_{lj}^{(\alpha)} = (2j+1)\ |\sum_{j'} B((j')^2 0(0000)0;0)\ A((j')^2 0\ j(0000)0;j)|^2 \qquad (5\text{-}8)$$

where this spectroscopic factor is normalized so that

$$\sum_{\alpha} S_{l_j}^{(\alpha)} = 2j+1. \qquad (5\text{-}9)$$

CUPPLE3 calculations were carried out for all the odd mass In isotopes with $113 \leq A \leq 123$ and for all the odd mass Sb isotopes with $115 \leq A \leq 125$. Table 8 lists the input parameters used during the calculations, while tables 9 and 10 compare the model calculated eigenvalues and spectroscopic facors with experimental values. Figs. 19 and 20 compare the model generated eigenvalues with the experimentally measured level energies for the lowest single-hole states in In, and the lowest single-particle and 2p1h states in Sb. The data illustrated in figs. 19 and 20 is taken from tables 9a and 10a.

Model calculations were carried out on the In nuclei in order to deduce the relative separations of the 1g9/2,

Input Parameters	^{115}Sb	^{117}Sb	^{119}Sb	^{121}Sb	^{123}Sb	^{125}Sb
ξ_2	1.5	1.6	1.7	1.8	1.8	1.8
ξ_3	1.7	1.7	1.5	1.3	1.3	1.5
$\hbar\omega_2$	1.300	1.294	1.230	1.171	1.140	1.131
$\hbar\omega_3$	2.275	2.266	2.310	2.400	2.492	2.612
1g7/2	0.35	0.15	0.0	0.0	0.0	0.0
2d5/2	0.0	0.0	0.05	0.20	0.40	0.70
2d3/2	1.30	1.20	1.20	1.40	1.50	1.70
3s1/2	1.10	1.10	1.30	1.45	1.55	1.75
1h11/2	1.30	1.30	1.40	1.65	1.95	2.40
1g9/2	2.10	2.25	2.40	2.70	3.05	3.45
2d1/2	2.90	2.95	3.05	3.30	3.65	4.15
2d3/2	3.60	3.65	3.65	3.85	4.20	4.85
	^{113}In	^{115}In	^{117}In	^{119}In	^{121}In	^{123}In
1g9/2	0.0	0.0	0.0	0.0	0.0	0.0
2d1/2	0.80	0.70	0.65	0.60	0.60	0.70
2d3/2	1.50	1.40	1.25	1.15	1.15	1.40
1g7/2	3.35	3.15	3.0	3.0	3.0	3.0
2d5/2	3.0	3.0	3.05	3.20	3.40	3.70

All energy parameters are measured in MeV.

Table 8 Input parameters for CUPPLE3.

Experimental Data[a]

Isotope	^{113}In	^{115}In	^{117}In	^{119}In	^{121}In	^{123}In
References[b]	1	2	3	4	5	6
Levels						
$9/2^+$	0	0	0	0	0	0
$1/2^-$	392	336	315	311	310 (6)	320 (10)
$3/2^-$	647	597	589	604	610 (12)	660 (20)

Model Calculations

$9/2^+$	0	0	0	0	0	0
$1/2^-$	401	315	328	339	327	311
$3/2^-$	648	602	597	610	603	645

[a]All energies are in keV. Experimental errors for levels with uncertainties greater than 1 keV are listed in parentheses.

[b]References: 1-Ra71, 2-Ra75, 3-Gr72, 4-McD74, 5-We71, 6-Au72.

Table 9a Experimentally measured and model calculated energies for the lowest single-hole levels in the odd mass In nuclei.

Isotope	^{113}In	^{115}In	^{117}In	^{119}In	^{121}In	^{123}In
References[b]	1	1,2	1,2	1,2	1,2	2
Experimental Data[a]						
Levels						
$9/2^+$	0.60	0.67	0.67	0.65	0.72	
		0.57	0.58	0.59	0.65	0.72
$1/2^-$	0.65	0.75	0.75	0.80	0.70	
		0.60	0.55	0.60	0.45	0.70
$3/2^-$	0.42	0.48	0.58	0.45	0.52	
		0.42	0.52	0.52	0.40	0.42
Model Calculations						
$9/2^+$	0.86	0.83	0.82	0.81	0.81	0.83
$1/2^-$	0.84	0.83	0.83	0.82	0.83	0.83
$3/2^-$	0.58	0.58	0.61	0.63	0.64	0.60

[a] Normalization of spectroscopic factors is explained in the text.

[b] References: 1-Co69, 2-We71.

Table 9b Experimentally measured and model calculated spectroscopic factors for the lowest single-hole levels in the odd mass In nuclei.

Table 10a Experimentally measured and model calculated energies for the lowest single-particle and 2p1h levels in the odd mass Sb nuclei.

Experimental Data[a]

Isotope	^{115}Sb	^{117}Sb	^{119}Sb	^{121}Sb	^{123}Sb	^{125}Sb
References[b]	1,3	1,2, 4	1,2, 5	6,7, 8	6,9, 10	6,11
Levels						
$7/2^+$	724	527	270	37	0	0
$5/2^+$	0	0	0	0	160	332
$3/2^+$	1072	924	700	508	542	643
$1/2^+$	771	720	644	573	712	922
$11/2^-$	1300	1323	1366	1420 (20)	1630 (30)	1890
$9/2^+$	1380	1160	971	948	1337	1813 (10)
$1/2^-$	---	1355 (10)	1337 (10)	1448 (10)	1729 (10)	2118 (10)
$3/2^-$	---	---	1416 (10)	1659 (10)	1884 (10)	2299 (10)

Model Calculations

$7/2^+$	743	549	284	45	0	0
$5/2^+$	0	0	0	0	161	335
$3/2^+$	1073	916	702	530	536	602
$1/2^+$	757	699	631	588	686	925
$11/2^-$	1314	1323	1371	1453	1672	1908
$9/2^+$	1373	1164	940	1024	1358	1839
$1/2^-$	1612	1634	1395	1428	1690	1962
$3/2^-$	1620	1688	1466	1567	1864	2270

[a]All energies are in keV. Experimental errors for levels with uncertainties greater than 1 keV are listed in parentheses.

[b]References: 1-Ga75, 2-Ke71, 3-Ka76, 4-Fr75, 5-Du75, 6-Co73, 7-Is67, 8-Ho71, 9-Co68, 10-Au72, 11-Au72a.

Table 10b Experimentally measured and model calculated spectroscopic factors for the lowest single-particle and 2p1h levels in the odd mass Sb nuclei.

Experimental Data[a]

Isotope	^{115}Sb	^{117}Sb	^{119}Sb	^{121}Sb	^{123}Sb	^{125}Sb
References[b]	1	1,2	1,2,	1,2, 3	1,3	1,3, 4
Levels						
$7/2^+$	0.85	0.81 0.70	0.79 0.66	0.70	0.84	0.74
$5/2^+$	0.70	0.70 0.90	0.75 0.93	0.67 0.92	0.80	0.82
$3/2^+$	0.58	0.42 0.42	0.44	0.28 0.30	0.30	0.32
$1/2^+$	0.50	0.60 0.51	0.41	0.30 0.38	0.35	0.25
$11/2^-$	---	0.52 0.9	0.63 1.0	0.63 1.1	0.49	0.75
$9/2^+$	---	---	---	1.52	1.60	2.0 2.70
$1/2^-$	---	---	---	0.78	0.91	0.80 1.13
$3/2^-$	---	---	---	0.62	0.85	0.39 0.78

Model Calculations

$7/2^+$	0.78	0.78	0.77	0.78	0.79	0.80
$5/2^+$	0.77	0.75	0.75	0.77	0.76	0.75
$3/2^+$	0.38	0.39	0.36	0.32	0.29	0.26
$1/2^+$	0.35	0.34	0.29	0.32	0.33	0.36
$11/2^-$	0.64	0.63	0.63	0.64	0.64	0.60
$9/2^+$	---	---	---	4.8	4.7	5.2
$1/2^-$	---	---	---	0.89	0.81	0.67
$3/2^-$	---	---	---	1.5	1.5	1.4

[a] Normalization of spectroscopic factors is explained in the text.

[b] References: 1-Co68, 2-Is67, 3-Co73, 4-Au68.

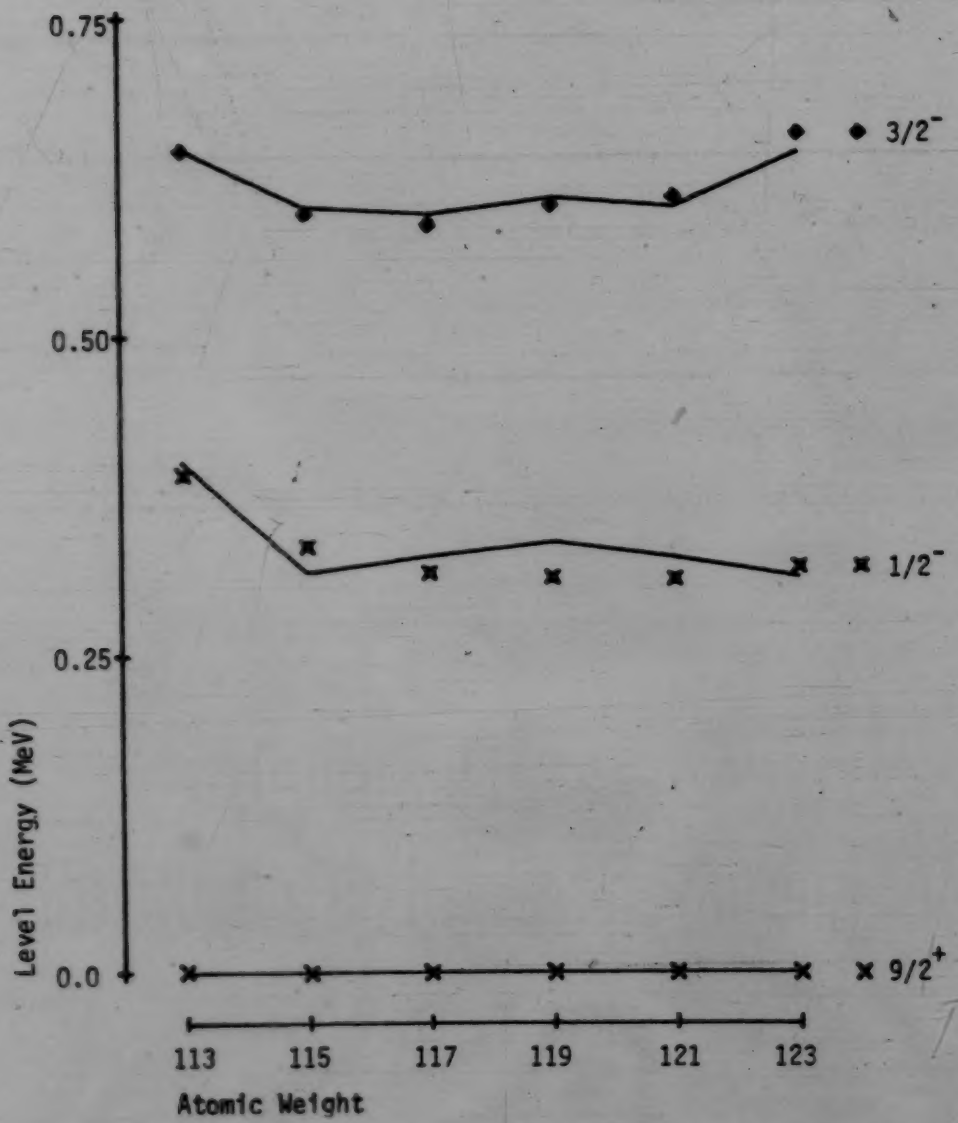

Fig. 19 A comparison of the model generated eigenvalues and the experimentally measured level energies for the lowest single-hole states in the odd mass In isotopes.

The solid lines represent the model results, while the symbols indicate the experimental measurements.

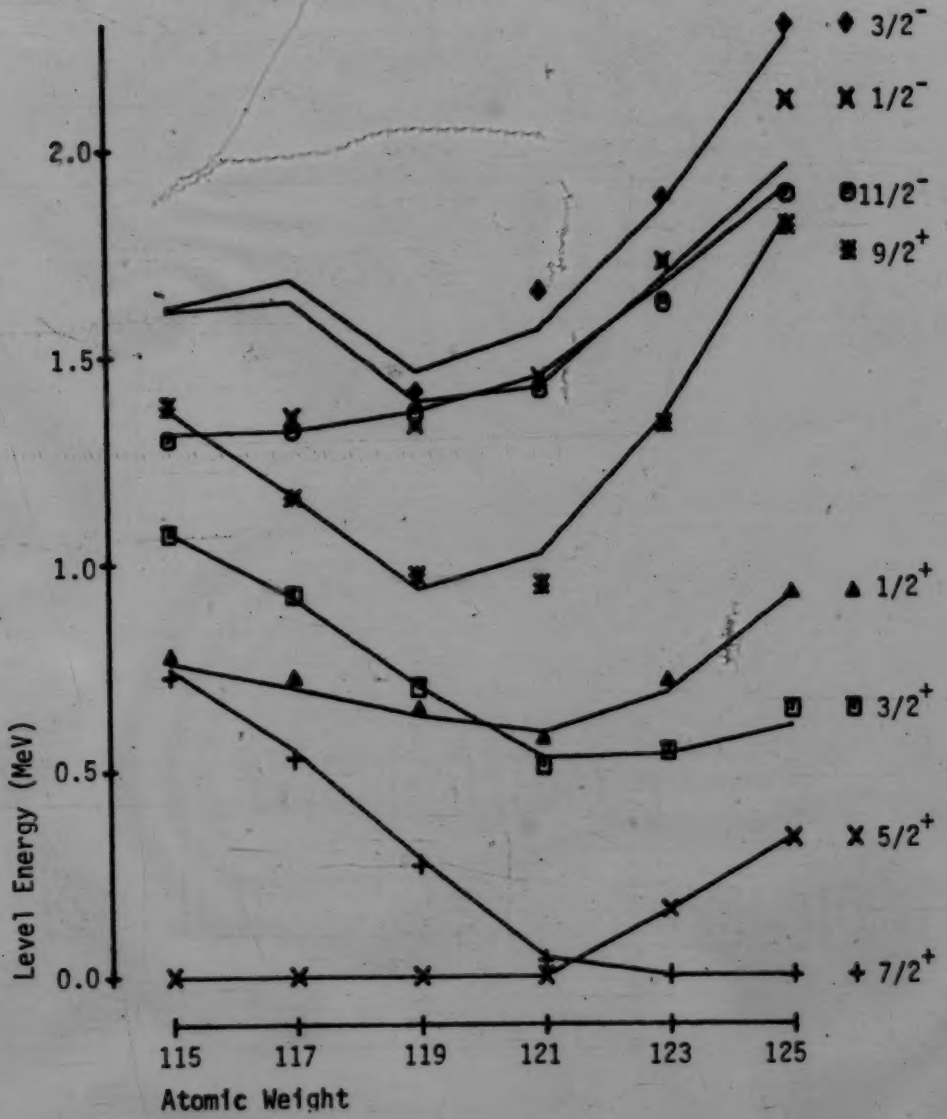

Fig. 20 A comparison of the model generated eigenvalues and the experimentally measured level energies for the lowest single-particle and two-particle-one-hole states in the odd mass Sb isotopes.

The solid lines represent the model results, while the symbols indicate the experimental measurements.

2p1/2 and 2p3/2 hole orbitals. The 1g7/2 and 2d5/2 particle states were also included in the calculations in order to determine if two-hole-one-particle (2h1p) terms were of any significance in the lowest In energy levels. Since the locations of the lowest $5/2^+$ and $7/2^+$ states have not been experimentally identified in many of the In nuclei, no attempt was made to determine exactly the energies of the 1g7/2 and 2d5/2 orbitals. Instead, particle state energies of about 3 MeV were used because for these energies the lowest $5/2^+$ and $7/2^+$ states predicted in In would have energies somewhere between 700 and 1000 keV above the ground state, which is what is expected experimentally. As it turned out, only the $1/2^-$ energy level was found to be significantly affected by the presence of 2h1p terms. For this level, the model calculations predicted that 2h1p terms of the form $|(1/2)^2 0\ 5/2(0013)3;1/2\rangle$ and $|(1/2)^2 0\ 7/2(0013)3;1/2\rangle$ did alter the level energy by between 100 and 150 keV. Since these terms would normally have been excluded by the 5 MeV upper energy cutoff on basis states, a higher energy cutoff was used for this level. Neither the $9/2^+$ ground state nor the first $3/2^-$ excited state contained significant 2h1p terms, nor were either of these states affected by raising the upper energy cutoff.

In carrying out the Sb calculations, the single-particle energies for the 1g7/2, 2d5/2, 2d3/2, 3s1/2 and 1h11/2 orbitals were deduced by comparing the model results

with experimentally measured energies for the lowest $7/2^+$, $5/2^+$, $3/2^+$, $1/2^+$ and $11/2^-$ levels. Since the $9/2^+$ 2p1h state had been identified experimentally in all of the Sb nuclei under consideration, it was also straightforward to deduce the energy separation of the 1g9/2 hole orbital and the lowest single-particle orbital (either the 2d5/2 or 1g7/2 orbital) by comparing the model calculated energy for this level with the experimental energy. Using the separations of the hole orbitals deduced from the In model calculations, it was then possible to predict where the lowest $1/2^-$ and $3/2^-$ 2p1h states should be in the various Sb nuclei.

Finally, it should be explained how the final values of the coupling strength parameters, ξ_2 and ξ_3, were chosen. From table 7 it will be noted that a wide range of ξ_3 values were predicted in many of the Sb isotopes. It was found that the model calculations were reasonably insensitive to values of ξ_3 within the given ranges. Hence, the values of ξ_3 used during the CUPPLE3 calculations were chosen, within the ranges predicted, so that ξ_3 varied fairly smoothly with A. No attempt was made to vary ξ_3 so as to obtain a best fit between the model calculations and the experimental results.

The model calculations in general, however, and the positions of the lowest $3/2^+$ and $1/2^+$ levels in particular, were found to be quite sensitive to the value of ξ_2 used in

the CUPPLE3 calculations. This dependence is illustrated in fig. 21. Using the values of ξ_2 listed in table 7, the CUPPLE3 claculations predicted energies for the lowest $3/2^+$ and $1/2^+$ states which were too low compared with experiment. These model energies could be increased by increasing the single-particle orbital energies for the 2d3/2 and 3s1/2 states, but then the spectroscopic factors for these levels were found to be too small. Hence, smaller values of ξ_2 than those predicted in table 7 were used during the final CUPPLE3 calculations in order to obtain a better fit between the experimental and model calculated energies and spectroscopic factors for the lowest $3/2^+$ and $1/2^+$ states.

The general results for all the In and Sb nuclei will not be discussed, except to note that the results of the model calculations, displayed in tables 9 and 10 and figs. 19 and 20, are in reasonable agreement with the experimental measurements. Also it will be noted that the CUPPLE3 input parameters listed in table 8 vary quite smoothly with A. A detailed discussion of the model calculations for ^{121}Sb and ^{123}Sb will be given in the next section.

b) The MOMENT Calculations

The calculation of various electromagnetic observables was accomplished by the computer program MOMENT. This

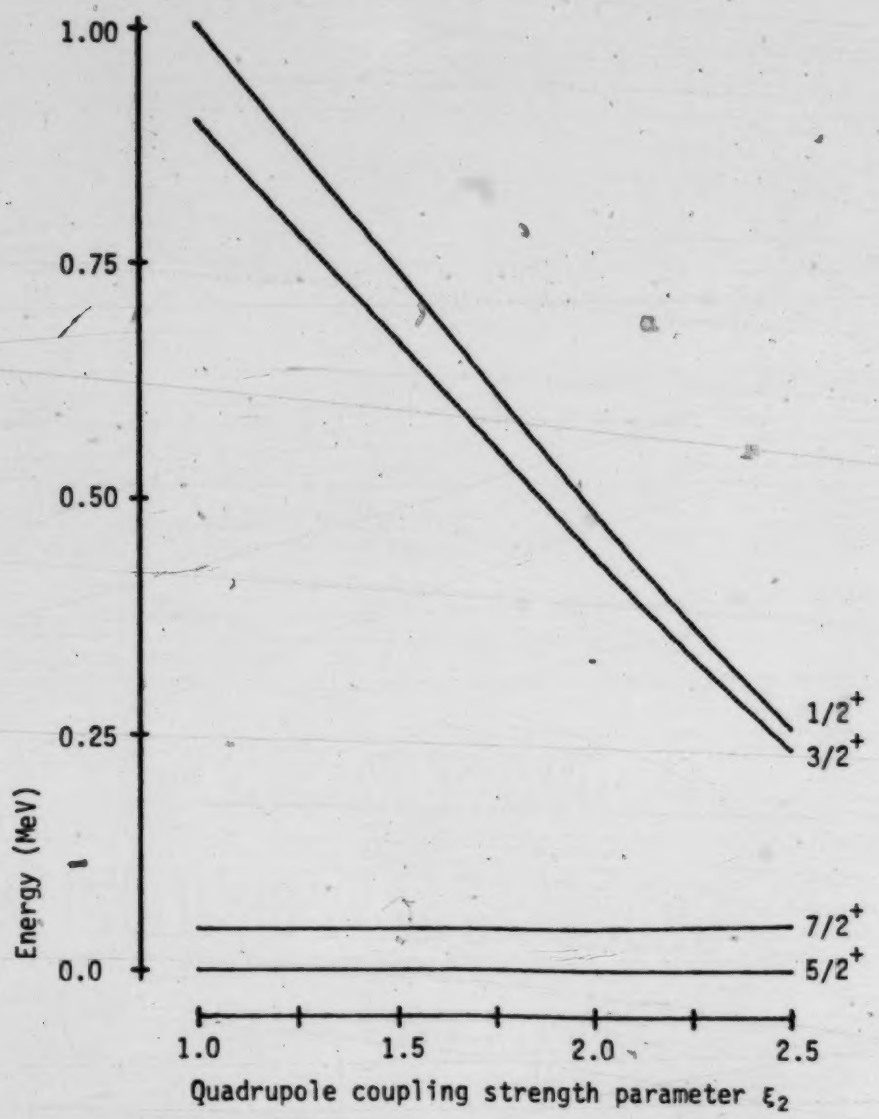

Fig. 21 Model calculated energies as a function of the quadrupole coupling strength parameter ξ_2 for the four lowest levels in ^{121}Sb.

program could calculate magnetic dipole and electric quadrupole moments, γ-ray branching and mixing ratios, and reduced matrix elements for electric quadrupole transitions (B(E2)'s) for any of the eigenstates generated by CUPPLE3. Input parameters to MOMENT included the values of $\hbar\omega_2$ and ξ_2 used in the CUPPLE3 calculations, the energy eigenvectors generated by CUPPLE3, the atomic number Z and weight A of the nucleus being studied, the radial parameter k (defined in chapter IV), and the magnetic g factors, g_l, g_s and g_R. All of these parameters were fixed during the calculations, with values of $g_l = 1$, $g_s = 2.62$ and $g_R = Z/A$ as specified in He67, and a value of $k = 40$ MeV as suggested in Br60 and He67. Detailed calculations were carried out only for the ^{121}Sb and ^{123}Sb nuclei, and these results will be discussed in the next section.

5.2 Energy Levels of ^{121}Sb and ^{123}Sb Below 2 MeV

Extensive model calculations were made for excited states below 2 MeV in ^{121}Sb and ^{123}Sb. Figs. 22 and 23 compare these deduced energy levels with known experimental levels, while tables 11 and 12 list the model deduced eigenvectors for many of the levels. It should be noted that correlations made between experimental levels and model calculated levels shown in figs. 22 and 23 and tables 11 and 12 are probable, but not certain. Tables 13 and 14 compare the electromagnetic observables calculated by MOMENT with experimental measurements.

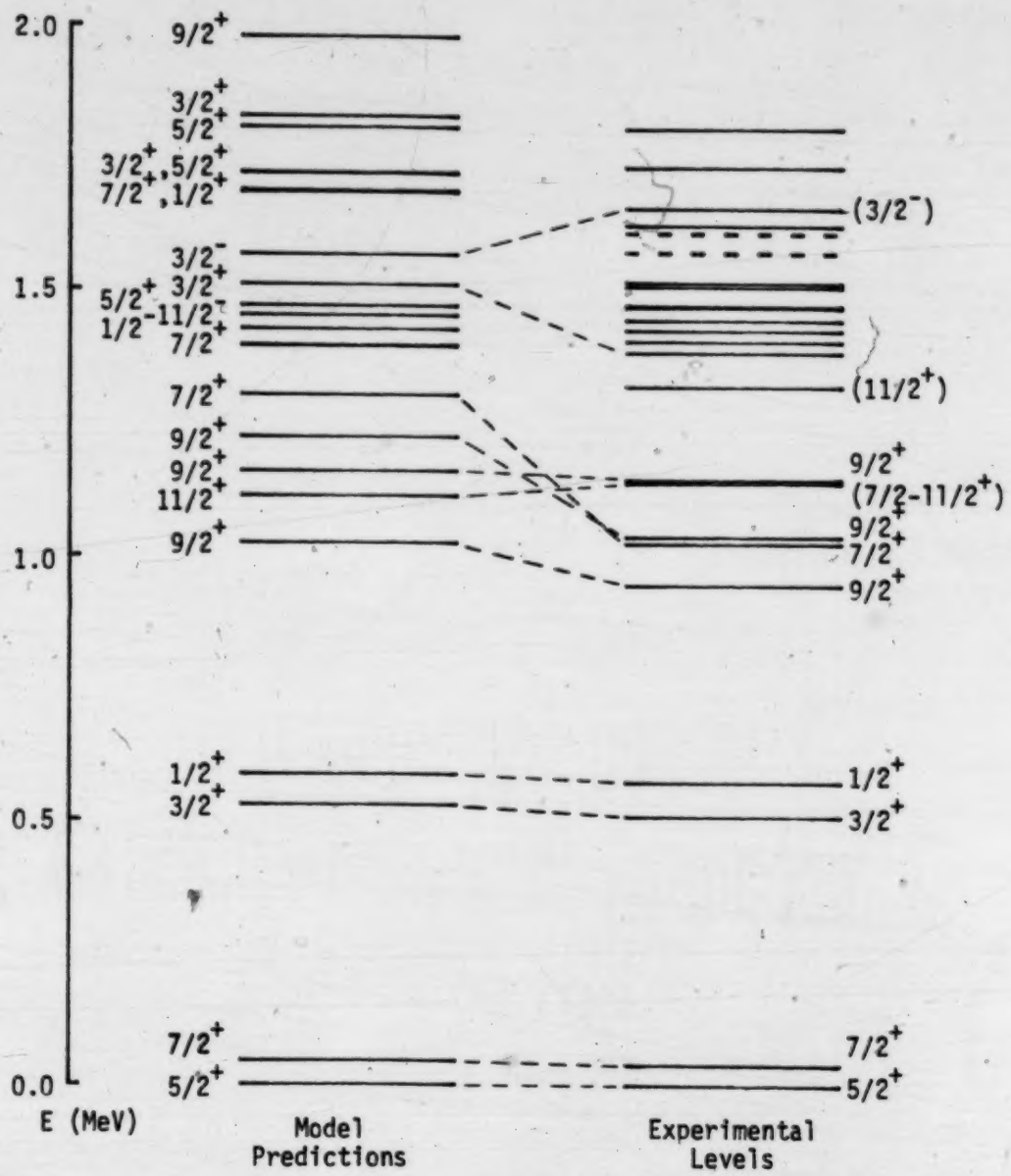

Fig. 22 A comparison of model predicted and experimental energy levels in ^{121}Sb.

The experimental levels are the same as those listed in table 15. Experimental levels represented by dashed lines are tentative. Correlations made between model predicted and experimental levels are probable, but not certain.

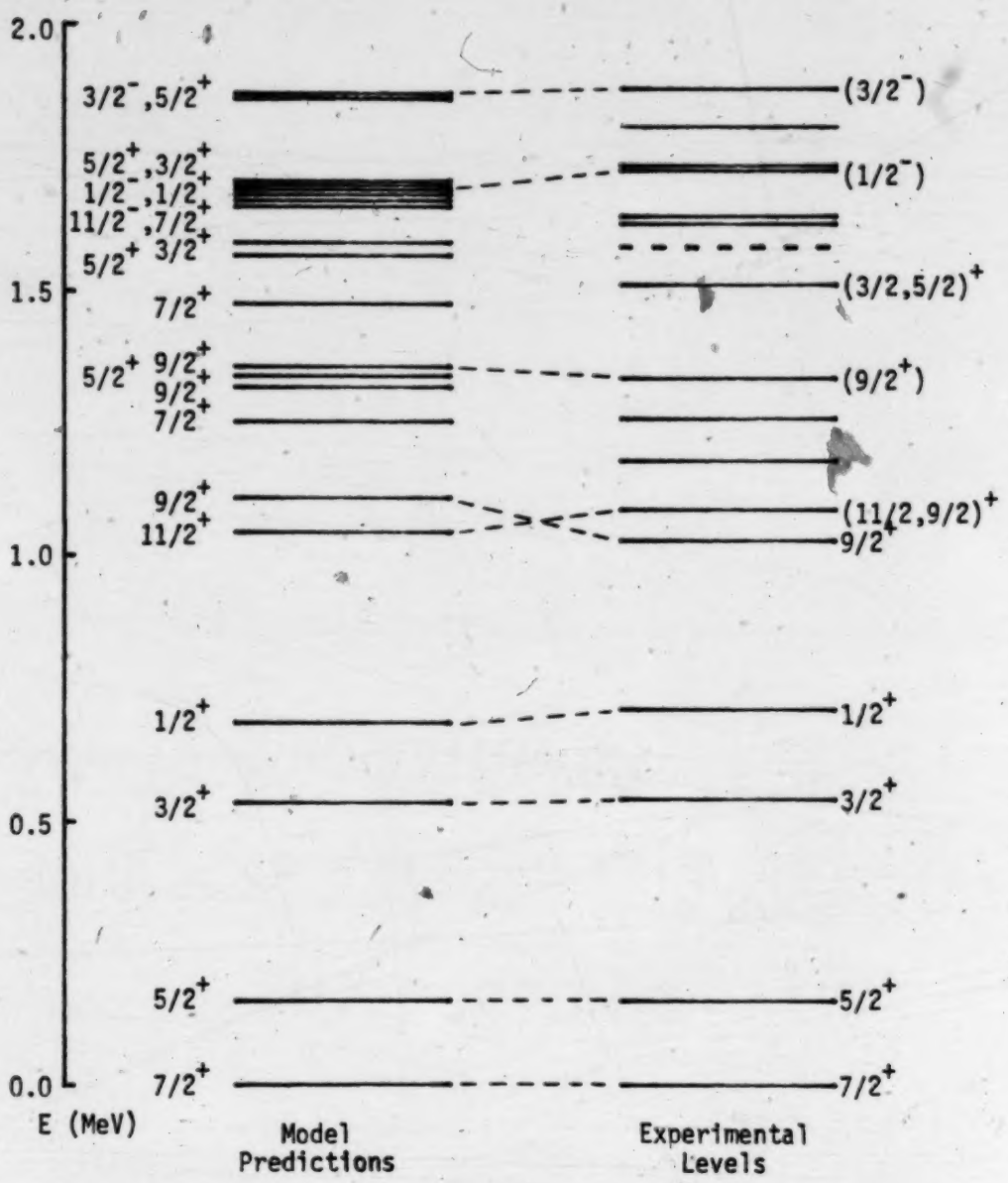

Fig. 23 A comparison of model predicted and experimental energy levels in ^{123}Sb.

The experimental levels are the same as those listed in table 16. Experimental levels represented by dashed lines are tentative. Correlations made between model predicted and experimental levels are probable, but not certain.

$$|0.000;5/2^+\rangle = 0.88|5/2(0000)0\rangle+0.14|7/2(1200)2\rangle -0.30|5/2(1200)2\rangle+0.17|1/2(1200)2\rangle -0.21|11/2(0013)3\rangle-0.12|(5/2)^20\ 9/2(1200)2\rangle$$

$$|0.037;7/2^+\rangle = 0.88|7/2(0000)0\rangle-0.36|7/2(1200)2\rangle -0.11|5/2(1200)2\rangle+0.20|3/2(1200)2\rangle$$

$$|0.507;3/2^+\rangle = 0.56|3/2(0000)0\rangle+0.63|7/2(1200)2\rangle +0.22|5/2(1200)2\rangle-0.21|3/2(1200)2\rangle -0.20|1/2(1200)2\rangle+0.16|3/2(2000)0\rangle -0.23|7/2(2200)2\rangle-0.12|7/2(2400)4\rangle -0.14|5/2(2400)4\rangle$$

$$|0.573;1/2^+\rangle = 0.56|1/2(0000)0\rangle+0.65|5/2(1200)2\rangle +0.32|3/2(1200)2\rangle+0.16|1/2(2000)0\rangle -0.23|5/2(2200)2\rangle-0.11|3/2(2200)2\rangle +0.21|7/2(2400)4\rangle-0.10|(5/2)^20\ 9/2(2400)4\rangle$$

$$|0.947;9/2^+\rangle = 0.24|7/2(1200)2\rangle+0.88|(7/2)^20\ 9/2(0000)0\rangle +0.34|(7/2)^20\ 9/2(1200)2\rangle +0.15|(7/2)^20\ 3/2(0013)3\rangle$$

$$|1.025;7/2^+\rangle = -0.20|7/2(0000)0\rangle+0.60|7/2(1200)2\rangle -0.58|5/2(1200)2\rangle-0.11|7/2(2000)0\rangle +0.18|7/2(2200)2\rangle-0.19|5/2(2200)2\rangle +0.10|3/2(2200)2\rangle-0.31|7/2(2400)4\rangle +0.17|5/2(2400)4\rangle$$

$$|1.036;9/2^+\rangle = -0.76|7/2(1200)2\rangle-0.34|5/2(1200)2\rangle -0.27|7/2(2200)2\rangle+0.28|7/2(2400)4\rangle +0.20|5/2(2400)4\rangle+0.19|(7/2)^20\ 9/2(0000)0\rangle +0.13|(5/2)^20\ 9/2(0000)0\rangle +0.11|(7/2)^20\ 9/2(1200)2\rangle$$

$$|1.140;11/2^+\rangle = 0.86|7/2(1200)2\rangle-0.19|7/2(2200)2\rangle -0.31|7/2(2400)4\rangle-0.12|5/2(2400)4\rangle +0.27|3/2(2400)4\rangle$$

$$|1.145;9/2^+\rangle = -0.33|7/2(1200)2\rangle+0.76|5/2(1200)2\rangle -0.16|5/2(2200)2\rangle+0.22|7/2(2400)4\rangle -0.23|5/2(2400)4\rangle-0.15|3/2(2400)4\rangle +0.21|1/2(2400)4\rangle+0.12|(7/2)^20\ 9/2(0000)0\rangle -0.25|(5/2)^20\ 9/2(0000)0\rangle$$

(continued on next page)

$$|1.386;3/2^+\rangle = -0.32|7/2(1200)2\rangle + 0.83|5/2(1200)2\rangle + 0.10|3/2(1200)2\rangle - 0.11|1/2(1200)2\rangle - 0.17|5/2(2200)2\rangle - 0.11|3/2(2200)2\rangle + 0.11|1/2(2200)2\rangle + 0.25|7/2(2400)4\rangle - 0.16|5/2(2400)4\rangle - 0.15|(5/2)^2 0\ 9/2(2400)4\rangle$$

$$|1.420;11/2^-\rangle = 0.80|11/2(0000)0\rangle - 0.34|11/2(1200)2\rangle - 0.15|7/2(0013)3\rangle + 0.42|5/2(0013)3\rangle - 0.12|5/2(1213)3\rangle - 0.10|5/2(1213)4\rangle$$

$$|1.448;1/2^-\rangle = -0.40|7/2(0013)3\rangle + 0.84|(7/2)^2 0\ 1/2(0000)0\rangle - 0.32|(7/2)^2 0\ 1/2(1200)2\rangle$$

$$|1.659;3/2^-\rangle = -0.16|7/2(0013)3\rangle + 0.79|(7/2)^2 0\ 3/2(0000)0\rangle + 0.29|(7/2)^2 0\ 1/2(1200)2\rangle + 0.26|(7/2)^2 0\ 3/2(1200)2\rangle - 0.41|(7/2)^2 0\ 9/2(0013)3\rangle$$

$$|1.770;1/2^+\rangle = -0.44|5/2(1200)2\rangle + 0.53|3/2(1200)2\rangle + 0.11|5/2(2200)2\rangle - 0.18|3/2(2200)2\rangle + 0.63|7/2(2400)4\rangle + 0.11|3/2(3200)2\rangle - 0.23|7/2(3400)4\rangle$$

Table 11 Model predicted energy eigenvectors for ^{121}Sb. Only components which contribute more than 1% are listed.

$$|0.000;7/2^+\rangle = 0.89|7/2(0000)0\rangle - 0.36|7/2(1200)2\rangle - 0.10|5/2(1200)2\rangle + 0.19|3/2(1200)2\rangle$$

$$|0.160;5/2^+\rangle = 0.87|5/2(0000)0\rangle + 0.16|7/2(1200)2\rangle - 0.31|5/2(1200)2\rangle - 0.10|3/2(1200)2\rangle + 0.18|1/2(1200)2\rangle - 0.20|11/2(0013)3\rangle$$

$$|0.542;3/2^+\rangle = 0.54|3/2(0000)0\rangle + 0.67|7/2(1200)2\rangle + 0.19|5/2(1200)2\rangle - 0.20|3/2(1200)2\rangle - 0.18|1/2(1200)2\rangle + 0.16|3/2(2000)0\rangle - 0.25|7/2(2200)2\rangle - 0.13|7/2(2400)4\rangle - 0.12|5/2(2400)4\rangle$$

$$|0.712;1/2^+\rangle = 0.57|1/2(0000)0\rangle + 0.62|5/2(1200)2\rangle + 0.34|3/2(1200)2\rangle + 0.16|1/2(2000)0\rangle - 0.22|5/2(2200)2\rangle - 0.12|3/2(2200)2\rangle + 0.24|7/2(2400)4\rangle$$

$$|1.030;9/2^+\rangle = 0.85|7/2(1200)2\rangle - 0.11|5/2(1200)2\rangle + 0.23|7/2(2200)2\rangle + 0.10|5/2(2200)2\rangle - 0.36|7/2(2400)4\rangle + 0.13|3/2(2400)4\rangle + 0.18|(7/2)^2 0\ 9/2(0000)0\rangle$$

$$|1.089;11/2^+\rangle = 0.87|7/2(1200)2\rangle - 0.19|7/2(2200)2\rangle - 0.32|7/2(2400)4\rangle - 0.11|5/2(2400)4\rangle + 0.26|3/2(2400)4\rangle$$

$$|1.337;9/2^+\rangle = -0.17|7/2(1200)2\rangle - 0.16|5/2(1200)2\rangle + 0.87|(7/2)^2 0\ 9/2(0000)0\rangle - 0.35|(7/2)^2 0\ 9/2(1200)2\rangle + 0.15|(7/2)^2 0\ 3/2(0013)3\rangle$$

$$|1.630;11/2^-\rangle = 0.80|11/2(0000)0\rangle - 0.33|11/2(1200)2\rangle - 0.17|7/2(0013)3\rangle + 0.43|5/2(0013)3\rangle - 0.11|5/2(1213)3\rangle - 0.10|5/2(1213)4\rangle$$

$$|1.729;1/2^-\rangle = -0.47|7/2(0013)3\rangle + 0.82|(7/2)^2 0\ 1/2(0000)0\rangle - 0.30|(7/2)^2 0\ 3/2(1200)2\rangle$$

$$|1.884;3/2^-\rangle = 0.20|7/2(0013)3\rangle - 0.78|(7/2)^2 0\ 3/2(0000)0\rangle - 0.28|(7/2)^2 0\ 1/2(1200)2\rangle - 0.26|(7/2)^2 0\ 3/2(1200)2\rangle + 0.41|(7/2)^2 0\ 9/2(0013)3\rangle$$

Table 12 Model predicted energy eigenvectors for ^{123}Sb. Only components which contribute more than 1% are listed.

Electromagnetic Observable	Level or Transition (keV)	Experimental Values [a]	Calculated Values
Magnetic Dipole Moment μ	0	3.359 nm	3.21 nm
	37	2.51 nm	2.75 nm
Electric Quad. Moment Q	0	-0.29 eb	-0.33 eb
	Q(37)/Q(0)	1.34±0.01	1.32
Branching Ratios	507-->0	94%	96%
	-->37	6%	4%
	947-->0	8%	2%
	-->37	92%	98%
	1025-->0	100%	75%
	-->37	0%	25%
	1036-->0	0%	10%
	-->37	100%	90%
	1145-->0	50%	68%
	-->37	50%	32%
	1386-->0	100%	98%
	-->37	0%	2%
Mixing Ratios arctanδ	507-->0	16°±5° [b]	-4°
	947-->37	13°±6° or 67°±6°	49°
	1025-->0	4°->75°	40°
	1036-->37	19°±9° or 61°±9°	42°
	1145-->37	6°->74°	-35°
B(E2)↑ from Coulomb Excitation	37	<0.018 e^2b^2	0.0054 e^2b^2
	507	0.010 ±0.003 e^2b^2	0.0061 e^2b^2
		0.011 ±0.002 e^2b^2	
	573	0.024 ±0.003 e^2b^2	0.023 e^2b^2
		0.028 ±0.002 e^2b^2	
	947	0.0007±0.0002 e^2b^2	0.0001 e^2b^2
	1025	0.100 ±0.016 e^2b^2	0.022 e^2b^2
		0.070 ±0.005 e^2b^2	
	1036	0.004 ±0.001 e^2b^2	0.011 e^2b^2
		0.0029±0.0003 e^2b^2	
	1145	0.081 ±0.005 e^2b^2	0.064 e^2b^2
	1386	0.020 ±0.005 e^2b^2	0.011 e^2b^2
		0.007 ±0.002 e^2b^2	

[a] Experimental mixing ratios are taken from the present work, except for the 507-->0 keV transition which is from Ho71. Branching ratios are taken from Ba71, and B(E2)↑ values are from Ho71 and An75. Other experimental values are from Ho71.

[b] The sign of this mixing ratio has not been determined experimentally.

Table 13 Model predicted and experimentally observed electromagnetic properties of ^{121}Sb.

Electromagnetic Observable	Level or Transition (keV)	Experimental Values [a]	Calculated Values
Magnetic Dipole Moment μ	0	2.547 nm	2.76 nm
	160	---	3.20 nm
Electric Quad. Moment Q	0	-0.37 eb	-0.43 eb
	160	---	-0.33 eb
Branching Ratios	542-->0	(35±6)%	21%
	-->160	(65±6)%	79%
	1030-->0	100%	99%
	-->160	0%	1%
	1337-->0	73%	90%
	-->160	27%	10%
Mixing Ratios arctan δ	1030-->0	9°->72°	51°
	1337-->0	-90°->-88° -10°->90°	-11°
B(E2)↑ from Coulomb Excitation	160	0.0035±0.0007 e^2b^2	0.0040 e^2b^2
	542	0.028 ±0.004 e^2b^2	0.031 e^2b^2
		0.040 ±0.003 e^2b^2	
	1030	0.08 ±0.01 e^2b^2	0.044 e^2b^2
		0.073 ±0.009 e^2b^2	
	1089(11/2)	0.055 ±0.014 e^2b^2	0.065 e^2b^2
	(9/2)	0.076 ±0.008 e^2b^2	0.002 e^2b^2
	1337	---	0.0011 e^2b^2

[a] Experimental mixing ratios are taken from the present work, and B(E2)↑ values are from both Au72 and An75. All other experimental values are taken from Au72.

Table 14 Model predicted and experimentally observed electromagnetic properties of ^{123}Sb.

In order to compare the model calculations with experimental results and hence to gain a better understanding of the structure of the Sb nuclei, it is useful to consider the results of experiments which preferentially excite certain Sb energy levels. Tables 15 and 16 list qualitatively the results for a number of such experiments.

Since both ^{120}Sn and ^{122}Sn have zero phonon ground states, the Sn(^{3}He,d)Sb stripping reaction would be expected to excite single-particle levels of the form $|j(0000)0;J\rangle$ in the Sb nuclei. The ^{120}Sn(α,p)^{123}Sb reaction would also be expected to excite levels of this form, provided the two neutrons transfered are coupled to spin zero. The Te(t,α)Sb pickup reaction would be expected to excite both single-particle levels, and 2pih states of the form $|(j')^{2}0\ j(0000)0;J\rangle$.

(d,d') inelastic scattering and coulomb excitation experiments should preferentially excite collective states in the Sb nuclei, but which collective states are excited will depend on the ground state wavefunctions of the Sb nuclei. From tables 11 and 12 it can be seen that the ground state of ^{121}Sb is largely in the $|5/2(0000)0;5/2\rangle$ state, while the ground state of ^{123}Sb is predominantly $|7/2(0000)0;7/2\rangle$. Hence, these reactions should excite levels with large components in their wavefunctions of the form $|5/2(1200)2;J\rangle$ in ^{121}Sb, and $|7/2(1200)2;J\rangle$ in ^{123}Sb.

	(^{3}He,d)	(t,α)	(p,t)	(d,d')	Coulomb Exc.	(γ,γ')	(^{7}Li,α2n)
Ref.	1,2,3	4	5	1,6	7,8	9	10
Level (keV)							
0	***	*		*			
37	**	***	***	*	**		
507	**	*	*	***	**	*	
573	***	*		***	**		
947		**			*		**
1025	*			***	***	***	
1036			**		*		
1140	*		**				
1145				***	***	***	
1322						•	**
1386	***			***	**	***	
1407						**	
1427	**			***	**		
1448	*	**		***			
1471							
1474							
1509							
1519						***	
(1575)							
(1613)							
1628	*					***	
1659		**					
1736	**					***	
1811							

References: 1-Ba66, 2-Is67, 3-Co68, 4-Co73, 5-Ba71, 6-Hj67, 7-Ho71, 8-An75, 9-Bo73, 10-St77.

Table 15 Qualitative results for experiments exciting ^{121}Sb. The level energies are taken from the present study, with the exception of the 1659 keV level. Levels in parentheses are tentative. Three stars (***) indicate that a level was strongly excited in a particular experiment, one star (*) that the level was weakly excited.

	(^{3}He,d)	(α,p)	(t,α)	(d,d')	Coulomb Exc.	(γ,γ')
Ref.	1,2	3	4	1,5	6,7	8
Level (keV)						
0	**	**	***	*		
160	***	***	*	*	*	
542	**	**	*	***	***	
712	**	**	*			
1030				***	***	***
1089				***	***	**
1182	*			*	**	
1260	*					
1337			**			
1515	**	**		***		***
(1586)	**	**				*
1643	**	***				**
1729			**			
1740	**	**		*		
1810				*		
1884			**			

References: 1-Ba66, 2-Co68, 3-Ka77, 4-Co73, 5-Hj67, 6-Ho71, 7-An75, 8-Bo73.

Table 16 Qualitative results for experiments exciting ^{123}Sb.
Level energies below 1600 keV are taken from the present study, while levels above this energy are taken from Au72 and Co73. Levels in parentheses are tentative. Three stars (***) indicate that a level was strongly excited in a particular experiment, one star (*) that the level was weakly excited.

The $^{123}Sb(p,t)^{121}Sb$ reaction, on the other hand, should excite collective terms with large $|7/2(1200)2;J\rangle$ components in ^{121}Sb. The (γ,γ') interaction will also be expected to excite collective levels in these nuclei, although other levels may also be excited.

Finally, in table 15 an experiment using the $^{120}Sn(^{7}Li,\alpha 2n)^{121}Sb$ reaction is listed. This experiment was intended to excite any high spin rotational levels in ^{121}Sb.

With the information available in tables 10 through 16, it is possible to discuss in some detail the structure of the individual Sb levels. It can be seen from table 15 that the first four levels in ^{121}Sb are strongly excited in the $(^{3}He,d)$ stripping reaction, and hence must have sizable single-particle components. Both the 507 and 573 keV levels are also excited in the (d,d') and coulomb excitation experiments, and therefore must have significant collective terms. This fact is born out by the spectroscopic factors listed in table 10b and the model deduced wavefunctions listed in table 11. The 0 and 37 keV levels are almost entirely single-particle states, while the 507 and 573 keV levels have much smaller single-particle components and many collective terms.

All of these states are excited in the $^{122}Te(t,\alpha)$ reaction. The fact that the 37 keV level is most strongly excited indicates that the ground state wavefunction for

^{122}Te is dominated by a term with two protons in the 1g7/2 orbital coupled to spin zero. The 37 keV level is also strongly excited in the ^{123}Sb(p,t) reaction, which is expected since this level is the analogue of the ^{123}Sb ground state.

The model calculated magnetic dipole and electric quadrupole moments for the 0 and 37 keV levels are in good agreement with the experimental values listed in table 13, as are the branching ratios for the 507 keV level and the B(E2)↑ values for the 37, 507 and 573 keV levels. The deduced mixing ratio for the 507-->0 keV transition is only in fair agreement with experiment, however.

The 947 keV level, which has been assigned a definite spin of 9/2 in the present study, was excited in the ^{122}Te(t,α) reaction with an transfer of 4, suggesting that the wavefunction for this level is dominated by a 2p1h term of the form $|(7/2)^2 0\ 9/2(0000)0;9/2\rangle$. The model calculations for this level were able to reproduce this feature (table 11), although the model predicted spectroscopic factors (table 10b) are considerably larger than the experimental spectroscopic factors. It should be noted, however, that many of the model predicted spectroscopic factors for 2p1h states were larger than the experimental values, and that the (2j+1) sum rule was far from being exhausted by the experimental values. The authors of the (t,α) study (Co73) noted that either the

absolute values of their calculations were incorrect, or that the remaining strength for the (2j+1) sum rule lay over many levels above 3 MeV in excitation.

The model predictions listed in table 13 for the electromagnetic observables associated with the 947 keV level are in reasonable agreement with experiment.

The 947 keV level was also excited in the ^{120}Sn(^{7}Li,α2n) reaction, and identified as the band head for a ΔJ=1 rotational band. It would thus appear that the 2p1h excitation predicted by the intermediate coupling model introduces a permanent deformation to the nucleus, and hence permits rotational bands to be built on this level. The 1322 keV level is presumed to be the first excited state in this rotational band. This level would not, of course, be predicted in the present model calculations.

The four levels between 1.0 and 1.2 MeV appear to be largely collective in nature. Both the 1025 and 1145 keV levels are strongly excited in the (d,d'), coulomb excitation and (γ,γ') reactions, but not in the (p,t) reaction, indicating that they have large $|5/2(1200)2;j\rangle$ components in their wavefunctions. The 1036 and 1140 keV levels, however, are excited in the (p,t) reaction but only weakly in the other reactions indicating the presence of large $|7/2(1200)2;j\rangle$ components in their wavefunctions. The 1036 and 1145 keV levels have been assigned spins of

9/2 in the present study, and can therefore be readily correlated with model calculated levels which have the same dominant components as those specified above. The 1025 keV level, which was assigned a definite spin of 7/2 in this study, can also be correlated with a model calculated level. In this case, however, the model appears to predict too large a |5/2(1200)2;7/2> component in the wavefunction; if this component were as large the model predicts (see table 11), then this level should be appreciably excited in the (p,t) reaction. The 1140 keV level presumably corresponds to the lowest $11/2^+$ model predicted level. In this case the model correctly predicts a large |7/2(1200)2;11/2> component in the wavefunction.

The model calculated electromagnetic observables for these levels are in reasonable agreement with experiment, although the agreement is not nearly as good as that for the lower levels. The branching ratio predicted for the 1025-->37 keV transtion is certainly too large, while the B(E2)↓ value for this level is too small. As well, the B(E2)↓ value for the 1036 keV level is a little too large, and the sign of the mixing ratio predicted for the 1145--> 37 keV transition disagrees with experiment.

The 1386 keV level has been observed in (^{3}He,d), (d,d'), coulomb excitation and (γ,γ') experiments. However, the (^{3}He,d) results for this level are somewhat ambiguous. In one study (Ba66), a level with an energy of

1380 ± 10 keV was strongly excited, but no ℓ transfer was measured. In two other studies (Is67 and Co68), levels with energies of 1420 ± 20 keV and 1440 ± 30 keV were observed with ℓ transfers of 2 + 5. It is not obvious that the levels observed in these last two experiments are related to the level observed in the first experiment. A spin-parity of $3/2^+$ has previously been proposed for this level (Bo73), and indeed, only for a spin 3/2 level did the model calculations reproduce the large branching ratio of this level to the ground state. The B(E2)↑ value for this level was also correctly predicted by the model calculations. However, the wavefunction for this level, listed in table 11, contains virtually no single-particle term. Therefore, if the model calculations are correct, this level should not be observed in a (^{3}He,d) stripping experiment. The model predicted wavefunction does contain a large collective term of the form $|5/2(1200)2;3/2\rangle$, which is what would be expected from the (d,d'), coulomb excitation and (γ,γ') experiments.

The experimental information available for levels above 1400 keV in ^{121}Sb is not nearly as decisive as it is for levels below this energy. As was mentioned above, levels at energies of 1420 ± 20 keV and 1440 ± 30 keV have been observed in (^{3}He,d) experiments with ℓ transfers of 2 + 5. The measured spectroscopic factor for an ℓ transfer of 5 is quite large (see table 10b), and hence an $11/2^-$ state with a large single-particle component is most likely

somewhere in this energy range. From the present study the most likely candidate for this level is the 1427 keV level, which decays to the two $9/2^+$ levels at 1036 and 1145 keV. This assignment would be unlikely if this level were excited by the (γ,γ') reaction, since a transition from the $5/2^+$ ground state of ^{121}Sb to an $11/2^-$ level must proceed via E3 radiation, and the (γ,γ') reaction tends to only proceed via E1 or E2/M1 radiation. A scattered 1423 ± 3 keV γ-ray was in fact observed in the (γ,γ') experiment (Bo73) and assigned to ^{121}Sb, but it has been assumed in this analysis that this γ-ray came from the 1586 keV level of ^{123}Sb proposed earlier in the discussion of the present experimental work. The fact that this level is strongly excited in the (d,d') and coulomb excitation experiments could be due to the presence of a one octupole phonon collective term, $|5/2(0013)3;11/2\rangle$, in the $11/2^-$ wavefunction, as shown in table 11.

Levels with energies of 1448 ± 10 keV and 1659 ± 10 keV have been observed in the (t,α) experiment with moderately sized spectroscopic factors for ℓ transfers of 1. These states must therefore have 2p1h components in their wavefunctions, with the one hole occuring in the 2p1/2 and 2p3/2 states respectively. The model calculated spectroscopic factor listed in table 10b for the $3/2^-$ level is about twice as large as the experimental value, as was the case for the $9/2^+$ 2p1h level at 947 keV. The spectroscopic factor calculated for the $1/2^-$ level is,

however, in reasonable agreement with experiment.

There is contradictory evidence concerning the properties of the excited state at 1736 keV. A level with an energy of 1735 ± 10 keV was originally observed to be moderately excited in a (^{3}He,d) experiment (Ba66), but no ℓ transfer was measured. A later (^{3}He,d) experiment (Is67) noted a level with an energy of 1770 ± 20 keV and having a measured spectroscopic factor of 0.16 ± 0.03 for an ℓ transfer of 0. On the basis of these measurements, the level at 1736 keV was assigned a spin-parity of $1/2^+$ by Nuclear Data Sheets (Ho71). This assignment was challenged in a (γ,γ') scattering experiment (Bo73), however, on the grounds that the E2 strength required to populate this level, assuming a spin-parity of $1/2^+$, was too large. The measured B(E2)$\uparrow$ for this level assuming this spin-parity was 0.09 ± 0.02 e^2b^2. The present model calculations tend to support this last experiment. The model does predict a $1/2^+$ level in this energy region, and the wavefunction for this level is listed in table 11. The model calculated B(E2)$\uparrow$ for this level is 0.0006 e^2b^2, however, which is at least two orders of magnitude lower than the experimental value quoted above. Furthermore, the spectroscopic factor predicted by the theory for this level is less than 0.01, in clear disagreement with the measured value. On the basis of the B(E2)$\uparrow$ results, it would appear that the 1736 keV level is not the $1/2^+$ level predicted in the (^{3}He,d) study. The exact location and properties of a $1/2^+$ energy

level in this region have still to be determined.

The first four states in ^{123}Sb are quite similar in structure to the four lowest levels in ^{121}Sb, except that the $5/2^+$ level now lies above the $7/2^+$ level in energy. All four levels are excited by the ^{124}Te(^{3}He,d) stripping reaction with the lowest two levels having large spectroscopic factors and the next two levels having smaller spectroscopic factors. As shown in table 16, the 542 keV level is also strongly excited in the (d,d'), coulomb excitation and (γ,γ') experiments, indicating that it has a large collective component of the form |7/2(1200)2;3/2> in its wavefunction. The 712 keV level would not be expected to be excited in any of these reactions because, with a spin-parity of $1/2^+$, it is 3 units of angular momentum above the ground state.

The model calculated wavefunctions (table 12) and spectroscopic factors (table 10b) for these levels are in agreement with the experimental results discussed above. The model calculated electromagnetic observables for these levels, shown in table 14, are also in good agreement with experimental values.

These four levels are also moderately excited in the ^{124}Te(t,α) reaction, with the ground state of ^{123}Sb being very strongly excited by this reaction. This suggests that, as was the case for ^{122}Te, the dominant term in the wavefunction for the ground state of ^{124}Te contains two

protons outside the Z = 50 core both occupying the 1g7/2 orbital and coupled to spin zero.

The level at 1030 keV has been assigned a definite spin of 9/2 in the present study. From table 16 it can also be seen that this level is strongly excited by the (d,d'), coulomb excitation and (γ,γ') experiments, which suggests that this level has a large collective component of the form |7/2(1200)2;9/2>. The model calculations successfully predict a level with these properties, and the wavefunction of this level is listed in table 12. The model calculated branching ratios for this level are in good agreement with experiment, and the calculated mixing ratio has the correct sign. The model calculated B(E2)$\uparrow$ is smaller than the experimental measurements, although the agreement is still reasonable.

The 1089 keV level was assigned possible spin-parities of $7/2^+$, $9/2^+$ or $11/2^+$ by Nuclear Data Sheets (Au72), but the $7/2^+$ assignment was rejected earlier in the present study (see chapter III). In table 14, measured B(E2)$\uparrow$ values for this level of 0.055 ± 0.014 e^2b^2 and 0.076 ± 0.008 e^2b^2 are compared with model calculations for levels in this region with spins of 9/2 and 11/2. The calculation for an $11/2^+$ level, 0.065 e^2b^2, is in good agreement with the experimental values, while the result for a $9/2^+$ level, 0.002 e^2b^2, is much too small. The wavefunction listed in table 12 for the 1089 keV level is

that of the $11/2^+$ model calculated level. It will be noted that this wavefunction has a large component of the form $|7/2(1200)2;11/2\rangle$, which agrees with the experimental finding that this level is strongly excited in the (d,d'), coulomb excitation and (γ,γ') experiments.

The levels at 1182 and 1260 keV are not strongly excited in any of the experiments listed in table 16, which suggests that these levels are largely collective in nature with the single proton outside the Z = 50 core residing in an orbital other than the 1g7/2. Terms of the form $|5/2(1200)2;j\rangle$ are probable, since the 2d5/2 orbital is next lowest in energy to the 1g7/2 orbital. Since experimental spin-parities for these levels have not been measured, any further discussion of their structure would be highly speculative.

The 1337 keV level is strongly excited by the ^{124}Te (t,α) reaction for an ℓ transfer of 4. This suggests that this level is similar to the 947 keV level in ^{121}Sb, being a 2p1h state with a proton hole occuring in the 1g9/2 orbital and having two protons in the 1g7/2 orbital coupled to spin zero. The model calculated wavefunction for this level is listed in table 12, and the calculated spectroscopic factor is compared with experiment in table 10b. As in the case of the 947 keV level in ^{121}Sb, the calculated spectroscopic factor is between two and three times larger than the experimental one. The calculated

branching ratios shown in table 12 for this level are in reasonable agreement with experiment, and the calculated mixing ratio for the 1337-->0 keV transition is also in general agreement with the rather poor experimental measurement.

As was the case for ^{121}Sb, the experimental information on levels above 1400 keV in ^{123}Sb is somwhat confusing. The 1515 keV level listed in table 16 is assumed to correspond to levels at 1502 ± 10 keV and 1500 ± 30 keV observed in two (^{3}He,d) experiments (Ba66 and Co68), levels at 1510 ± 5 keV and 1526 ± 15 keV seen in two (d,d') experiments (Ba66 and HJ67), and a level at 1512 ± 2 keV observed in a (γ,γ') experiment (Bo73). This level was also observed in an (α,p) experiment (Ka77), but measured excitation energies were not reported in this study. An ℓ transfer of 2 was measured for this level in the second (^{3}He,d) experiment.

The 1586 keV level proposed in the present study should correspond to a level at energy 1574 ± 10 keV observed in a (^{3}He,d) study (Ba66), a level at 1601 ± 15 keV observed in a (d,d') experiment (Hj67), and a level at 1583 ± 3 keV possibly seen in a (γ,γ') experiment (Bo73). It has been assumed that the 1423 ± 3 keV γ-ray observed in the (γ,γ') experiment originated from the ^{123}Sb nucleus. This level was also observed in the (α,p) study, and may correspond to a peak with energy 1630 ± 30 keV observed to

have an ℓ transfer of 2 + 5 in a (^{3}He,d) study (Co68).

A level at an energy of 1643 keV proposed by Nuclear Data Sheets (Au72) appears to correspond to levels at 1644 ± 10 keV and 1630 ± 30 keV observed in the two (^{3}He,d) experiments mentioned above, a level at 1653 ± 5 keV seen in one of the (d,d') experiments (Ba66), a level observed in the (α,p) experiment, and perhaps to a level at 1643 ± 3 keV excited in the (γ,γ') experiment. However, a spin-parity of $11/2^-$ was proposed for this level in the (α,p) study, whereas the (γ,γ') study proposed spin-parities of $3/2^+$ or $5/2^+$.

Finally, a level at 1740 keV was observed in a (^{3}He,d) experiment (Co68) with an energy of 1740 ± 30 keV, in the (α,p) study, and in a (d,d') study (Hj67) with an energy of 1750 ± 15 keV. However, the ℓ transfer of 2 measured in the (^{3}He,d) study suggests spin-parities of $3/2^+$ or $5/2^+$ for this level, whereas a spin-parity of $7/2^+$ was proposed in the (α,p) study.

A correlation between the model calculated levels and any of the four levels just discussed cannot be made with the information available. Indeed because the model predicts many more levels in this energy region than are observed experimentally, and in light of the contradictory experimental results noted above, it is quite possible that some of the levels discussed above are doublets.

The model calculated wavefunction for the $11/2^-$ single-particle state is listed in table 12, and is assumed to have an energy of 1630 ± 30 keV. The spectroscopic factor calculated for this level is in good agreement with experimental results.

Finally, levels with energies of 1729 ± 10 keV and 1884 ± 10 keV have been observed in a (t,α) experiment with ℓ transfers of 1. These two levels should therefore correspond to 2p1h levels with proton holes occuring in the 2p1/2 and 2p3/2 states respectively, and must have spin-parities of $1/2^-$ and $3/2^-$. The wavefunction for these levels are listed in table 12, and their spectroscopic factors in table 10b. As was the case for the $1/2^-$ and $3/2^-$ levels in ^{121}Sb, the calculated spectroscopic factor for the $1/2^-$ level is in agreement with experiment, but the spectroscopic factor calculated for the $3/2^-$ level is about twice as large as the experimental value.

Chapter VI

Conclusions

The present study has demonstrated that level spins can be deduced by measuring γ-ray angular distributions produced by the $(n,n'\gamma)$ reaction. The count rates encountered when using the $(n,n'\gamma)$ reaction are much smaller than the count rates obtained when doing, for example, (p,n) work on lighter nuclei. Hence, the mixing ratios deduced in this work have relatively large errors associated with them.

Four definite spin assignments were made in ^{121}Sb but only one assignment was made in ^{123}Sb. This was because the ground state spin of ^{123}Sb is larger than the ground state spin of ^{121}Sb, and hence excited states in ^{123}Sb are not as strongly aligned as states in ^{121}Sb. Alternate experiments to determine level spins, such as measuring γ-γ correlations, were impractical due to the low count rates.

It was noted in the discussion of experimental results that angular distribution measurements could not be made for levels above 1.4 MeV in ^{121}Sb because these levels were weakly excited by the $(n,n'\gamma)$ reaction. This observation can be explained by noting that the level density in ^{121}Sb increases considerably at this energy. Hence there are many more exit channels available for the compound nucleus to decay to, and the yield to each of the exit channels decreases.

The intermediate coupling model calculations are in reasonable agreement with the experimental results. The model correctly predicts the large one quadrupole phonon components in the lowest $1/2^+$ and $3/2^+$ states in the Sb nuclei, and also explains many of the features of the predominantly one quadrupole phonon levels grouped in the 1.0 to 1.2 MeV region. There is insufficient experimental data available to extend the comparison to higher levels, where two quadrupole phonon states would start to become important. In this region a comparison between experimental results and model calculations might begin to break down, however, because the experimentally observed two quadrupole phonon states in the Sn nuclei are split in energy, whereas the model two phonon states are degenerate.

The 2p1h terms included in the model calculations appear to couple only weakly to the single-particle terms. Most of the eigenstates predicted by the model below 2 MeV do not have both large single-particle and large 2p1h components, but instead have either single-particle terms, or 2p1h terms, coupled to vibrational components. If the 2p1h terms were removed from the model calculations, the model predictions for most states would not change appreciably, except of course that levels with large 2p1h components would be overlooked.

In the discussion of the model results it was noted that a $\Delta J=1$ rotational band has been discovered

experimentally with a band head corresponding to the $9/2^+$ 2p1h state in ^{121}Sb. It is possible that rotational bands may also be built on the $1/2^-$ and $3/2^-$ 2p1h states in the Sb nuclei, although no experimental evidence exists as yet for such bands. The intermediate coupling model does not account for the permanent nuclear deformation which must exist if a rotational band is observed. Hence another type of model, most likely a microscopic calculation, must be used in order to explain the $9/2^+$ rotational band, and to investigate the possibility of other rotational bands.

Comparison of the model predictions and present results with previous studies for a variety of reactions leads to a consistent picture of the structure of the low lying levels in the Sb isotopes. As excitation energy increases, however, the structure can no longer be interpreted in terms of a simple model.

Further experimental investigation of higher energy rotational bands in ^{121}Sb and ^{123}Sb would be of considerable interest, and hopefully will be undertaken. A study of the analogue reactions ^{123}Sb(p,t)^{121}Sb and ^{121}Sb(t,p)^{123}Sb would also be useful. The poor energy resolution noted in many of the previous charged particle experiments could be significantly improved if γ-ray-particle coincidence experiments were carried out. Forinstance, the energies of the lowest $1/2^-$ and $3/2^-$ states could be measured with greater accuracy if the α-

particle emitted in the Te(t,α)Sb reaction was detected in coincidence with de-excitation γ-rays.

Other experiments of theoretical interest which may be feasible are the two proton transfer reactions $^{115}In(^{7}Li,p)^{121}Sb$ and $^{127}I(d,^{6}Li)^{123}Sb$, and the three proton transfer reaction $^{116}Cd(^{6}Li,n)^{121}Sb$.

References

Ab64 M. Abramowitz and I.A. Stegun, Handbook of Mathmatical Functions, U.S. National Bureau of Standards, 1964.

Al64 D.G. Alkhazov, Yu.P. Gangrskii, I.Kh. Lemberg and Yu.I. Udralov, Bull. Acad. Sci. USSR 28, 149 (1964).

An75 D.S. Andreev, K.I. Erokhina, V.S. Zvonov and I.N. Chugunov, Bull. Acad. Sci. USSR 39 #8, 55 (1975).

Au68 R.L. Auble, J.B. Ball and C.B. Fulmer, Nucl. Phys. A116, 14 (1968).

Au72 R.L. Auble, Nucl. Data B7, 363 (1972).

Au72a R.L. Auble, Nucl. Data B7, 465 (1972).

Ba60 M. Baranger, Phys. Rev. 120, 957 (1960).

Ba66 P.D.Barnes, E. Ellegaard, B. Herskind and M.C. Joshi, Phys. Lett. 23, 266 (1966).

Ba71 E. Barnard, N. Coetzee, J.A.M. De Villiers, D. Reitmann and P. Van der Merwe, Nucl. Phys. A172, 215 (1971).

Ba71a E.U. Baranger, Adv. Nucl. Phys. 4, 261 (1971).

Be72 F.E. Bertrand, Nucl. Data 7, 419 (1972).

Be73 F.E. Bertrand, Nucl. Data 10, 91 (1973).

Bo73 E.C. Booth, R.G. Arnold and W.J. Alston III, Phys. Rev. C7, 1500 (1973).

Br60 D.M. Brink, Prog. Nucl. Phys. 8, 99 (1960).

Ca75 G.H. Carlson, W.L. Talbert, Jr. and S. Raman, Nucl. Data 14, 247 (1975).

Ca76 G.H. Carlson, W.L. Talbert, Jr. and S. Raman, Nucl. Data 17, 1 (1976).

Co68 M. Conjeaud, S. Harar and Y. Cassagnou, Nucl. Phys. A117, 449 (1968).

Co69 M. Conjeaud, S. Harar and E. Thuriere, Nucl. Phys. A129, 10 (1969).

Co73 M. Conjeaud, S. Harar, M. Caballero and N. Cindro, Nucl. Phys. A215, 383 (1973).

Da76 J.M. Davidson, H.R. Hooper, D.M. Sheppard and G.C. Neilson, Nucl. Instrum. Methods 134, 291 (1976).

Da76a J.M. Davidson, Internal Report No. 79, Nuclear Research Centre, University of Alberta, 1975 (unpublished).

deS63 A. deShalit and I. Talmi, Nuclear Shell Theory, Academic Press, New York, (1963).

deS74 A. deShalit and H. Feshbach, Theoretical Nuclear Physics Vol. 1: Nuclear Structure, John Wiley & Sons Inc., Toronto, (1974).

Du75 R. Duffait, A. Charvet and R. Chery, Z. Phys. 272, 315 and 321 (1975).

En64 P.M. Endt and C. Van der Leun, At. Data Nucl. Data Tables 13, 67 (1974).

Fr75 W.D. Fromm, H.F. Brinckmann, F. Donau, C. Heiser, F.R. May, V.V. Pashkevich and H. Rotter, Nucl. Phys. A243, 9 (1975).

Ga75 A.K. Gaigalas, R.E. Shroy, G. Schatz and D.B. Fossan, Phys. Rev. Lett. 35, 555 (1975).

Gr72 P.R. Gregory and M.W. Johns, Can. J. Phys. 50, 2012 (1972).

Gr73 P.W. Green, Internal Report No. 62, Nuclear Research Centre, University of Alberta, 1973 (unpublished).

He67 K. Heyde and P.J. Brussaard, Nucl. Phys. A104, 81 (1967).

Hj67 S.A. Hjorth, Ark. Fys. 33 #12, 183 (1967).

Ho71 D.J. Horen, Nucl. Data B6, 75 (1971).

Is67 T. Ishimatsu, K. Yagi, H. Ohmura, Y. Nakajima, T. Nakagawa and H. Orihara, Nucl. Phys. A104, 481 (1967).

Ka76 R. Kamermans, T.J. Ketel and H. Verheul, Z. Phys. A279, 99 (1976).

Ka77 R. Kamermans, J.W. Smits, J. Van Driel and R.H. Siemssen, Phys. Lett. 66B, 226 (1977).

Ke71 R. L. Kernell, H.J. Kim, R.L. Robinson and C.H. Johnson, Nucl. Phys. A176, 449 (1971).

Ki63 L.S. Kisslinger and R.A. Sorensen, Rev. Mod. Phys. 35, 853 (1963).

Ki75 H.J. Kim, Nucl. Data 16, 107 (1975).

Ko76 D.C. Kocher, Nucl. Data 17, 39 (1976).

McD74 J. McDonald, B. Fogelberg, A. Backlin and Y. Kawase, Nucl. Phys. A224, 13 (1974).

Ra71 S. Raman and H.J. Kim, Nucl. Data 5, 181 (1971).

Ra74 S. Raman, R.L. Auble and F.F. Dyer, Phys. Rev. C8, 426 (1974).

Ra75 S. Raman and H.J. Kim, Nucl. Data 16, 195 (1975).

Ro67 H.J. Rose and D.M. Brink, Rev. Mod. Phys. 39, 306 (1967).

Ro75 D.W.O. Rogers, Nucl. Instrum. Methods 126, 253 (1975).

Se70 S. Sen and B.K. Sinha, Nucl. Phys. A157, 497 (1970).

Sh66 E. Sheldon and D.M. van Patter, Rev. Mod. Phys. 38, 143 (1966).

St70 P.H. Stelson, F.K. McGowan, R.L. Robinson and W.T. Milner, Phys. Rev. C2, 2015 (1970).

St77 P.M. Stwertka, T.P. Sjoreen, U. Garg and D.B. Fossan, Bull. Am. Phys. Soc. 22, 1026 (1977).

Va70 G. Vanden Berghe and K. Heyde, Phys. Lett. 32B, 173 (1970).

Va71 G. Vanden Berghe and K. Heyde, Nucl. Phys. A163, 478 (1971).

Va73 G. Vanden Berghe and E. Degrieck, Z. Phys. 262, 25 (1973).

We71 C.V. Weiffenback and R. Tickle, Phys. Rev. C3, 1668 (1971).

Wi64 D. Wilmore and P.E. Hodgson, Nucl. Phys. 55, 673 (1964).

Appendix A

Phase Consistent Electromagnetic Multipole Operators

In order to calculate theoretically any electromagnetic observable, it is inevitably necessary to calculate the reduced transition matrix element $\langle E^{(\beta)}; J_\beta \| \mathcal{M}(A) \| E^{(\alpha)}; J_\alpha \rangle$, where $\mathcal{M}(A)$ is any electromagnetic multipole operator. Many electromagnetic observables are proportional to the square of this number, and do not provide any information concerning the phase of the operator. A few observables, however, are proportional to the matrix element itself, and hence measure its phase as well as its amplitude. The γ-ray multipole mixing ratio δ is an observable of this type. When comparing model calculations with experimental results for these observables, it is important to ensure that the phase of the multipole operator used in the model calculations is consistent with the phase of the operator used during the experimental analysis.

In the present study, the experimental measurements were analysed according to the phase convention of Rose and Brink (Ro67). A derivation will therefore be made of the magnetic dipole and electric quadrupole operators, and of the γ-ray mixing ratio δ, which corresponds to this phase convention.

In the long wavelength approximation, Rose and Brink define their magnetic and electric operators as

$$T^{m}_{\lambda\mu} \equiv \alpha^{m}_{\lambda} \left(M_{\lambda\mu} + M'_{\lambda\mu} \right) \tag{A-1}$$

$$T^{e}_{\lambda\mu} \equiv \alpha^{e}_{\lambda} \left(Q_{\lambda\mu} + Q'_{\lambda\mu} \right) \tag{A-2}$$

where

$$\alpha^{e}_{\lambda} = \frac{(iK)^{\lambda}}{(2\lambda-1)!!} \left(\frac{\lambda+1}{2\lambda} \right)^{1/2} \tag{A-3}$$

$$\alpha^{m}_{\lambda} = -i\, \alpha^{e}_{\lambda} \tag{A-4}$$

$$Q_{\lambda\mu} = 2 g_e \left(\frac{m\beta}{\hbar^2 K} \right) \left[H, r^{\lambda} C_{\lambda\mu} \right] \tag{A-5}$$

$$Q'_{\lambda\mu} = -g_s \beta \frac{K}{\lambda+1} \vec{L} \left(r^{\lambda} C_{\lambda\mu} \right) \cdot \vec{S} \tag{A-6}$$

$$M_{\lambda\mu} = 2 g_e \frac{\beta}{\lambda+1} \vec{\nabla} \left(r^{\lambda} C_{\lambda\mu} \right) \cdot \vec{l} \tag{A-7}$$

$$M'_{\lambda\mu} = g_s \beta \vec{\nabla} \left(r^{\lambda} C_{\lambda\mu} \right) \cdot \vec{S} \tag{A-8}$$

and

$$C_{\lambda\mu} \equiv \left(\frac{4\pi}{2\lambda+1} \right)^{1/2} Y_{\lambda\mu} \tag{A-9}$$

$$\beta \equiv \frac{e\hbar}{2 m_p c} \tag{A-10}$$

Consider first the magnetic dipole operator T_1. It can be shown that[1]

$$\vec{\nabla} \left(r^{\lambda} Y_{\lambda\mu} \right) \cdot \vec{v} = \sqrt{\lambda(2\lambda+1)}\, r^{\lambda-1} \left[Y_{\lambda-1} \times \vec{v} \right]^{\lambda}_{\mu} \tag{A-11}$$

where $\vec{v}$ is any vector. Thus equations A-7 and A-8 become

$$M_{1\mu} = 2 g_e \frac{\beta}{2} \sqrt{\frac{4\pi}{3}}\, \vec{\nabla} \left(r Y_{1\mu} \right) \cdot \vec{l}$$

$$= g_e \beta \sqrt{\frac{4\pi}{3}} \sqrt{\frac{3}{4\pi}}\, l_{\mu}$$

$$= g_e \beta\, l_{\mu} \tag{A-12}$$

[1] See deS63 page 164

$$M'_{1\mu} = g_s \beta \sqrt{\frac{4\pi}{3}} \vec{\nabla}(r Y_{1\mu}) \cdot \vec{S}$$

$$= g_s \beta S_\mu . \qquad \text{(A-13)}$$

Noting that $\alpha_1^m = k$,

$$\therefore T_{1\mu}^m = \beta K (g_\ell l_\mu + g_s S_\mu) . \qquad \text{(A-14)}$$

Now consider a nucleus with atomic weight A and Z protons, described by a vibrating core coupled to one extra-core nucleon.

$$T_{1\mu}^m = \sum_{core} \beta K (g'_\ell l'_\mu + g'_s S'_\mu) + \beta K (g_\ell l_\mu + g_s S_\mu) \qquad \text{(A-15)}$$

where the primed variables refer to nucleons in the core, and the unprimed variables refer to the extra nucleon. This equation may be simplified by noting that

$$\sum_{core} g'_\ell l'_\mu + g'_s S'_\mu = \sum_{core} g'_\ell l'_\mu \equiv g_R R_\mu \qquad \text{(A-16)}$$

where $\vec{R}$ is the angular momentum of the core.

$$\therefore T_{1\mu}^m = \beta K (g_\ell l_\mu + g_s S_\mu + g_R R_\mu) . \qquad \text{(A-17)}$$

In order to be consistent with other authors (He67), the magnetic dipole operator used in this study, $\mathcal{M}(M1,\mu)$, is defined as

$$\mathcal{M}(M1,\mu) \equiv \frac{1}{K} \sqrt{\frac{3}{4\pi}} T_{1\mu}^m$$

$$= \sqrt{\frac{3}{4\pi}} \beta (g_\ell l_\mu + g_s S_\mu + g_R R_\mu) . \qquad \text{(A-18)}$$

When evaluating the electric quadrupole operator $T_{2\mu}^e$, the spin term $Q'_{2\mu}$ defined in equation A-6 above is normally ignored since it is much smaller than $Q_{2\mu}$. From equation

A-3 it is obvious that

$$\alpha_2^2 = \frac{-K^2}{2\sqrt{3}} . \qquad \text{(A-19)}$$

Therefore, substituting A-19 and A-5 back into A-2 yields

$$T^e_{2\mu} = -\sqrt{\frac{\pi}{15}}\, g_a\, \frac{2m\beta}{\hbar^2}\, K\, [H, r^2 Y_{2\mu}]$$

$$= -\sqrt{\frac{\pi}{15}}\, g_a\, \frac{Ke}{\hbar c}\, [H, r^2 Y_{2\mu}] . \qquad \text{(A-20)}$$

Returning to the case of a nucleus with a vibrating core and one extra-core proton ($g_\ell = 1$),

$$\sum_{\substack{\text{all}\\ \text{Nucleons}}} g_a\, e\, r^2 Y_{2\mu} = \sum_{\text{core}} g_a'\, e (r')^2 Y_{2\mu}(\theta', \phi') + r^2 Y_{2\mu}(\theta, \phi) . \qquad \text{(A-21)}$$

where the primed variables again refer to nucleons in the core, and the unprimed variables refer to the extra-core proton. The sum over the core nucleons may be expressed alternately as an integration over the core,

$$\sum_{\text{core}} g_a' e (r')^2 Y_{2\mu}(\theta', \phi') \rightarrow \int \rho(\vec{r})\, r^2\, Y_{2\mu}\, d\vec{r} \qquad \text{(A-22)}$$

where $\rho(r)$ is the charge density. For a vibrating core,

$$R = R_0 \left(1 + \sum_{\lambda\mu} \alpha^*_{\lambda\mu} Y_{\lambda\mu}\right) . \qquad \text{(A-23)}$$

Therefore, for $\alpha_{\lambda\mu} \ll 1$,

$$\rho(\vec{r}, R) \simeq \frac{(Z-1)\, e}{(4\pi/3) R_0^3}\, \Theta(R-r) \qquad \text{(A-24)}$$

Performing a Taylor expansion of $\rho(r)$ about R_0,

$$\rho(\vec{r}, R) = \rho(\vec{r}, R_0) + (R-R_0) \left.\frac{\partial \rho}{\partial R}\right|_{R_0} + \cdots$$

$$= \rho(\vec{r}, R_0) + \frac{3}{4\pi} \frac{(Z-1)\, e}{R_0^3}\, \delta(R_0 - r) \sum_{\lambda\mu} \alpha^*_{\lambda\mu} Y_{\lambda\mu} \qquad \text{(A-25)}$$

where, since $\alpha_{\lambda\mu} \ll 1$, only first order terms in $\alpha_{\lambda\mu}$ have

been kept. Thus, evaluating the integral in equation A-22 and introducing the quadrupole phonon creation and annihilation operators defined in equation 4-9 of chapter IV,

$$\int \rho(\vec{r})\, r^2 Y_{2\mu}\, d\vec{r}$$

$$= \frac{3}{4\pi}\frac{(Z-1)e}{R_0^2} R_0^4\, \alpha_{2\mu}$$

$$= \frac{3}{4\pi}(Z-1)e R_0^2 \sqrt{\frac{\hbar\omega_2}{2C_2}}\left[b^+_{2\mu} + (-)^{\mu} b_{2,-\mu}\right] \quad \text{(A-26)}$$

Substituting equations A-26 and A-21 back into equation A-20 yields

$$T^e_{2\mu} = -\sqrt{\frac{\pi}{15}}\frac{Ke}{\hbar c}\left[H_1\left\{(Z-1)\frac{3}{4\pi} R_0^2 \sqrt{\frac{\hbar\omega_2}{2C_2}} \times \left[b^+_{2\mu} + (-)^{\mu} b_{2,-\mu}\right]\right\} + r^2 Y_{2\mu}\right] \quad \text{(A-27)}$$

For a γ-ray transition <u>from</u> state $E^{(\alpha)}$ <u>to</u> state $E^{(\beta)}$

$$E_\gamma = E^{(\alpha)} - E^{(\beta)}$$

$$= \hbar c K \quad \text{(A-28)}$$

$$\therefore \langle E^{(\beta)}; j_\beta m_\beta | T^e_{2\mu} | E^{(\alpha)}; j_\alpha m_\alpha \rangle$$

$$= -\sqrt{\frac{\pi}{15}}\frac{K}{\hbar c}(E_\beta - E_\alpha)\langle E^{(\beta)}; j_\beta m_\beta | \mathcal{M}(E2_\mu) | E^{(\alpha)}; j_\alpha m_\alpha \rangle$$

$$= \sqrt{\frac{\pi}{15}} K^2 \langle E^{(\beta)}; j_\beta m_\beta | \mathcal{M}(E2,\mu) | E^{(\alpha)}; j_\alpha m_\alpha \rangle \quad \text{(A-29)}$$

where $\mathcal{M}(E2,\mu)$ is defined as

$$\mathcal{M}(E2,\mu) \equiv e r^2 Y_{2\mu}(\theta,\phi) + \frac{3}{4\pi} e (Z-1) R_0^2 \sqrt{\frac{\hbar\omega_2}{2C_2}}\left[b^+_{2\mu} + (-)^{\mu} b_{2,-\mu}\right] \quad \text{(A-30)}$$

This definition is equivalent to that of Heyde and Brussaard (He67).

Rose and Brink define the multipole mixing ratio for an E2/M1 transition <u>from</u> state $E^{(\alpha)}$ <u>to</u> state $E^{(\beta)}$ as

$$\delta \equiv \sqrt{\frac{3}{5}} \frac{\langle E^{(\alpha)}; j_\alpha \| T_2^e \| E^{(\beta)}; j_\beta \rangle}{\langle E^{(\alpha)}; j_\alpha \| T_1^m \| E^{(\beta)}; j_\beta \rangle} \qquad \text{(A-31)}$$

Since under time reversal the operators $T_{\lambda\mu}$ transform as

$$\Theta T_{\lambda\mu} \Theta^{-1} = (-)^{\lambda-\mu} T_{\lambda,-\mu} \qquad \text{(A-32)}$$

it can easily be shown that

$$\begin{aligned} \delta &\equiv \sqrt{\frac{3}{5}} \frac{\langle E^{(\alpha)}; j_\alpha \| T_2^e \| E^{(\beta)}; j_\beta \rangle}{\langle E^{(\alpha)}; j_\alpha \| T_1^m \| E^{(\beta)}; j_\beta \rangle} \\ &= -\sqrt{\frac{3}{5}} \frac{\langle E^{(\beta)}; j_\beta \| T_2^e \| E^{(\alpha)}; j_\alpha \rangle}{\langle E^{(\beta)}; j_\beta \| T_1^m \| E^{(\alpha)}; j_\alpha \rangle} \end{aligned} \qquad \text{(A-33)}$$

and therefore

$$\begin{aligned} \delta &= -\sqrt{\frac{3}{5}}\sqrt{\frac{\pi}{15}}\, K^2 \sqrt{\frac{3}{4\pi}} \frac{1}{K} \frac{\langle E^{(\beta)}; j_\beta \| \mathcal{M}(E2) \| E^{(\alpha)}; j_\alpha \rangle}{\langle E^{(\beta)}; j_\beta \| \mathcal{M}(M1) \| E^{(\alpha)}; j_\alpha \rangle} \\ &= -\sqrt{\frac{3}{100}} \frac{E_\gamma}{\hbar c} \frac{\langle E^{(\beta)}; j_\beta \| \mathcal{M}(E2) \| E^{(\alpha)}; j_\alpha \rangle}{\langle E^{(\beta)}; j_\beta \| \mathcal{M}(M1) \| E^{(\alpha)}; j_\alpha \rangle} \end{aligned} \qquad \text{(A-34)}$$

For completeness, equations for other electromagnetic observables used in this study are outlined below. The magnetic dipole moment for a level E is defined as (He67)

$$\mu \equiv \sqrt{\frac{4\pi}{3}} \langle E; I, M=I | \mathcal{M}(M1,\mu) | E; I, M=I \rangle \qquad \text{(A-35)}$$

$$\begin{aligned} \therefore \mu &= \sqrt{\frac{4\pi}{3}} \frac{1}{I} (I1; I0 | II) \langle E; I \| \mathcal{M}(M1) \| E; I \rangle \\ &= \sqrt{\frac{4\pi}{3}} \sqrt{\frac{I}{(I+1)(2I+1)}} \langle E; I \| \mathcal{M}(M1) \| E; I \rangle \end{aligned} \qquad \text{(A-36)}$$

Similarly, the electric quadrupole moment is defined as (He67)

$$Q \equiv \sqrt{\frac{16\pi}{5}} \langle E; I, M=I \mid \mathcal{M}(E2,\mu) \mid E; I, M=I \rangle \qquad \text{(A-37)}$$

$$\therefore Q = \sqrt{\frac{16\pi}{5}} \frac{1}{\hat{I}} (I2; I0 \mid II) \langle E; I \| \mathcal{M}(E2) \| E; I \rangle$$

$$= \sqrt{\frac{16\pi}{5}} \sqrt{\frac{I(2I-1)}{(2I+3)(2I+1)(I+1)}} \langle E; I \| \mathcal{M}(E2) \| E; I \rangle \qquad \text{(A-38)}$$

In both equations A-36 and A-38 above the Clebsch-Gordon coefficients were evaluated using the Handbook of Mathmatical Functions (Ab64).

In the long wavelength approximation, the transition probability for a γ-ray transition of angular momentum L between states $E^{(\alpha)}$ and $E^{(\beta)}$ is given by[1]

$$\omega(L) = \frac{8\pi c e^2}{\hbar c} \frac{(L+1)}{L[(2L+1)!!]^2} K^{2L+1} B(L) \qquad \text{(A-39)}$$

where for E2/M1 radiation

$$B(E2) = \frac{1}{2j_\alpha+1} \frac{1}{e^2} \langle E^{(\beta)}; j_\beta \| \mathcal{M}(E2) \| E^{(\alpha)}; j_\alpha \rangle^2$$

$$B(M1) = \frac{1}{2j_\alpha+1} \frac{1}{e^2} \langle E^{(\beta)}; j_\beta \| \mathcal{M}(M1) \| E^{(\alpha)}; j_\alpha \rangle^2 \qquad \text{(A-40)}$$

Thus

$$\omega(E2/M1) = 8\pi c \frac{e^2}{\hbar c} \left[\frac{2}{9} K^3 B(ML) + \frac{1}{150} K^5 B(E2) \right]$$

$$= \frac{16\pi}{9} \frac{c e^2}{(\hbar c)^4} E_\gamma^3 \left[B(M1) + \frac{3}{100} \left(\frac{E_\gamma}{\hbar c} \right)^2 B(E2) \right] \qquad \text{(A-41)}$$

[1]See deS63 page 160 or deS74 page 698

Appendix B

Computing Details of the Programs CUPPLE3 and MOMENT

B.1 The Program CUPPLE3

CUPPLE3 is a FORTRAN IV computer program designed to carry out the intermediate coupling model calculations discussed in chapter IV of this thesis. The format of this program is quite similar to that of the program CUPPLE-1 (Gr73).

Input is read by this program from unit 5 and output is written, unless otherwise specified, on unit 6. Input data is read in the standard form

```
      READ(5,100) IC,(DUM(J),J=1,7)
100 FORMAT(I2,8X,7F10.0)
```

where IC is a control integer which specifies to the program which input parameters are contained on the remainder of the card. Table 17 lists the various IC values and input parameters read by the program. All energy parameters are measured in MeV.

One option available in CUPPLE3 permits results to be written, in a special format, to unit 7 as well as on unit 6. This output is designed to be read by the program MOMENT. In the present version of CUPPLE3 only results for positive parity states, and only the eigenvectors for the lowest ten eigenstates in energy for each spin, are written to unit 7.

Table 17

Input Cards for CUPPLE3

IC	DUM(J) J = ?	NAME	REMARKS
-1	-	-	Causes program to stop.
0	-	-	Ignored
01	-	-	The remainder of this card is ignored. The program then expects a card containing a descriptive TITLE in (20A4) format.
02	1	NFONON	Number of quadrupole phonons. ($0 \leq$ NFONON ≤ 3)
	2	EFONON	Energy of quadrupole phonons.
	3	NOCTF	Number of octupole phonons. ($0 \leq$ NOCTF ≤ 2)
	4	EOCTF	Energy of octupole phonons.
	5	IPAR	Parity of states for which calculations will be done.
03	1	NPART	Number to particle orbitals. ($0 \leq$ NPART ≤ 5)
	2	NHOLE	Number of hole orbitals. ($0 \leq$ NHOLE ≤ 5) ($NPART + NHOLE \geq 1$)
	3	GPAIR	Pairing interaction energy G_{pair}.
	4	IWHICH	=0 Do calculations for single-particle and two-particle-one-hole states.
			=1 Do calculations for single-hole and two-hole-one-particle states.
			Following the 03 card, the program expects to read NPART data cards with IC=0, and NHOLE data cards with IC=1, containing the following information for each orbital.

IC	DUM(J) J = ?	NAME	REMARKS
00 or 01	1	N1(I) or NH1(I)	The radial quantum number n_i.
	2	PARTL(I) or HOLEL(I)	The orbital angular momentum l_i.
	3	PARTJ(I) or HOLEJ(I)	The total angular momentum j_i.
	4	PARTE(I) or HOLEE(I)	The single-particle (-hole) energy ϵ_j (ϵ_{j_3}).
			This series of orbital information cards in terminated by a card with IC=-1.
04	1	XIMIN	Minimum value of ξ_2.
	2	XISTP	Increment for stepping ξ_2.
	3	XIMAX	Maximum value of ξ_2.
	4	XI3MIN	Minimum value of ξ_3.
	5	XI3STP	Increment for stepping ξ_3.
	6	XI3MAX	Maximum value for ξ_3.
			To do calculations for only one value of XI (XI3) set XISTP = 0 (XI3STP = 0) and XIMIN = XIMAX (XI3MIN = XI3MAX).
05	1	LPUNCH	=1 Write ouput to unit 7 as well as unit 6. The output in unit 7 is in a special format readible by the computer program MOMENT.
			=0 Suppress extra output.
	2	LFULL1	Should always equal 0. If LFULL1 > 0 then an extensive printout is generated. This facility was useful when writing the program.

IC	DUM(J) J = ?	NAME	REMARKS
05	3	LCOEFF	=1 Print eigenvalues and eigenvectors. =0 Print only eigenvalues.
	4	KMSTRT	Only used of LPUNCH = 1. The starting ID number for ouput written to unit 7. Subsequent sets are numbered sequentially.
	5	MAXDIA	Maximum number of diagonalizations.
	6	MAXRNK	Maximum matrix rank (≤ 75).
	7	NSTOP	The maximum number of eigenstates for which output will be printed on unit 6. Eigenstates are printed in ascending order of eigenvalue six to a line, and hence NSTOP is always rounded up to the next multiple of six. In order to print results for all eigenstates set NSTOP < 0. NOTE: NSTOP does not effect the output to unit 7.
06	-	-	Not used. Ignored.
07	1	NSPIN	Number of total spin I values for which calculations will be done. ($1 \leq$ NSPIN ≤ 6)
	2	RSPIN(1)	First I value.
	3	RSPIN(2)	Second I value. etc.
08	1	NENG	Number of maximum cutoff energies to be given. NENG must equal NSPIN.
	2	EMAX(1)	Upper energy cutoff for levels with RSPIN(1).
	3	EMAX(2)	Upper energy cutoff for levels with RSPIN(2). etc.
09	-	-	Not used. Ignored.

IC	DUM(J) J = ?	NAME	REMARKS
10	-	-	End input. Current input parameters are checked for errors and, if none are found, calculation begins.

B.2 The Program MOMENT

MOMENT is a FORTRAN IV computer program designed to calculate various electromagnetic observables using as input the energy level eigenvectors calculated by CUPPLE3. The formulae used by MOMENT are discussed in chapter IV and appendix A of this thesis.

Input to MOMENT comes both from units 7 and 5, while output is through unit 6. MOMENT first reads the CUPPLE3 results from unit 7, and then reads all other input from unit 5. Input from unit 5 is identical in format to that used in the CUPPLE3 calculations and described above. Table 18 lists the various IC values and input parameters read by the program. All energy parameters are measured in MeV.

The IC = 04 to 08 cards each initiate the calculation of a particular electromagnetic observable. The 04 and 05 cards calculate magnetic dipole and electric quadrupole moments resectively, while the 06 and 07 cards are used to calculate γ-ray mixing and branching ratios respectively. The 08 card calculates B(E2) values for specified transitions. After reading one of these cards or, in the case of a branching ratio calculation, a set of cards, the program calculates the required observable, prints the result, and then returns to read the next input card.

Energy levels or eigenstates are identified on these

Table 18

Input Cards for MOMENT

IC	DUM(J) J = ?	NAME	REMARKS
-1	-	-	Causes program to stop.
0	-	-	Ignored.
01	-	-	The program immediately prints out all the parameters read from the CUPPLE3 output. These include the quadrupole phonon energy and coupling strength parmeter, and the eigenvectors for the first ten eigenstates of each spin.
02	1	ZN	Atomic number Z of nucleus.
	2	AN	Atomic weight A of nucleus.
	3	XKR	Radial parameter k.
03	1	GS	Spin g factor.
	2	GR	Core g factor.
	3	GL	Orbital angular momentum g factor.
04	1	SPINI	Total angular momentum of level.
	2	JSPI	Level number relative to other levels with angular momentum SPINI. (See text for explanation.)
			The program now calculates and prints the magnetic dipole moment for this level.
05	1	SPINI	Total angular momentum of level.
	2	JSPI	Level number relative to other levels with angular momentum SPINI.
			The program now calculates and prints the electric quadrupole moment for this level.
06	1	SPINI	Total angular momentum of the initial level in a γ-ray transition.

IC	DUM(J) J = ?	NAME	REMARKS
06	2	JSPI	Level number relative to other levels with angular momentum SPINI.
	3	SPINF	Total angular momentum of the final level in a γ-ray transition.
	4	JSPF	Level number relative to other levels with angular momentum SPINF.
	5	EGAMMA	Energy of γ-ray.
			The program now calculates and prints the γ-ray multipole mixing ratio for an E2/M1 transition between these two levels.
07	1	SPINI	Total angular momentum of a level decaying via γ-ray emission.
	2	JSPI	Level number relative to other levels with angular momentum SPINI.
	3	NBR	The number of branches through which this level can decay. (NBR $\leq$ 10)
			The program now expects to read NBR cards with IC=0 containing the following information about the final levels in the various γ-ray branches.
	1	XSPF(I)	Total angular momentum of the I'th final state.
	2	MSPF(I)	Level number relative to other levels with angular momentum XSPF(I).
	3	XGAM(I)	Energy of I'th γ-ray transition.
			After reading NBR cards, the program calculates and prints the branching ratios for the specified transitions.
08	1	SPINI	Total angular momentum of initial level in transition.

IC	DUM(J) J = ?	NAME	REMARKS
08	2	JSPI	Level number relative to other levels with angular momentum SPINI.
	3	SPINF	Total angular momentum of final level in transition.
	4	JSPF	Level number relative to other levels with angular momentum SPINF.
			The program now calculates and prints the B(E2) value for a transition between these two levels.

cards by two parameters, the level spin and level number. The level number refers to the position of a state with respect to other states of the same spin; level 1 is the lowest level of a particular spin, level 2 the second lowest level of that spin, etc. Experimental γ-ray energies are used for transitions between states.